Electronic Supplementary information (ESI)

Sulphur-Atom Positional Engineering in Perylenimide: Structure-Property Relationships and H-aggregation Directed Type-I Photodynamic Therapy

Mst Nasima Khatun[a], Satyendu Nandy[b], Hirakjyoti Roy[b], Siddhartha Sankar Ghosh[b,c], Sachin Kumar*[b], and Parameswar Krishnan Iyer*[a,c]*

[a]Department of Chemistry, Indian Institute of Technology Guwahati, Guwahati-781039, Assam, India.

[b]Department of Bioscience and Bioengineering, Indian Institute of Technology Guwahati, Guwahati-781039, Assam, India

[c]Centre for Nanotechnology, Indian Institute of Technology Guwahati, Guwahati-781039, Assam, India.

FAX: +913612582349; E-mail: pki@iitg.ac.in.

Contents

1. **Experimental Section**

1.1. Materials and Instrumentations: All reagents and starting materials, including Perylene-3,4,9,10-tetracarboxylic acid anhydride (PDA), imidazole, Zinc acetate [Zn $(OAc)_2$], and various boronic acid derivatives such as phenylboronic acid, thianthrenyl boronic acid, and 2,2'-bithiophene-5-boronic acid pinacol ester, and other reactive oxygen species detector such as 2',7'-Dichlorodihydrofluorescein diacetate were (DCFDA), 2,2,6,6-Tetramethylpiperidin (TEMP), 9,10-Anthracenediyl-bis(methylene)dimalonic acid (ABDA), Terephthalic acid (TA), Dihydrorhodamine 123 (DHR 123), 2,3-Bis-(2-methoxy-4-nitro-5-sulfophenyl)-2H-tetrazolium-5-carboxanilide (XTT) and 5,5-dimethyl-1-pyrroline-N-oxide (DMPO) were purchased from were purchased from Sigma Aldrich (INDIA) in reagent-grade quality. HPLC-grade solvents were obtained from Fisher Scientific Ltd. and RANKEM. Nuclear magnetic resonance (NMR) spectra, including ^{1}H and ^{13}C, were recorded using a Bruker Avance 400 MHz spectrometer. The residual solvent signal was used as an internal reference for all solutions used in the NMR experiments. Mass spectra were obtained using MALDI-TOF spectrometry. UV/visible (UV/vis) and photoluminescence (PL) spectra were recorded using a Perkin-Elmer Model Lambda-750 spectrophotometer and a Horiba Fluoromax-4 spectrofluorometer, respectively. Measurements were performed at 298 K using 4 mm quartz cuvettes. A laser diode at 375 nm (DeltaDiode-375) was the excitation source for both UV/vis and PL experiments. The compounds' hydrodynamic diameter and Zeta potential were measured using a Malvern Zetasizer instrument. Field emission scanning electron microscopy (FESEM) images were obtained using a Sigma Carl ZEISS field emission scanning electron microscope. Single crystal data were collected using a Bruker SMART APEX diffractometer with a CCD area detector. The electron spin resonance (ESR) technique was recorded using Bruker EMXplus-10/12 Bruker. For photodynamic therapy studies, a white light source with an intensity of 50 mW cm^{-2}, specifically the "Pick Ur Needs 120W Plastic Lithium Battery Search Light Long 1 Km Range with Multi-Functional + Blinker Rechargeable Handheld Torch" in black, was utilized. DMEM, Propidium iodide (PI), and Calcein-AM (AM) were purchased from High Media.

1.2. Preparation of the Test Solution: Stock solutions of **RPNI-O** materials, including **PPI**, **THPI**, and **API**, as well as derivatives of **RPNI-S** such as **PPIS**, **THPIS**, and **APIS**, were prepared at a concentration of 20 mM in dimethyl sulfoxide (DMSO). To study the aggregation behavior, test solutions of the materials were prepared at a concentration of 100 μM. These test

solutions were prepared by varying the water fraction in DMSO. Before recording the spectra, the resulting solutions were thoroughly shaken at room temperature to ensure proper mixing and dispersion of the compounds.

1.3. Preparation of FESEM samples:

The morphological analysis of the supramolecular self-assembly was conducted using field emission scanning electron microscopy (FESEM). A simple methodology was employed to prepare the samples for imaging, as depicted in Fig. S8b. A dilute suspension of the perylene derivatives at a concentration of 100 μM was prepared using a mixture of 99.9% water and -0.1% DMSO. Subsequently, this suspension was drop-casted onto a glass surface coated with aluminum foil. The samples were then allowed to air dry overnight at room temperature before analysis.

1.4. Theoretical Studies: Density functional theory (DFT) calculations were employed to evaluate the electronic properties of **RPNI-O** and **RPNI-S** derivatives. The Gaussian 16 package, incorporating the B3LYP hybrid functional, was utilized to perform these calculations. For each derivative, the ground state optimized geometries were obtained, and the electron density and energy of the highest occupied molecular orbital (HOMO) and lowest unoccupied molecular orbital (LUMO) were determined. The calculations employed the 6-31G basis set, which is known to provide accurate results within a reasonable computational time. [1,2]

1.5. Photoluminescence quantum Yield Calculations: The fluorescence quantum yields (Φ_{PL}) of **RPNI-O** and **RPNI-S** derivatives were determined by comparing them to the fluorescence quantum yield of Rhodamine 6G (Φ_r = 0.95 in ethanol) using a specific equation. The equation used is as follows:

$$\Phi_{PL} = \Phi_r (A_r F_s / A_s F_r) (\eta_s^2 / \eta_r^2) \quad \text{(S1)}$$

In this equation, s and r refer to the sample and reference, respectively. Φ represents the quantum yield, A denotes the absorbance, F signifies the relative integrated fluorescence intensity, and η represents the refractive index.

1.6. Synthesis of RPNI-O and RPNI-S derivatives

Synthetic procedures for peryleneimide (PNI-O): PNI-O was synthesized through a simple condensation reaction employing hydrothermal reaction procedures. Perylene-3,4,9,10-

tetracarboxylic acid anhydride (PDA) (2.54 mmol), amine (1.35 mmol), Zn $(OAC)_2$ (1.72 mmol), imidazole (5g), and water (1ml) were combined in a Teflon sleeve and thoroughly mixed until a homogeneous mixture was obtained. The homogeneous mixture was transferred to a hydrothermal autoclave reactor vessel and sealed. The reactor was then subjected to a pressure of 15 bar and placed in an oven. The temperature inside the autoclave reactor was gradually increased to 190 °C over 20 hours. The reaction was allowed to proceed under these conditions. After 20 hours, the heat was turned off, and the reaction mixture was allowed to cool down to room temperature. The resulting dark reddish crude product was extracted with chloroform (200 ml) and water (50 ml) under acidic PH. The extraction process was repeated four times to ensure adequate separation. The extracted product was washed four times with water, dried over Na_2SO_4, and subsequently filtered. The filtered solution was concentrated using a rotary evaporator to remove the solvent, resulting in a concentrated residue. The concentrated residue was purified using column chromatography with chloroform as the eluent. This purification step yielded the desired dark reddish compound (400 mg) with a 40% yield.

Characterization data for PNI-O: ^{1}H NMR (400 MHz, CDCl3) 0.84 (t, 3H),1.28-1.44 (m, 6H), 1.70 (dd, 2H), 4.09-4.14 (t, 2H), 7.52 (t, 2H), 7.80 (d, 2H), 8.24 (d, 2H), 8.29 (d, 2H), 8.44 (d, 2H)). ^{13}C NMR (101 MHz, CDCl3) δ 14.09, 22.58, 26.92, 28.19, 31.64, 40.49, 120.12, 120.83, 123.67, 126.73, 126.96, 127.75, 129.10, 130.90, 131.29, 134.35, 136.94, 163.86. MALDI-TOF: calculated for $C_{28}H_{23}NO_2$: 405.17 $[M]^+$, Found: 404.95 $[M-H]^+$

Synthetic Route

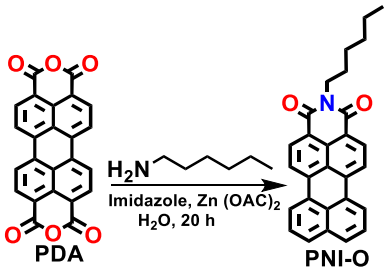

Scheme S1. The synthetic method employed to prepare **PNI-O.**

Synthetic procedures for BrPNI-O: PNI-O (1 mmol) was dissolved in 5 mL of chlorobenzene with gentle heating. Subsequently, bromine (4.5 mmol) was added to the solution, and the resulting mixture was stirred for 4.5 hours at 50 °C. After completion of the reaction, chlorobenzene and any unreacted bromine were removed under vacuum. The resulting solid, which appeared red, was subjected to crystallization using methanol. This process yielded a 95% yield of the desired compound.

Characterization data for 8-bromo-2-hexyl-1H-benzo[5,10]anthra[2,1,9-def]isoquinoline-1,3(2H)-dione (BrPNI-O): ^{1}H NMR (400 MHz, CDCl3) δ 0.93 (t, 3H), 1.3-1.6 (m, 6H), 1.88 (dd, 2H), 3.77 (t, 2H), 7.69 (t, 1H),7.86 (d, 1H), 8.13 (d, 1H), 8.27 (d, 2H), 8.33 (d, 1H). 8.38 (d, 1) 8.55 (dd, 2H). ^{13}C NMR (101 MHz, CDCl3) δ.14.09, 22.58, 26.92, 28.19, 31.64, 40.49, 120.12, 123.67, 126.96, 127.75, 129.15, 130.80, 131.32, 172.56 MALDI-TOF: calculated for $C_{28}H_{22}BrNO_2$: 484.38 $[M]^+$, Found: 483.39 $[M-H]^+$

Synthetic Route

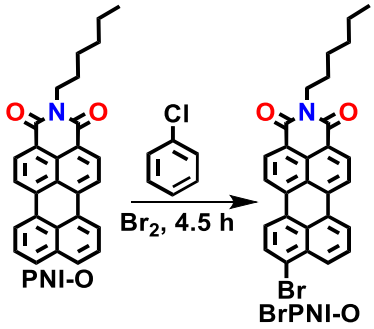

Scheme S2. The synthetic method employed to prepare **BrPNI-O.**

Synthetic procedures for RPNI-O: In a 50 mL round-bottom flask, Compound **BrPNI-O** (0.5 mmol) and the corresponding boronic acid (1 mmol) were combined with 5 mg of Pd $(PPh_3)_4$ catalyst. The mixture was then subjected to nitrogen gas for 30 min to remove any oxygen. Then, 6 mL of THF (tetrahydrofuran) was added to the flask, followed by 2 mL of a 2.0 M potassium carbonate solution. The resulting mixture was stirred at 85 °C under a nitrogen atmosphere, and the progression of the reactions was monitored using thin-layer chromatography (TLC). After 24 hours, the solutions were cooled and extracted using $CHCl_3$ (chloroform). The organic layers were subsequently dried using anhydrous sodium sulfate. The solvent was evaporated, and the resulting product was purified using column chromatography, yielding a 60% yield of the desired Red solid for **PPI** and **API** and **THPI** (brownish solid) compound.

Characterization data for 2-hexyl-8-phenyl-1H-benzo[5,10]anthra[2,1,9-def]isoquinoline-1,3(2H)-dione (PPI): ^{1}H NMR (400 MHz, CDCl3) δ 0.89 (t, 3H), 1.41 (m, 6H), 1.76 (dt, 2H), 4.14 (t, 2H), 7.53 (m, 7H),7.98 (d, 1H) 8.37 (d, 2H), 8.42 (t, 2H), 8.55 (m, 2H). ^{13}C NMR (101 MHz, CDCl3) δ 14.07, 22.62, 26.77, 28.07, 29.02, 31.56, 40.39, 114.10, 120.13, 119.69, 123.56, 126.05, 128.52, 129.20, 130.01, 131.99, 132.66, 136.66, 139.74, 143.11, 163.73. MALDI-TOF: calculated for $C_{34}H_{29}NO_2$: 481.20 $[M]^+$, Found: 481.321$[M]^+$

Characterization data for 8-([2,2'-bithiophen]-5-yl)-2-hexyl-1H-benzo[5,10]anthra[2,1,9-def]isoquinoline-1,3(2H)-dione (THPI): ^{1}H NMR (400 MHz, CDCl3) δ 0.88 (t, 3 H), 1.39 (m,5H), 1.75 (dt,3H), 4.19 (t,2H), 7.08 (t, 1H), 7.29 (m, 4H), 7.64 (t, 1H), 7.70 (d, 1H), 8.35 (m, 3H), 8.41 (t, 2H), 8.54 (m, 2H). ^{13}C NMR (101 MHz, CDCl3) δ 12.98, 22.92, 26.64, 27.25, 28.02, 30.90, 32.50, 39.56, 113.69, 118.96, 119.56, 122.50, 126.83, 127.54, 128.52, 131.29, 135.54, 138.75, 142.01, 162.55. MALDI-TOF: calculated for $C_{36}H_{27}NO_2S_2$: 569.14 $[M]^+$, Found:569.43 $[M]^+$

Characterization data for 2-hexyl-8-(thianthren-1-yl)-1H-benzo[5,10]anthra[2,1,9-def]isoquinoline-1,3(2H)-dione (API): ^{1}H NMR (400 MHz, CDCl3) δ 0.89 (t, 3H), 1.39 (m, 6H), 1.77 (m, 2H), 4.22 (t, 2H), 7.15 (t, 3H), 7.34 (d, 1H), 7.40 (t, 3H), 7.54 (dd, 3H), 7.65 (d, 3H). 8.50 (m, 1) 8.64 (dd, 2H). ^{13}C NMR (101 MHz, CDCl3) δ 14.09, 27.09, 28, 59, 31.57, 40.49, 120.36, 121.25,126.28, 127.84, 128.67, 129.12, 132.4, 135.44, 136.43, 137.39, 139.66, 164.12. MALDI-TOF: calculated for $C_{40}H_{29}NO_2S_2$: 619.79 $[M]^+$, Found: 620.79 $[M+H]^+$

Synthetic Route

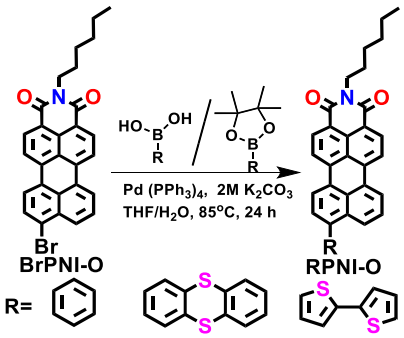

Scheme S3. The synthetic method employed to prepare **RPNI-O.**

Synthetic procedures for RPNI-S: In a 20 mL flask, **RPNI-O** (0.5 mmol) and Lawesson's reagent (1.5 mmol) were dissolved in dry toluene. The resulting solution was refluxed under a nitrogen atmosphere for 24 hours. After completion of the reaction, the mixture was allowed to cool down to room temperature, and the solvent was evaporated under reduced pressure. The residue was purified using column chromatography on silica gel, employing a hexane/dichloromethane (DCM) mixture as the eluent. Subsequent drying under vacuum conditions yielded a bluish powder (53-58% yield).

Characterization data for 2-hexyl-8-phenyl-1H-benzo[5,10]anthra[2,1,9-def]isoquinoline-1,3(2H)-dithione (PPIS): ^{1}H NMR (400 MHz, CDCl3) δ 0.90 (t, 3H), 1.40 (m,6H), 1.78 (dt, 2H

), 4.21 (m, 2H), 7.16 (q, 3H), 7.34 (d, 3H), 7.41 (t, 1H), 7.53 (d, 1H), 7.56 (d,1H), 7.65 (d,1H), 8.48 (dd, 1H), 8.54 (d, 1H) 8.63 (dd, 2H). ^{13}C NMR (101 MHz, CDCl3) δ 13.07, 21.66, 25.87, 27.03, 28.67, 30.57, 49.54, 113.04, 118.31, 119.47, 121.45, 122.33, 125.63, 126.94, 127.56, 128.09, 129.95, 131.95, 132.25, 138.75, 142.09, 165.3. MALDI-TOF: calculated for $C_{34}H_{27}NS_2$: 513.15 $[M]^+$, Found: 513.29 $[M]^+$

Characterization data for 8-([2,2'-bithiophen]-5-yl)-2-hexyl-1H-benzo[5,10]anthra[2,1,9-def]isoquinoline-1,3(2H)-dithione (THPIS): ^{1}H NMR (400 MHz, CDCl3) δ 0.89 (t, 3H), 1.41 (m, 6H), 1.76 (dt, 2H) 4.19 (t,2H), 7.08 (t, 1H), 7.29 (m, 6H), 7.64 (t, 1H), 7.71 (d, 1H), 8.35 (m, 3H), 8.40 (dd, 1H), 8.54 (t, 2H). ^{13}C NMR (101 MHz, CDCl3) δ 13.09, 21.59, 25.67, 27.04, 28.77, 30.67, 48.54, 114.04, 117.31, 118.57, 120.55, 121.43, 123.73, 125.74, 125.56, 127.01, 128.95, 130.05, 131.25, 141.45, 142.09, 169.3. MALDI-TOF: calculated for $C_{36}H_{27}NS_4$: 601.10 $[M]^+$, Found: 601.19 $[M]^+$

Characterization data for 2-hexyl-8-(thianthren-1-yl)-1H-benzo[5,10]anthra[2,1,9-def]isoquinoline-1,3(2H)-dithione (APIS): ^{1}H NMR (400 MHz, CDCl3) δ 0.91 (t, 3H), 1.42 (m, 6H), 1.78 (dt, 2H), 4.21 (t, 2H), 7.16 (t, 3H), 7.34 (t, 1H), 7.40 (t, 1H), 7.51 (d, 4H), 7.56 (m, 1H), 7.65 (d, 2H), 8.47 (m, 1H), 8.54 (d, 1H), 8.63 (dd, 2H). ^{13}C NMR (101 MHz, CDCl3) δ 14.10, 22.61, 26.89, 28.12, 31.62, 42.4, 120.36, 121.25, 123.40, 124.03, 126.89, 127.13, 128.67, 129.21, 132.43, 135.44, 136.01, 137.89, 139.66, 170.30. MALDI-TOF: calculated for $C_{40}H_{29}$NS4: 651.11 $[M]^+$, Found: 650.40 $[M-H]^+$

Synthetic Route

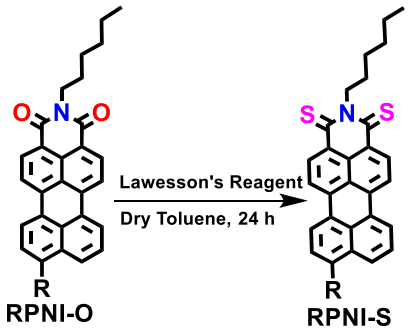

Scheme S4. The synthetic method employed to prepare **RPNI-S.**

1.7. Computational studies

This study examined the optimization and frequencies of triplet excited states, excitation energies, and transition properties of these peryleneimide materials RPNI-O and RPNI-S

derivatives. These calculations were performed using the time-dependent B3LYP/6-31G (d, p) method within the Tamm-Dancoff approximation (TDA). The computational software used for these calculations was the Gaussian 16 package, with the ORCA 5.0 module utilized at the B3LYP DEF2-SVP level. Furthermore, the spin-orbit coupling (SOC) constants for **PPI, THPI, API, PPIS, THPIS,** and **APIS** were also computed at the abovementioned level, employing the ORCA 5.0 software.[3,4]

1.8. $^1O_2$ generation quantum yield Estimation: In this study, dilute solutions of Rose Bengal were used as a reference (Φ_Δ = 0.76 in ethanol). To eliminate the inner filter effect, the absorbance maxima of Rose Bengal and Photosensitizer were maintained at 0.2. Additionally, various solutions of **RPNI-O** and **RPNI-S** derivatives were prepared at a concentration of 100 μM. Then, 100 uM ABDA was added to these solutions. The absorbance of ABDA at 378 nm was measured at various irradiation times using white light (400-700 nm, 50 mW cm^{-2}). This measurement allowed the determination of the decay rate of the photosensitizing process. The Φ_Δ of **RPNI-O** and **RPNI-S** derivatives in 99% PBS in DMSO was then calculated using the following equations:

$$\Phi_{AIEgen} = \Phi_{RB} (K_{AIEgen} A_{RB}/K_{RB} A_{AIEgen}) \quad \text{(S2)}$$

Where Φ_{AIE} is the $^1O_2$ generation quantum yield of AIEgen in 99% PBS in DMSO. A_{RB} and A_{AIEgen} represent the light absorbed by Rose Bengal and AIEgen, respectively, at an absorbance 0.2. The absorption bands were integrated into the 400-700 nm wavelength range to determine these values. K_{RB} and K_{AIEgen} are the decomposition rate constants of ABDA by Rose Bengal and AIEgen, respectively. These constants were determined by plotting Ln (A_0/A) against time, where A_0 and A are the absorbances of ABDA at 378 nm by photosensitizers under white light irradiation at different time points.[5,6]

1.9. Reactive oxygen species (ROS) Generation/Measurement

Singlet Oxygen ($^1O_2$) Test: This experiment was conducted to quantify the generation $^1O_2$. Singlet oxygen, produced through the photoirradiation of PSs at 99% PBS in DMSO, was detected using ESR spectroscopy in the presence of TEMP. The ESR signals from the free-radical TEMPO, formed from the reaction of singlet oxygen with TEMP, were recorded after irradiation with white light. Solutions containing 100 μM TEMP and 100 μM **RPNI-O** or **RPNI-S** PSs were inserted quantitatively into quartz capillaries at 99% PBS in DMSO. These solutions were then subjected to white light irradiation at a power density of 50 mW cm^{-2} for

30 min. ESR spectra of the spin-trapped radicals were recorded in the range of 3000-3600 G after irradiation. Background interference was corrected using a sample before irradiation.[7]

Further, a mixed solution containing 100 μM ABDA (a singlet oxygen sensor) and 100 μM of various **RPNI-O** and **RPNI-S** derivatives solutions was prepared in 99% PBS in DMSO. The solution was irradiated with white light at a power density of 50 mW cm^{-2} for different durations: 0, 2, 4, 6, 8, 10, and 20 min. The degradation of ABDA's absorbance at 378 nm was measured promptly after each interval.

Total ROS Test: The total ROS test measures the overall reactive oxygen species (ROS) levels. DCFDA, a chemically reduced form of fluorescein, was used as a fluorescent indicator for ROS. A solution of 10 μM DCFDA and 100 μM of various solutions of **RPNI-O** and **RPNI-S** derivatives was prepared at 99% PBS in DMSO. The solution was irradiated with white light at a power density of 50 mW cm^{-2} for different durations: 0, 5, 10, 15, 20, 25, and 30 min. The fluorescence spectra of the mixed solution were rapidly measured.

Typ-I ROS :

Superoxide Anion Radical ($O_2^{\bullet-}$) Test:

1) The feasibility of the reaction producing $O_2^{\bullet-}$ was checked through theoretical calculations using the ORCA 5.0 software.

2) ESR analysis was conducted to verify the generation of $O_2^{\bullet-}$ utilizing DMPO as the spin-trapping agent. The experimental samples were quantitatively inserted into quartz capillaries, comprising 100 μM DMPO at 99% PBS in DMSO and 100 μM of **PPIS**, **THPIS**, or **APIS**. Subsequently, the spin spectra were monitored after subjecting the solutions to 10 min white light irradiation (50 mW cm^{-2}).

3) XTT was employed as the indicator for $O_2^{\bullet-}$, which undergoes conversion to XTT formazan in the presence of $O_2^{\bullet-}$. A mixed solution of XTT (100 μM) and **PPIS**, **THPIS**, or **APIS** PSs (100 μM) was prepared. Subsequently, the solution was irradiated with white light for durations of 0, 5, 10, 20, and 30 min, and the UV-vis spectra of the mixed solution were promptly measured. Additionally, UV-vis spectra of XTT irradiated solely by white light were recorded as the control.

4) DHR123 was utilized as the indicator for superoxide anion radicals, which undergo conversion to Rhodamine 123 in the presence of $O_2^{\bullet-}$. Solutions containing 100 μM **PPIS**, **THPIS**, or **APIS** at 99% PBS in DMSO were prepared. Subsequently, the cuvette containing the solution was exposed to white light (400-700 nm, 50 mW cm^{-2}) for varying durations (5-30 min), and the fluorescence spectra were promptly recorded after each irradiation. In the control group, a DHR123 solution without photosensitizers was irradiated. (λ_{ex} = 500 nm, λ_{em} = 527 nm).

Hydroxyl Radical (HO$^{\bullet}$) Test: This test aimed to measure the generation of hydroxyl radicals (HO$^{\bullet}$). A mixed solution containing 100 μM TA and 100 μM of various solutions of **RPNI-O** and **RPNI-S** derivatives compounds was prepared in 99% PBS in DMSO. The subsequent testing process was the same as determining total ROS using DCFDA as the probe. Upon trapping with HO$^{\bullet}$, TA was converted to hydroxyl terephthalic acid, resulting in an enhanced fluorescent intensity (λ_{ex} = 315 nm).

1.10. The Point of Zero Zeta Potential Evaluation

According to the literature,[8] the points of zero zeta potential (PZZP) for **RPNI-O** and **RPNI-S** derivatives were calculated. The aqueous solutions of these Perylenimide materials were initially at a neutral pH of about 7. However, by introducing a dilute solution of sodium hydroxide or dilute hydrochloric acid, the pH of the solutions could be adjusted to either alkaline or acidic conditions. When the pH values of the **RPNI-O** and **RPNI-S** materials were altered within 9, 7.4, 5.6, to 3 and 1, a noticeable change in the zeta potential was observed. Specifically, the zeta potential transitioned from negative to positive as the pH values changed from alkaline to acidic.

1.11. The Energy of the Valence Band and Conduction Band Calculations

The valence band energy (E_V) was determined by calculating the energy of the

band (E_V) from X-ray photoelectron spectroscopy (XPS) data. To calculate the conduction band energy (E_C), the energy gap was first estimated from the onset absorption data from UV-visible spectroscopy. Subsequently, E_C was calculated concerning the normal hydrogen electrode (NHE) using Equations S3 and S4, as shown below:

$$E_V = -E_{HOMO} - 4.5 \quad \text{(S3)}$$

$$E_C = -E_{LUMO} - 4.5 \quad \text{(S4)}$$

The calculated E_V and E_C values for the **RPNI-O** and **RPNI-S** derivatives were recorded in Table S17. Additionally, E_C and E_V at a point of zero zeta potential (PZZP) with a pH of 5.6 were computed based on literature data using Equations S5 and S6, respectively:

$$E_{C,pH} = E_C + 0.059 \times (PZZP - pH) \quad (S5)$$

$$E_{V,pH} = E_V + 0.059 \times (PZZP - pH) \quad (S6)$$

Where PZZP represents the points of zero zeta potential for the **RPNI-O** and **RPNI-S** materials at pH 5.6. The estimated E_C and E_V values at a pH of 5.6 for **PPI, THPI, API, PPIS, THPIS,** and **APIS** were also included in Table S17.

1.12. Cell studies

1.12.1. Cell culture: HeLa (cervical cancer cells) and MCF 7 (breast cancer cells) were procured from the National Centre for Cell Sciences (NCCS) in Pune, India. These cells were cultured in Dulbecco's Modified Eagle Medium (DMEM), supplemented with 10% fetal bovine serum and 100 U/ml each of penicillin and streptomycin. The cell cultures were maintained in a controlled environment with 5% CO_2 at 37 ℃.

1.12.2. Dark & Light Cytotoxicity Evaluated by MTT assay: In the cell viability assay conducted on cancer cells (HeLa and MCF7 cell lines), the 3-(4,5-dimethylthiazol-2-yl)-2,5-diphenyltetrazolium bromide (MTT) method was employed. Initially, 5000 cells were seeded into individual wells of a 96-well plate and incubated in DMEM media inside a 5% CO_2 humidified incubator at 37 °C for 24 hours. Subsequently, the cells were treated with different concentrations of **RPNI-O** and **RPNI-S** compounds for 4 hours. After the 4-hour treatment, specific cell samples were exposed to white light using a handheld torch, 50 mW cm^{-2}, for 20 min. Following irradiation, the cells were further incubated with other treatment groups for 24 hours at 37 °C in the same 5% CO_2 humidified incubator. Upon completion of the incubation period, the MTT assay was performed. The MTT assay measures cell viability based on the reduction of MTT by mitochondrial enzymes in viable cells, producing a formazan product. This formazan product is detected spectrophotometrically at 570 nm, with a reference filter set at 655 nm. The resulting absorbance of the formazan product is directly proportional to the number of viable cells present in the samples.

1.12.3. Cellular Uptake: After an overnight incubation period, Hela cells were seeded into 96-well plates with a cell density of 1×10^4 cells per well. Twenty-four hours later, the Hela cells

were treated with varying concentrations of **RPNI-S** derivatives such as **PPIS**, **THPIS,** and **APIS**, respectively, at 20 μM, while HEK 293T cells were treated with 100 μM of the same compounds. Additionally, Hela cells were exposed to **RPNI-O** derivative at a concentration of 20 μM and 100 μM, and HEK 293T cells were treated with 100 μM of the corresponding compound. These treatments were performed at different intervals under normal oxygen conditions ranging from 0, 1, 2, 3, 4, 5, and 6 hours. Subsequently, the cells were washed three times with DPBS to remove any excess **RPNI-O** and **RPNI-S** compounds. Each well's optical density (OD) values were then measured using a multifunction microplate reader (BioTek, Synergy H1). (BioTek, Synergy H1, $\lambda_{abs.max}$ = 500 nm for **PPI**, **THPI,** and **API**, whereas $\lambda_{abs.max}$ = 590 nm for **PPIS**, $\lambda_{abs.max}$ = 580 nm for **THPIS,** and 636 nm for **APIS**).

1.12.4. Live/dead cell co-staining assay: In the study, HeLa cells were initially seeded in 35-mm glass-bottomed dishes at a density of 3 x 10^5 cells per dish and cultured overnight in standard culture media. Subsequently, the cells were treated with **RPNI-S** derivatives**,** such as **PPIS**, **THPIS**, and **APIS**, at a concentration of 50 µM for 4 hours. After the 4-hour treatment, the cells were subjected to white light irradiation using a handheld torch with a specific wavelength (50 mW cm^{-2}) for 20 min. The cells were co-stained with 2 μM Calcein AM and 4 μM propidium iodide (PI) for I h. After washing with DPBS (Dulbecco's Phosphate-Buffered Saline), fluorescence images of the cells were acquired using a fluorescence microscope. Additionally, another set of HeLa cells was treated with the same **RPNI-S** derivatives at a concentration of 50 µM for 4 hours. These cells were treated with 2',7'-dichlorodihydrofluorescein diacetate (DCFDA) at 10 μM for I h. After washing with DPBS, the cells were irradiated with the same handheld torch (50 mW cm^{-2}) for 20 min, and their fluorescence images were acquired. Moreover, HeLa cells were cultured in a normoxic environment (21% O_2) for 24 hours.

Table S1 Below is a comparison table of recently published heavy-atom-free materials, highlighting their design strategies, structure-property relationships, and photosensitizing behaviors for PDT efficacy.

References	**Present work**	*J. Am. Chem. Soc.* **2019**, *141*, 16243-16248

Materials		**THPIS**	**PPIS**	**API**	MANI-S
AIE		Non-fluorescent (a)	Non-fluorescent (a)	Red $AIEE_{gen}$ (a)	Non-fluorescent (b)
Stokes- shift (nm)		g	g	146	g
Φ_{PL}		g	g	0.85 (a)	g
Φ_{Δ}		0.29 (c)	0.11 (c)	g	1.00 (d)
Light used		$50mWcm^{-2}$ (e)	$50\ mWcm^{-2}$ (e)	$50\ mWcm^{-2}$ (e)	$100\ mW\ cm^{-2}$ (e)
ROS	**Types**	Type-I, Type-II ($^1O_2$, $O_2^{\cdot-}$)	Type-I ($O_2^{\cdot-}$)	Type-I ($O_2^{\cdot-}$)	Type-I, Type-II ($^1O_2$, $O_2^{\cdot-}$)
	Specificity	Specific	Specific	Specific	Not very specific
Total ROS	**DCFDA (μM)**	10	10	10	10
	T (min)	5	5	5	3

	I	$1x10^6$	$2.5x10^5$	$5x10^4$	$7.5x10^4$
ROS (mechanism)		DCFDA, ABDA, TA, ESR, Theoretical (ΔG, SOC), Band energy/NHE)	DCFDA, ABDA, TA, ESR, Theoretical (ΔG, SOC), Band energy/NHE)	DCFDA, ABDA, TA, ESR, Theoretical (ΔG, SOC), Band energy/NHE)	DCFDA, DPBF, DHE, Theoretical (SOC)
PDT (Cancer cell)	**In vitro**	Normoxia (Hela, MCF7, normal cell)	Normoxia (Hela, MCF7, normal cell)	g	Hypoxia (Hela cell)
	Selectivity	Selective	Selective	g	g
Liposome		x	x	g	Albumin
Design strategy		Structure-property relationship and application (H-aggregation unveiled PDT efficacy)			Application-based
		S-atom at the carbonyl and functional position			S-atom at the carbonyl position

a, b, c, and d, respectively, are the different solvent systems (a = 99% f_w, b = toluene, c = 99% PBS, and d = ethanol, respectively). In contrast, e is the white light used for the photosensitization [g = not observed, x = not used (normal cell non-toxic)].

Table S2 Comparison of the blue-shifted $\lambda_{abs.max}$ with the reported data has demonstrated enhanced H-aggregation, which is crucial for PDT efficacy by boosting the SOC value.

References		Materials	Blue-shifted $\lambda_{abs.max}$ (nm)	H-aggregation
Present work		**PPIS**	89	Highly pronounced
		THPIS	76	Highly pronounced
		APIS	23	Moderate
a	*Adv. Mater.* **2022**, *34*, 210814	PTTe	74	Pronounced
		PTSe	71	Pronounced
		PTS	30	Moderate
b	*Nature Materials* **2015**, *14*, 685-690	DPhCzT	14	Moderate
c	*Nanoscale* **2016**, *8*, 17422-17426	$(OB4)_4$	10	Moderate

a, b, and c are the references 41, 28, and 29 present in the main manuscript.

Table S3 CIE coordinates for the **RPNI-O** and **RPNI-S** derivatives in solution, aggregated, and solid state.

Materials	Solution		Aggregated		Solid	
	X	**Y**	**X**	**Y**	**X**	**Y**
PPI	0.562	0.437	0.638	**0.36**	0.689	**0.31**
THPI	0.635	0.364	0.644	**0.355**	0.725	0.274
API	0.504	0.493	0.617	0.382	0.684	**0.315**
PPIS	0.73	0.269	A	A	A	A
THPIS	0.724	0.275	A	A	A	A
APIS	0.734	0.265	A	A	A	A

A represents not observed due to non-emissive characteristics.

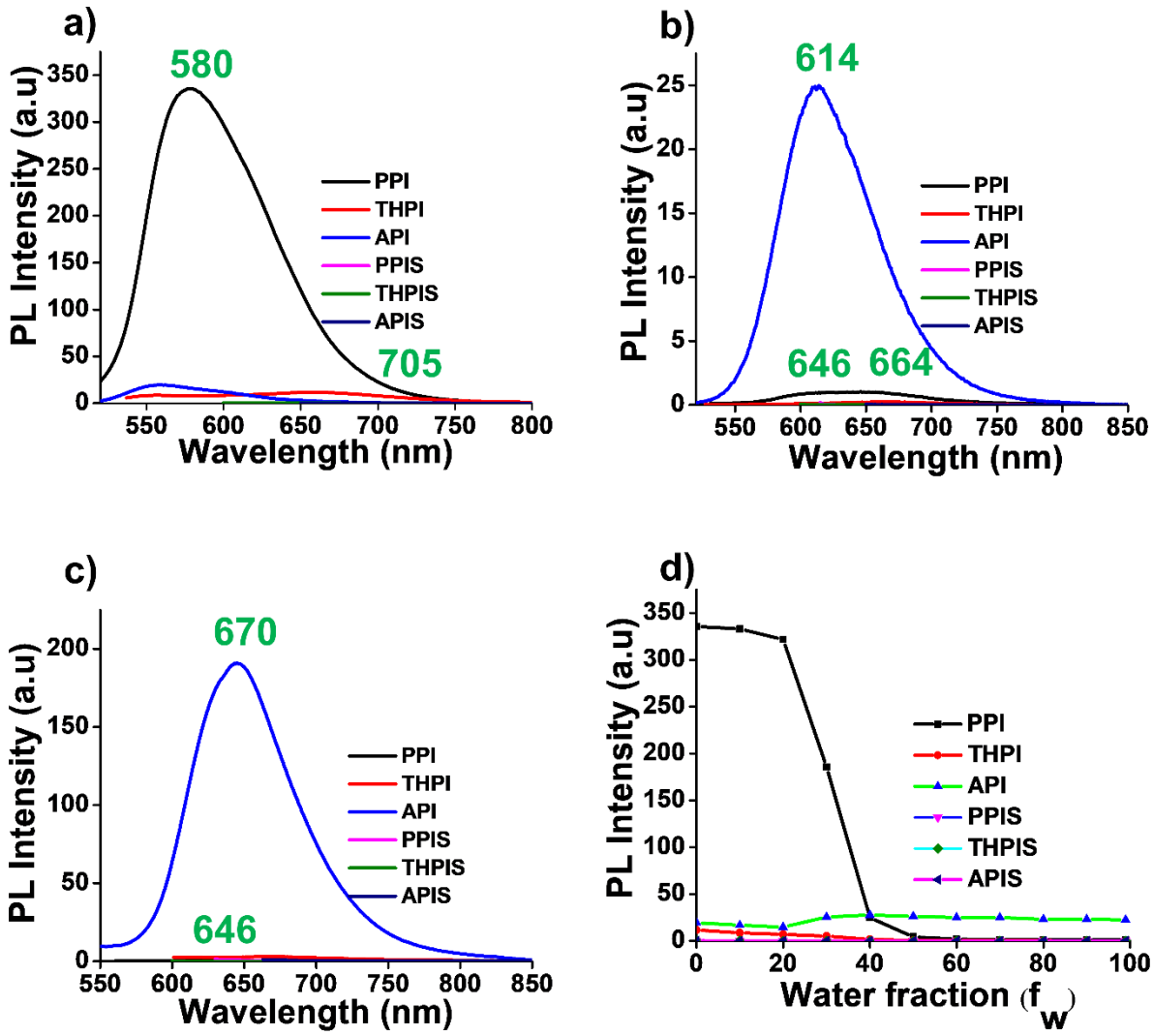

Fig. S1 Photophysical characteristics of all the **RPNI-O** (**PPI**, **THPI,** and **API**) and **RPNI-S** (**PPIS**, **THPIS,** and **APIS**) derivatives. (a) The PL spectra in their solution state represent monomeric emission (λ_{ex} = 500 nm). (b) PL spectra in their aggregated-state (at 99% f_w in DMSO) (λ_{ex} = 500 nm). (c) Solid state PL spectra (λ_{ex} = 500 nm). (d) Fluorescence intensity plot at various f_w in DMSO at their corresponding $\lambda_{em,max}$.

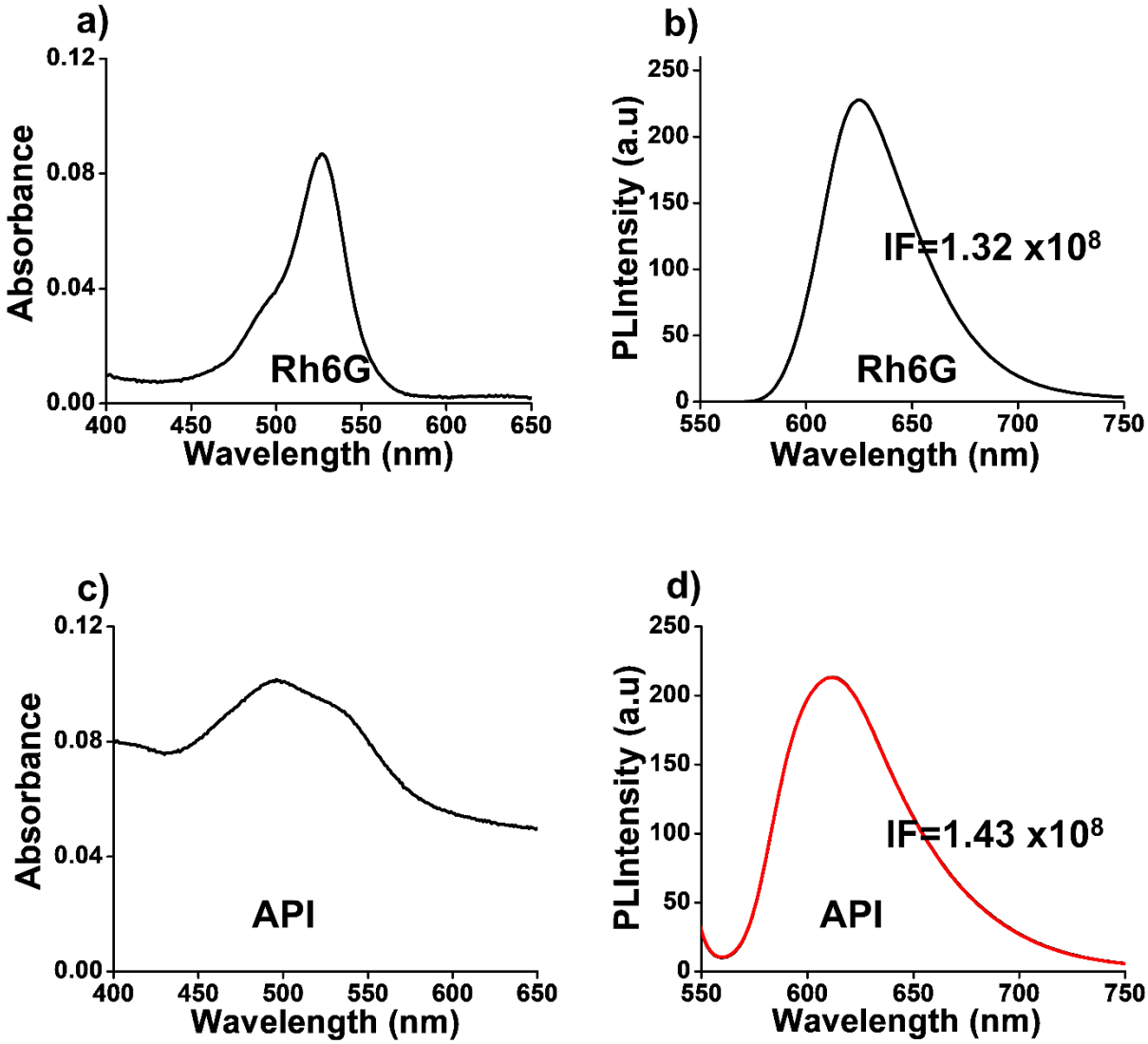

Fig. S2 (a and b) The absorbance and emission peak area of rhodamine 6G. (c and d) The absorbance and emission peak area of **API** at 40% f_w in DMSO. IF: integrated fluorescence intensity.

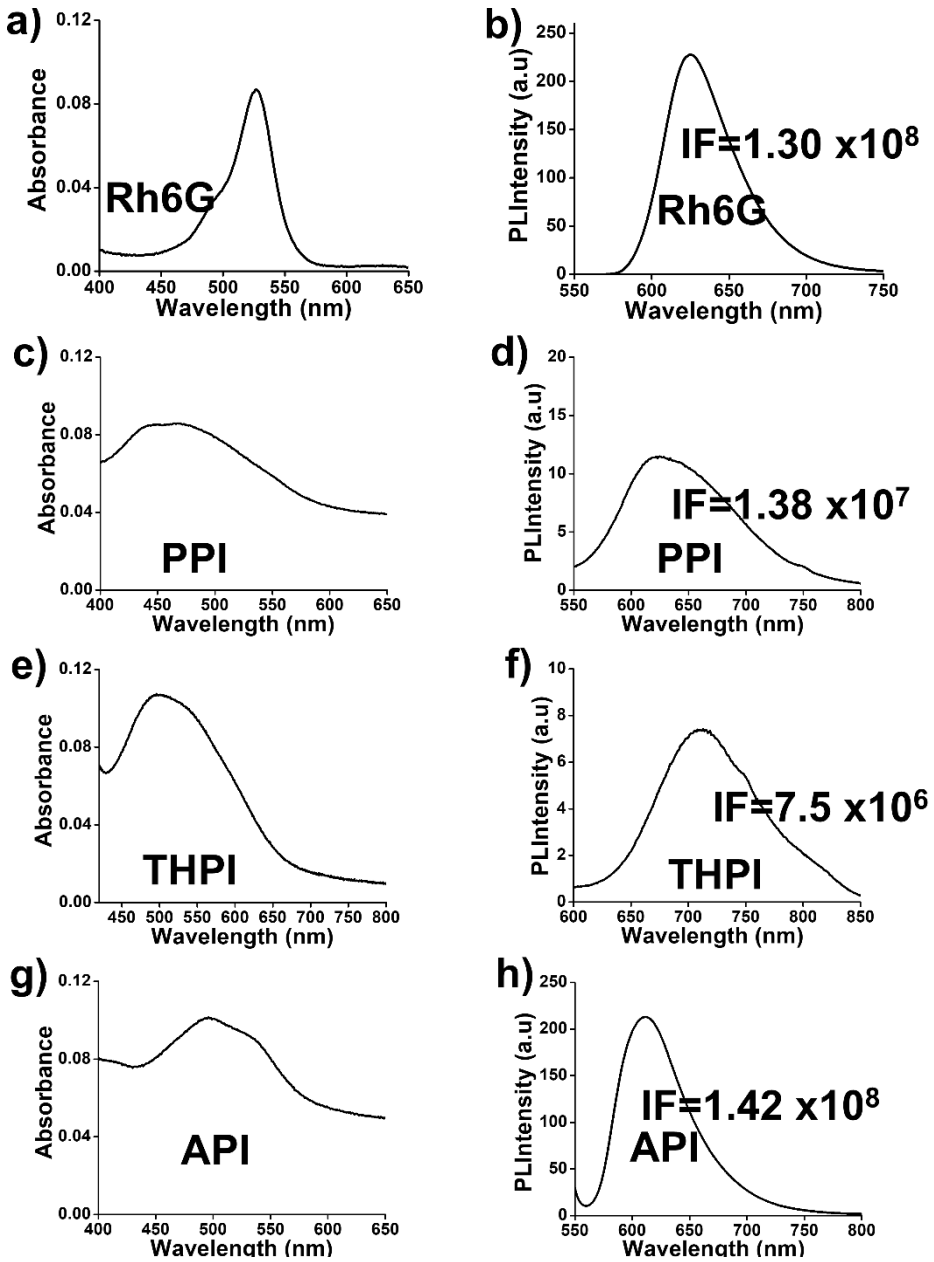

Fig. S3 (a and b) The absorbance and emission peak area of rhodamine 6G. (c, d), (e, f) and (g, h) The absorbance and emission peak area of **PPI, THPI,** and **API** at 99% f_w in DMSO. IF: integrated fluorescence intensity. Rh6G represent rhodamine 6G.

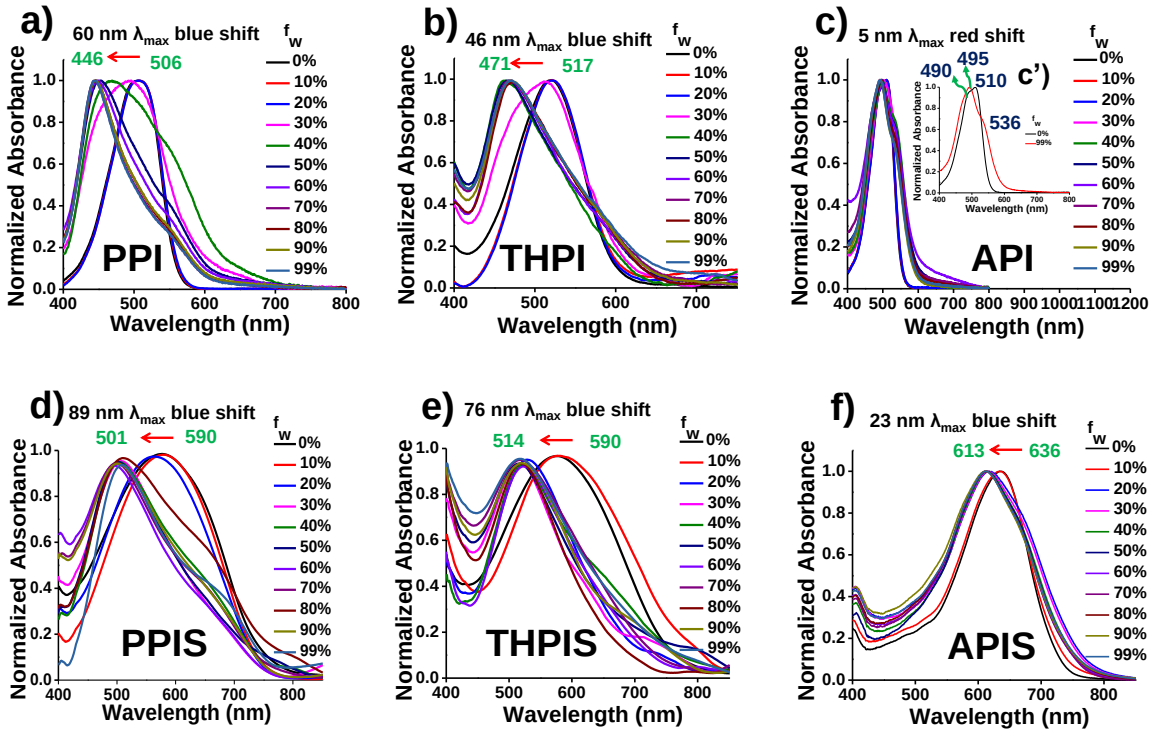

Fig. S4 Normalized UV-vis spectra (a-c) of **RPNI-O** derivatives (**PPI, THP**I, and **API),** and (d-f) **RPNI-S** derivatives (**PPIS, THPIS,** and **APIS)** at various water fractions (f_w) in DMSO. [**RPNI-O**] or [**RPNI-S**] = 100 µM. Inset **Fig. S4** (c') Altered normalized UV-vis spectra of 0 and 99 % f_w.

Table S4 UV-vis absorption data for the **RPNI-O** and **RPNI-S** derivatives.

Materials	**Water fraction (f_w)**	**$\lambda_{abs.max}$ (nm)**	**A**	**$\Delta\lambda$ (nm)**
PPI	0%	506	0.394105	60
	99%	446	0.159005	
THPI	0%	517	0.059899	46
	99%	471	0.021479	
API	0%	510	0.248319	10
	99%	500	0.151884	
PPIS	0%	590	0.053059	89
	99%	501	0.006136	

THPIS	0%	580	0.030367	76
	99%	514	0.012369	
APIS	0%	636	0.37716	23
	99%	613	0.220526	

A, Δλ, are the absorbance and wavelength maxima shifts in their absorption.

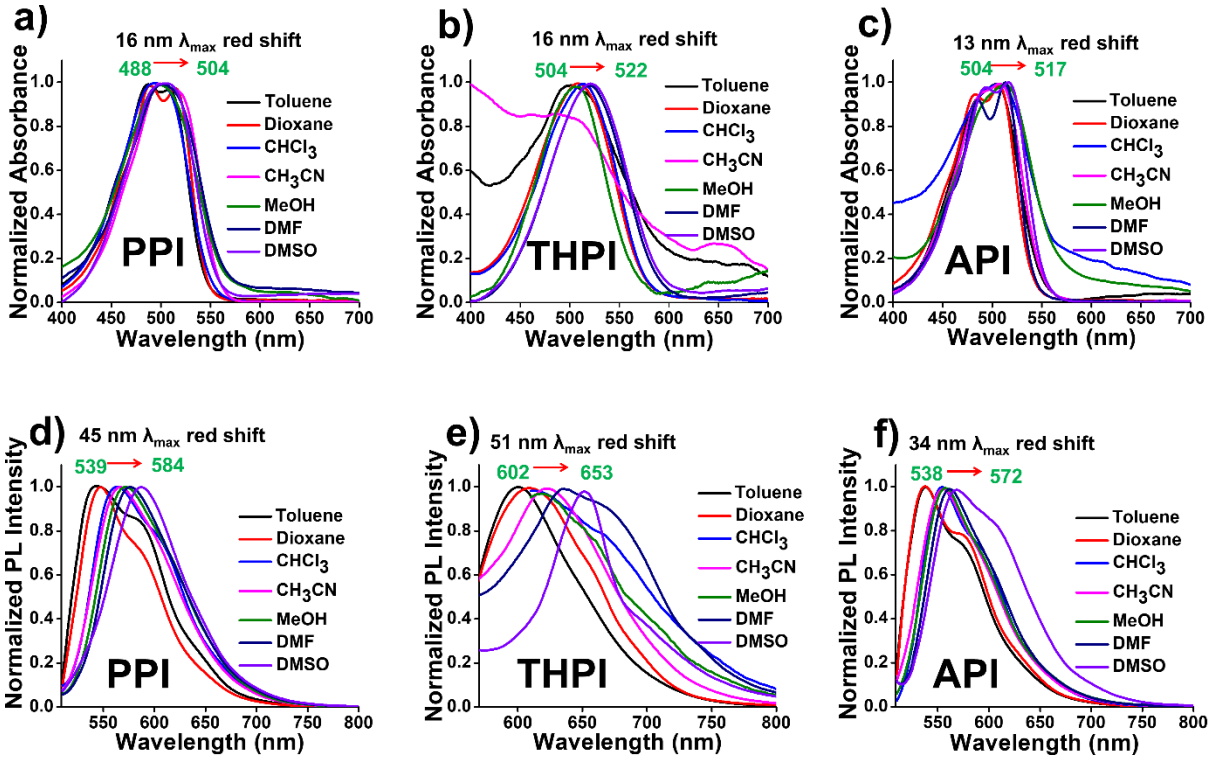

Fig. S5 Solvatochromic effect of the **RPNI-O** derivatives. (a-c) Normalized absorbance, (d-f) Normalized fluorescence spectra of **PPI**, **THPI**, and **API** in various solvents from nonpolar to polar (100 μM, λ_{ex} = 500 nm).

Table S5 The solvatochromic UV-vis data for the **RPNI-O** derivatives in various solvents from nonpolar to polar (100 μM, λ_{ex} = 500 nm).

Materials	**Solvents**	**$\lambda_{abs.max}$ (nm)**	**Δλ (nm)**
PPI	Toluene	488	16
	Dioxane	488	
	$CHCl_3$	494	

	CH_3CN	497	
	MeOH	498	
	DMF	502	
	DMSO	504	
THPI	Toluene	504	16
	Dioxane	508	
	$CHCl_3$	514	
	CH_3CN	514	
	MeOH	518	
	DMF	522	
	DMSO	522	
API	Toluene	504	13
	Dioxane	507	
	$CHCl_3$	507	
	CH_3CN	507	
	MeOH	512	
	DMF	513	
	DMSO	517	

Δλ is the wavelength maxima shift in their absorption

Table S6 The solvatochromic PL data for the **RPNI-O** derivatives in various solvents from nonpolar to polar (100 μM, λ_{ex} = 500 nm).

Materials	**Solvents**	**$\lambda_{em.max}$ (nm)**	**Δλ (nm)**
PPI	Toluene	539	45

	Dioxane	547	
	$CHCl_3$	562	
	CH_3CN	566	
	MeOH	573	
	DMF	578	
	DMSO	584	
THPI	Toluene	602	51
	Dioxane	609	
	$CHCl_3$	611	
	CH_3CN	622	
	MeOH	623	
	DMF	631	
	DMSO	653	
API	Toluene	538	34
	Dioxane	539	
	$CHCl_3$	554	
	CH_3CN	554	
	MeOH	559	
	DMF	559	
	DMSO	572	

$\Delta\lambda$, is the wavelength maxima shift in their absorption.

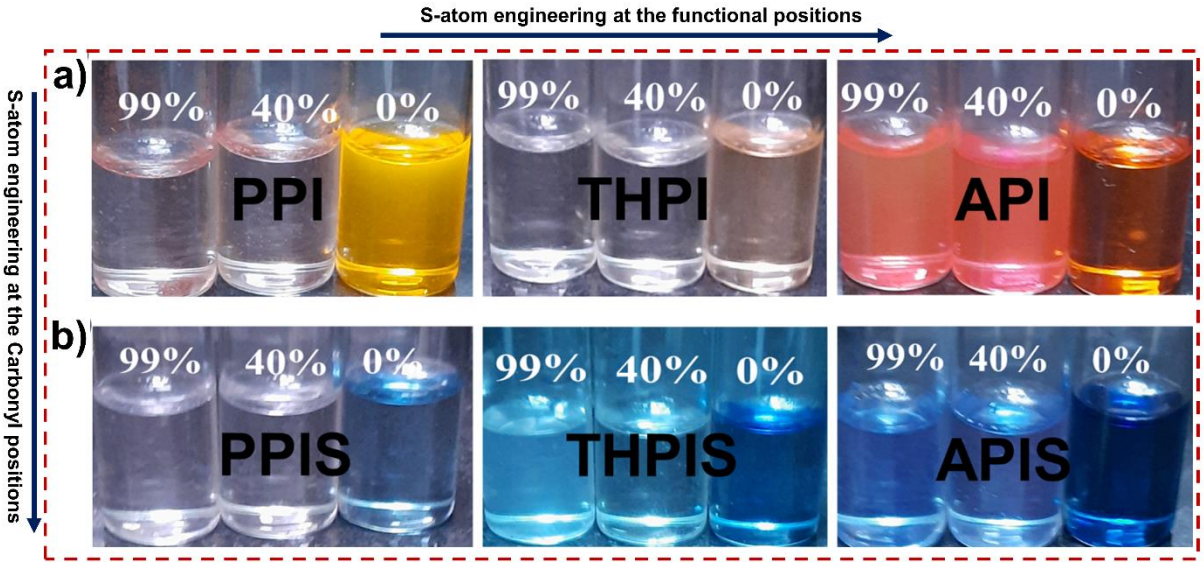

Fig. S6 Capturing daylight photographs of **RPNI-O** derivatives (**PPI, THP**I, and **API)** and **RPNI-S** derivatives (**PPIS, THPIS,** and **APIS),** respectively at 0%, 40%, and 99% f_w in DMSO.

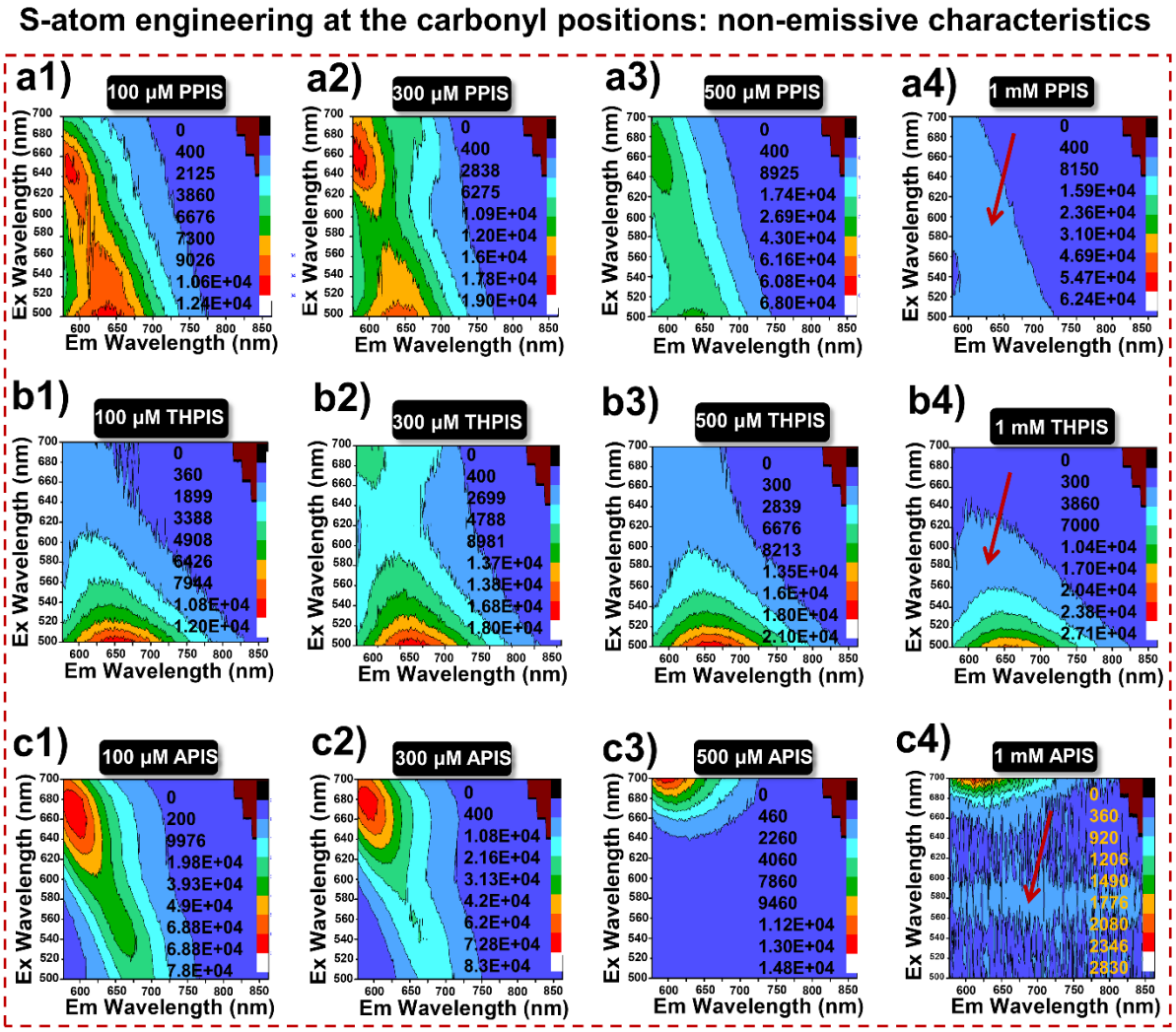

Fig. S7 (a1-c4) 2D Excitation-emission (EEM) contour projections of the **RPNI-S** derivatives at different concentrations (left: 100 μM; middle: 300 μM and 500 μM; right: 1 mM) in DMSO. [Inset: arrow represents the fluorescence intensity]**.**

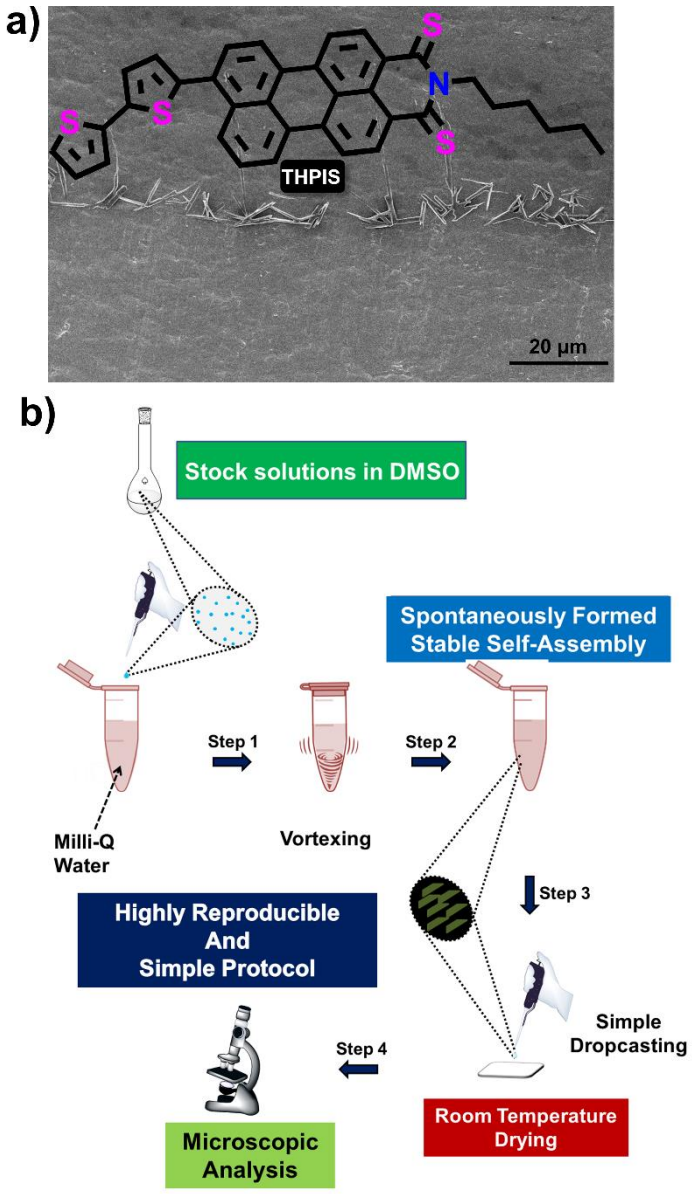

Fig. S8 (a) FESEM images of the micro-assembly of the **THPIS**, spontaneously formed at 99.9% f_w in DMSO (100 μM) by a simple drop-casting technique on aluminum foil coated on a glass slide, followed by drying at room temperature, as graphically represented in b. (b) Schematic illustration of the highly reproducible, simple, cost-effective, and feasible strategy for preparing micro- and nano-supramolecular self-assembly from **RPNI-O** and **RPNI-S** derivatives.

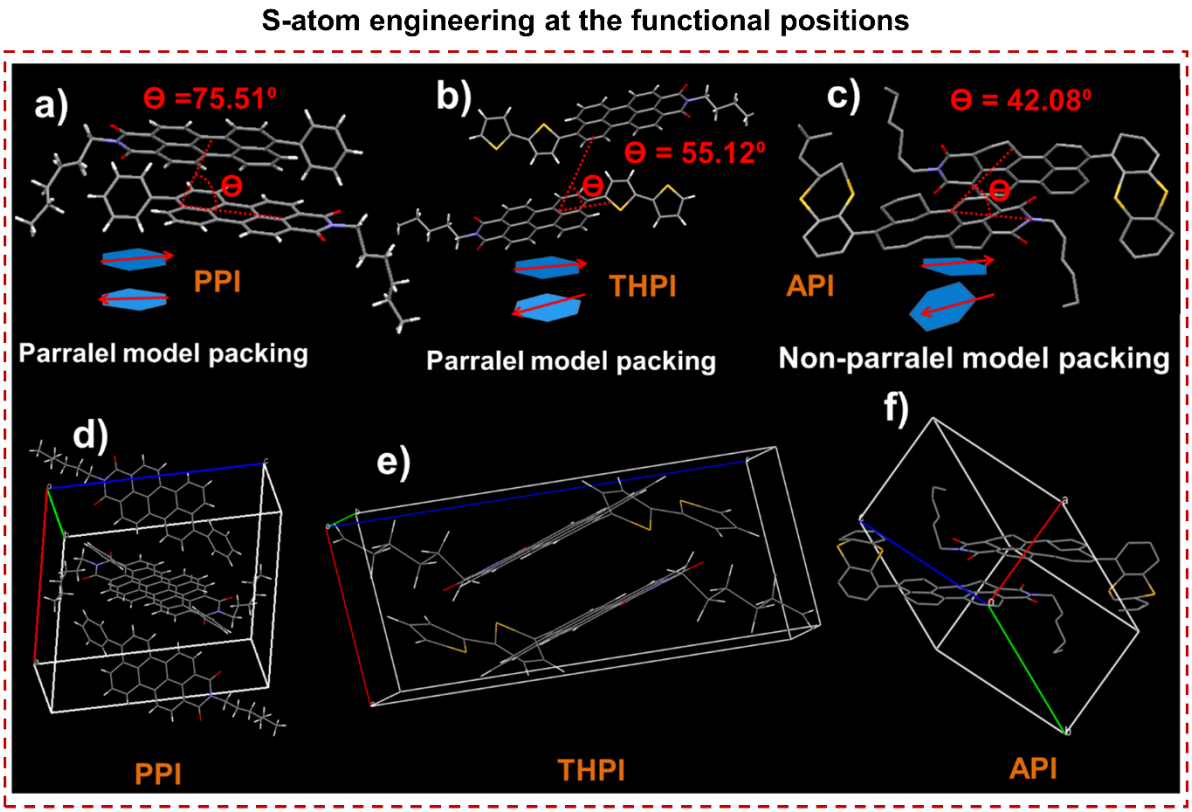

Fig. S9 Single crystal structures of (a) **PPI**, (b) **THPI**, and (c) **API**, respectively, show evidence of H- and J- aggregate formation in these molecules, corresponding to their schematic showing the π-π-stacking interaction among the **PNI-O** cores. The angle between the transition dipoles and the interconnected axis is indicated by θ. (d-f) single crystal unit cell of (d) **PPI**, (e) **THPI**, and (f) **API**, respectively.

Table S7 SCXRD data of the **RPNI-O** derivatives.

Name	**PPI**	**THPI**	**API**
Formula	$C_{34}H_{29}NO_2$	$C_{36}H_{27}NO_2S_2$	$C_{40}H_{29}NO_2S_2$
Formula weight	108.37	70.71	607.75
Wavelength (Å)	0.71073	0.71073	0.71073
Space Group	P -1	P -1	P -1
Crystal System	triclinic	triclinic	triclinic
Temperature	293 (K)	293 (K)	293 (K)
	a 17.6473(9)	a 7.3852(5)	a 8.766(6)

Cell Lengths (Å)	b 7.5383(4)	b 11.7473(8)	b 11.916(8)
	c 18.6063(9)	c 16.5975(11)	c 15.464(11)
Cell Angles (o)	α 89.999(2)	α 83.044(2)	α 101.43(2)
	β 94.196(2)	β 84.880(2)	β 92.94(2)
	γ 90.014(2)	γ 77.501(2)	γ 111.20(2)
Cell Volume (Å3)	2468.6(2)	1392.51(16)	1462.8(18)
Z	1	2	2
Density (g/cm3)	0.418	0.361	1.380
F(000)	78	98	636
hmax, kmax, lmax	2,8,2	8,1,3	9,13,16
CCDC	2325822	2325824	2325826

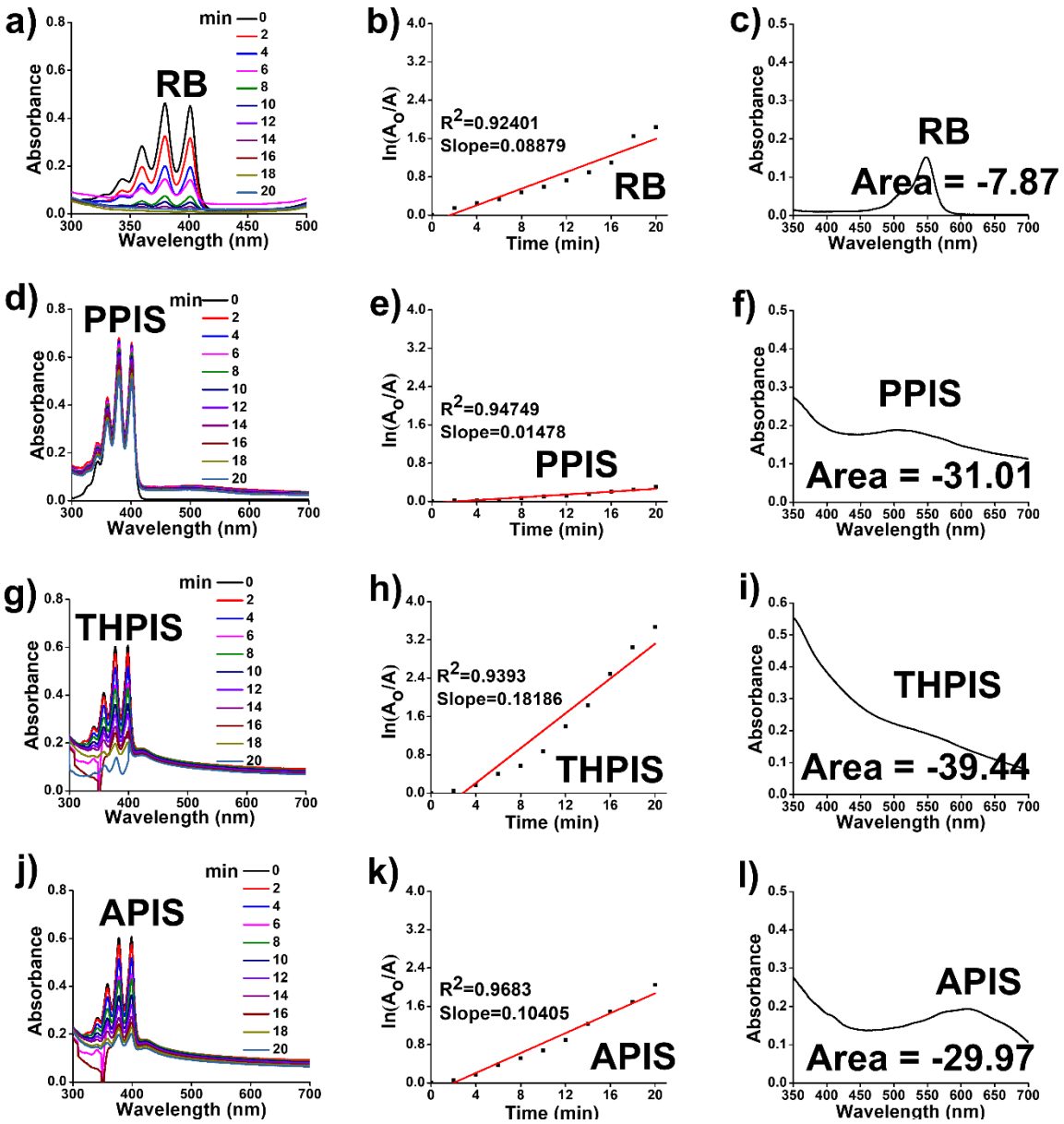

Fig. S10 The ROS quantum yield of **RPNI-S** was determined through chemical trapping measurements. ABDA is undergoing photodegradation with (a) Rose Bengal, (d) **PPIS**, (g) **THPIS,** and (j) **APIS**, respectively. Rate constants for the decomposition of ABDA in the presence of (b) Rose Bengal, (e) **PPIS**, (h) **THPIS,** and (k) **APIS**, respectively. The integrated area of the absorption peak for (c) Rose Bengal. (f) **PPIS**, (i) **THPIS,** and (l) **APIS**, respectively.

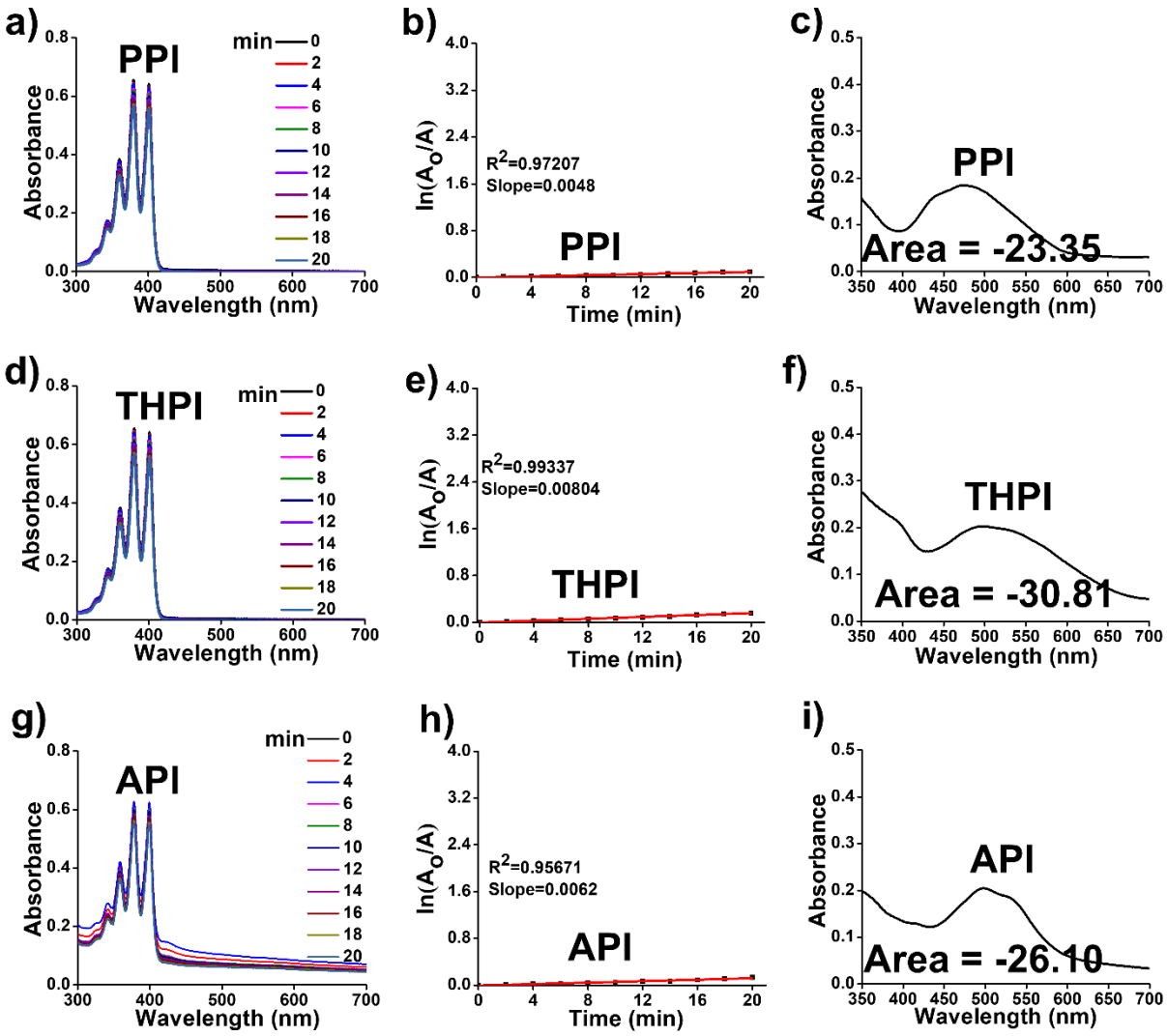

Fig. S11 The ROS quantum yield of **RPNI-O** was determined through chemical trapping measurements. ABDA is undergoing photodegradation with (a) **PPI**, (d) **THPI,** and (g) **API**, respectively. Rate constants for the decomposition of ABDA in the presence of (b) **PPI**, (e) **THPI,** and (h) **API**, respectively. The integrated area of the absorption peak for (c) **PPI**, (f) **THPI,** and (i) **API**, respectively.

Table S8 Spin-orbit coupling matrix elements (SOCMEs) of **PPIS** compound in optimized structure. $<S_m|H_{SO}|T_n>$, cm^{-1} and ΔE_{ST}, eV calculated using ORCA 5.0 at the B3LYP/6-31G (d, p) and B3LYP/DEF2SVP level.

Excite state electronic transition	**ΔE_{ST} (eV)**	**SOC (cm^{-1})**
$S_1 \leftrightarrow T_1$	0.402	8.33
$S_1 \leftrightarrow T_2$	0.205	3.00
$S_2 \leftrightarrow T_1$	0.794	6.53

$S_2 \leftrightarrow T_2$	0.597	4.16
$S_2 \leftrightarrow T_3$	0.251	7.24
$S_2 \leftrightarrow T_4$	0.096	10.80
$S_3 \leftrightarrow T_2$	0.99	7.88
$S_3 \leftrightarrow T_3$	0.637	5.46
$S_3 \leftrightarrow T_4$	0.482	4.25
$S_4 \leftrightarrow T_4$	0.99	6.00
$S_4 \leftrightarrow T_5$	0.637	1.34
$S_4 \leftrightarrow T_6$	0.482	0.75
$S_5 \leftrightarrow T_5$	0.681	3.01
$S_5 \leftrightarrow T_6$	0.36	3.69
$S_5 \leftrightarrow T_7$	0.16	2.63
$S_5 \leftrightarrow T_8$	0.092	1.25
$S_5 \leftrightarrow T_9$	0.046	5.01
$S_5 \leftrightarrow T_{10}$	0.02	6.57
$S_6 \leftrightarrow T_5$	0.72	5.09
$S_6 \leftrightarrow T_6$	0.3990	6.16
$S_6 \leftrightarrow T_7$	0.199	5.20
$S_6 \leftrightarrow T_8$	0.131	3.08
$S_6 \leftrightarrow T_9$	0.085	2.43
$S_6 \leftrightarrow T_{10}$	0.059	1.76
$S_7 \leftrightarrow T_5$	0.754	6.54

$S_7 \leftrightarrow T_6$	0.44	6.50
$S_7 \leftrightarrow T_7$	0.233	9.16
$S_7 \leftrightarrow T_8$	0.165	3.02
$S_7 \leftrightarrow T_9$	0.119	1.32
$S_7 \leftrightarrow T_{10}$	0.093	3.01
$S_8 \leftrightarrow T_5$	0.864	1.18
$S_8 \leftrightarrow T_6$	0.543	2.05
$S_8 \leftrightarrow T_7$	0.343	2.62
$S_8 \leftrightarrow T_8$	0.275	0.88
$S_8 \leftrightarrow T_9$	0.229	5.74
$S_8 \leftrightarrow T_{10}$	0.203	4.75
$S_9 \leftrightarrow T_5$	0.905	1.38
$S_9 \leftrightarrow T_6$	0.584	1.99
$S_9 \leftrightarrow T_7$	0.384	1.57
$S_9 \leftrightarrow T_8$	0.316	1.09
$S_9 \leftrightarrow T_9$	0.27	2.65
$S_9 \leftrightarrow T_{10}$	0.244	4.32
$S_{10} \leftrightarrow T_7$	0.46	2.79
$S_{10} \leftrightarrow T_8$	0.392	1.34
$S_{10} \leftrightarrow T_9$	0.346	4.79
$S_{10} \leftrightarrow T_{10}$	0.32	3.83

Table S9 SOCMEs of **THPIS** compound in optimized structure. $\langle S_m|H_{SO}|T_n\rangle$, cm^{-1} and $\Delta E_{ST,}$ eV calculated using ORCA 5.0 at the B3LYP/6-31G (d, p) and B3LYP/DEF2SVP level.

Excite state electronic transition	**ΔE_{ST} (eV)**	**SOC (cm^{-1})**
$S_1 \leftrightarrow T_1$	0.418	6.90
$S_1 \leftrightarrow T_2$	0.202	2.32
$S_2 \leftrightarrow T_1$	0.81	5.49
$S_2 \leftrightarrow T_2$	0.594	5.15
$S_2 \leftrightarrow T_3$	0.247	6.14
$S_2 \leftrightarrow T_4$	0.094	9.20
$S_3 \leftrightarrow T_2$	0.798	5.47
$S_3 \leftrightarrow T_3$	0.451	3.75
$S_3 \leftrightarrow T_4$	0.298	2.70
$S_3 \leftrightarrow T_5$	0.017	0.60
$S_3 \leftrightarrow T_3$	0.857	4.90
$S_4 \leftrightarrow T_4$	0.704	3.61
$S_4 \leftrightarrow T_5$	0.423	0.65
$S_4 \leftrightarrow T_6$	0.043	0.44
$S_5 \leftrightarrow T_4$	0.892	4.91
$S_5 \leftrightarrow T_5$	0.611	1.65
$S_5 \leftrightarrow T_6$	0.231	0.87
$S_5 \leftrightarrow T_7$	0.054	0.52
$S_6 \leftrightarrow T_5$	0.921	3.56

$S_6 \leftrightarrow T_6$	0.541	5.97
$S_6 \leftrightarrow T_7$	0.364	4.40
$S_6 \leftrightarrow T_8$	0.227	3.92
$S_6 \leftrightarrow T_9$	0.075	3.02
$S_6 \leftrightarrow T_{10}$	0.046	1.91
$S_7 \leftrightarrow T_5$	0.98	2.14
$S_7 \leftrightarrow T_6$	0.60	3.32
$S_7 \leftrightarrow T_7$	0.423	3.29
$S_7 \leftrightarrow T_8$	0.286	3.00
$S_7 \leftrightarrow T_9$	0.134	5.45
$S_7 \leftrightarrow T_{10}$	0.105	0.80
$S_8 \leftrightarrow T_6$	0.649	2.74
$S_8 \leftrightarrow T_7$	0.472	4.14
$S_8 \leftrightarrow T_8$	0.3350	4.50
$S_8 \leftrightarrow T_9$	0.183	0.57
$S_8 \leftrightarrow T_{10}$	0.154	0.75
$S_9 \leftrightarrow T_6$	0.724	2.13
$S_9 \leftrightarrow T_7$	0.547	1.57
$S_9 \leftrightarrow T_8$	0.41	2.00
$S_9 \leftrightarrow T_9$	0.258	4.21
$S_9 \leftrightarrow T_{10}$	0.229	1.41
$S_{10} \leftrightarrow T_6$	0.826	1.14

$S_{10}\leftrightarrow T_7$	0.649	0.80
$S_{10}\leftrightarrow T_8$	0.512	0.88
$S_{10}\leftrightarrow T_9$	0.36	2.33
$S_{10}\leftrightarrow T_{10}$	0.331	0.44

Table S10 SOCMEs of **APIS** compound in optimized structure. $\langle S_m|H_{SO}|T_n\rangle$, cm^{-1} and $\Delta E_{ST,}$ eV calculated using ORCA 5.0 at the B3LYP/6-31G (d, p) and B3LYP/DEF2SVP level.

Excite state electronic transition	**ΔE_{ST} (eV)**	**SOC (cm^{-1})**
$S_1\leftrightarrow T_1$	0.386	4.44
$S_1\leftrightarrow T_2$	0.207	1.62
$S_2\leftrightarrow T_1$	0.778	6.37
$S_2\leftrightarrow T_2$	0.599	4.47
$S_2\leftrightarrow T_3$	0.253	3.83
$S_2\leftrightarrow T_4$	0.098	5.73
$S_3\leftrightarrow T_2$	0.907	2.36
$S_3\leftrightarrow T_3$	0.561	2.58
$S_3\leftrightarrow T_4$	0.406	2.16
$S_4\leftrightarrow T_3$	0.682	5.63
$S_4\leftrightarrow T_4$	0.527	4.34
$S_4\leftrightarrow T_5$	0.121	2.16
$S_5\leftrightarrow T_4$	0.916	3.63
$S_5\leftrightarrow T_5$	0.51	1.34
$S_5\leftrightarrow T_6$	0.311	1.46

$S_5 \leftrightarrow T_7$	0.034	0.42
$S_6 \leftrightarrow T_4$	0.958	1.61
$S_6 \leftrightarrow T_5$	0.552	2.18
$S_6 \leftrightarrow T_6$	0.353	1.00
$S_6 \leftrightarrow T_7$	0.076	0.52
$S_7 \leftrightarrow T_5$	0.897	1.47
$S_7 \leftrightarrow T_6$	0.698	3.49
$S_7 \leftrightarrow T_7$	0.421	2.96
$S_7 \leftrightarrow T_8$	0.325	2.54
$S_7 \leftrightarrow T_9$	0.161	1.60
$S_7 \leftrightarrow T_7$	0.128	0.20
$S_8 \leftrightarrow T_5$	0.911	1.11
$S_8 \leftrightarrow T_6$	0.712	4.25
$S_8 \leftrightarrow T_7$	0.435	3.15
$S_8 \leftrightarrow T_8$	0.339	2.94
$S_8 \leftrightarrow T_9$	0.175	1.71
$S_8 \leftrightarrow T_{10}$	0.142	3.28
$S_9 \leftrightarrow T_5$	0.956	1.89
$S_9 \leftrightarrow T_6$	0.757	2.57
$S_9 \leftrightarrow T_7$	0.48	1.85
$S_9 \leftrightarrow T_8$	0.384	1.88
$S_9 \leftrightarrow T_9$	0.22	1.36

$S_9 \leftrightarrow T_{10}$	0.187	3.04
$S_{10} \leftrightarrow T_6$	0.853	1.16
$S_{10} \leftrightarrow T_7$	0.576	0.77
$S_{10} \leftrightarrow T_8$	0.48	0.97
$S_{10} \leftrightarrow T_9$	0.316	0.69
$S_{10} \leftrightarrow T_{10}$	0.283	2.04

Table S11 SOCMEs of **PPI** compound in optimized structure. $\langle S_m|H_{SO}|T_n\rangle$, cm^{-1} and $\Delta E_{ST,}$ eV calculated using ORCA 5.0 at the B3LYP/6-31G (d, p) and B3LYP/DEF2SVP level.

Excite state electronic transition	**ΔE_{ST} (eV)**	**SOC (cm^{-1})**
$S_1 \leftrightarrow T_1$	1.196	0.3
$S_1 \leftrightarrow T_2$	-0.17	0.77
$S_2 \leftrightarrow T_1$	1.678	3.70
$S_2 \leftrightarrow T_2$	0.305	2.14
$S_2 \leftrightarrow T_3$	0.207	2.39
$S_2 \leftrightarrow T_4$	0.19	3.53
$S_2 \leftrightarrow T_5$	0.048	3.72
$S_3 \leftrightarrow T_2$	0.609	0.39
$S_3 \leftrightarrow T_3$	0.511	1.93
$S_3 \leftrightarrow T_4$	0.352	0.95
$S_3 \leftrightarrow T_5$	0.21	1.56
$S_4 \leftrightarrow T_3$	0.576	3.81

$S_4 \leftrightarrow T_4$	0.559	1.51
$S_4 \leftrightarrow T_5$	0.417	3.22
$S_4 \leftrightarrow T_6$	0.275	2.14
$S_4 \leftrightarrow T_7$	0.143	1.89
$S_4 \leftrightarrow T_8$	0.174	3.69
$S_4 \leftrightarrow T_9$	0.083	3.13
$S_4 \leftrightarrow T_{10}$	0.024	0.78
$S_5 \leftrightarrow T_4$	0.594	2.45
$S_5 \leftrightarrow T_5$	0.452	3.54
$S_5 \leftrightarrow T_6$	0.31	3.00
$S_5 \leftrightarrow T_7$	0.209	0.88
$S_5 \leftrightarrow T_8$	0.178	2.49
$S_5 \leftrightarrow T_9$	0.118	2.77
$S_5 \leftrightarrow T_{10}$	0.059	0.95
$S_6 \leftrightarrow T_5$	0.53	3.17
$S_6 \leftrightarrow T_6$	0.388	3.12
$S_6 \leftrightarrow T_7$	0.287	1.67
$S_6 \leftrightarrow T_8$	0.256	1.23
$S_6 \leftrightarrow T_9$	0.196	1.74
$S_6 \leftrightarrow T_{10}$	0.137	0.79
$S_7 \leftrightarrow T_5$	0.585	2.62
$S_7 \leftrightarrow T_6$	0.443	2.64

$S_7 \leftrightarrow T_7$	0.342	1.49
$S_7 \leftrightarrow T_8$	0.311	1.54
$S_7 \leftrightarrow T_9$	0.251	1.32
$S_7 \leftrightarrow T_{10}$	0.192	0.59
$S_8 \leftrightarrow T_6$	0.522	2.35
$S_8 \leftrightarrow T_7$	0.421	1.92
$S_8 \leftrightarrow T_8$	0.39	2.75
$S_8 \leftrightarrow T_9$	0.33	1.58
$S_8 \leftrightarrow T_{10}$	0.271	0.35
$S_9 \leftrightarrow T_6$	0.614	2.07
$S_9 \leftrightarrow T_7$	0.513	3.03
$S_9 \leftrightarrow T_8$	0.482	2.49
$S_9 \leftrightarrow T_9$	0.422	1.32
$S_9 \leftrightarrow T_{10}$	0.363	0.26
$S_{10} \leftrightarrow T_6$	0.642	2.67
$S_{10} \leftrightarrow T_7$	0.541	2.15
$S_{10} \leftrightarrow T_8$	0.51	3.07
$S_{10} \leftrightarrow T_9$	0.45	1.58
$S_{10} \leftrightarrow T_{10}$	0.391	0.35

Table S12 SOCMEs of **THPI** compound in optimized structure. $\langle S_m|H_{SO}|T_n\rangle$, cm^{-1} and $\Delta E_{ST,}$ eV calculated using ORCA 5.0 at the B3LYP/6-31G (d, p) and B3LYP/DEF2SVP level.

Excite state electronic transition	**ΔE_{ST} (eV)**	**SOC (cm^{-1})**

$S_1 \leftrightarrow T_1$	0.981	0.65
$S_1 \leftrightarrow T_2$	0.036	0.85
$S_2 \leftrightarrow T_1$	1.442	0.91
$S_2 \leftrightarrow T_2$	0.497	0.74
$S_3 \leftrightarrow T_2$	0.761	2.33
$S_3 \leftrightarrow T_3$	0.257	1.33
$S_3 \leftrightarrow T_4$	0.203	1.07
$S_3 \leftrightarrow T_5$	0.176	0.3
$S_3 \leftrightarrow T_6$	0.153	1.85
$S_3 \leftrightarrow T_7$	0.04	3.37
$S_4 \leftrightarrow T_3$	0.554	0.32
$S_4 \leftrightarrow T_4$	0.50	1.47
$S_4 \leftrightarrow T_5$	0.473	0.92
$S_4 \leftrightarrow T_6$	0.45	0.47
$S_4 \leftrightarrow T_7$	0.337	1
$S_4 \leftrightarrow T_8$	0.184	0.4
$S_4 \leftrightarrow T_9$	0.091	0.97
$S_4 \leftrightarrow T_{10}$	0.05	1.66
$S_5 \leftrightarrow T_4$	0.568	2.26
$S_5 \leftrightarrow T_5$	0.541	1.55
$S_5 \leftrightarrow T_6$	0.518	1.07
$S_5 \leftrightarrow T_7$	0.405	1.36

$S_5 \leftrightarrow T_8$	0.252	0.51
$S_5 \leftrightarrow T_9$	0.159	1.63
$S_5 \leftrightarrow T_{10}$	0.118	2.25
$S_6 \leftrightarrow T_5$	0.56	2.67
$S_6 \leftrightarrow T_6$	0.537	2.01
$S_6 \leftrightarrow T_7$	0.424	3.44
$S_6 \leftrightarrow T_8$	0.271	2.55
$S_6 \leftrightarrow T_9$	0.178	1.81
$S_6 \leftrightarrow T_{10}$	0.137	3.50
$S_7 \leftrightarrow T_5$	0.683	1.90
$S_7 \leftrightarrow T_6$	0.66	1.58
$S_7 \leftrightarrow T_7$	0.547	2.98
$S_7 \leftrightarrow T_8$	0.394	3.06
$S_7 \leftrightarrow T_9$	0.301	1.54
$S_7 \leftrightarrow T_{10}$	0.26	0.51
$S_8 \leftrightarrow T_6$	0.687	0.37
$S_8 \leftrightarrow T_7$	0.574	0.24
$S_8 \leftrightarrow T_8$	0.421	0
$S_8 \leftrightarrow T_9$	0.328	0.32
$S_8 \leftrightarrow T_{10}$	0.287	0.2
$S_9 \leftrightarrow T_6$	0.728	1.59
$S_9 \leftrightarrow T_7$	0.651	1.68

$S_9 \leftrightarrow T_8$	0.462	1.55
$S_9 \leftrightarrow T_9$	0.369	1.82
$S_9 \leftrightarrow T_{10}$	0.328	1.73
$S_{10} \leftrightarrow T_6$	0.783	0.87
$S_{10} \leftrightarrow T_7$	0.67	1.08
$S_{10} \leftrightarrow T_8$	0.517	1.84
$S_{10} \leftrightarrow T_9$	0.424	1.65
$S_{10} \leftrightarrow T_{10}$	0.383	2.07

Table S13 SOCMEs of **API** compound in optimized structure. $\langle S_m|H_{SO}|T_n\rangle$, cm^{-1} and $\Delta E_{ST,}$ eV calculated using ORCA 5.0 at the B3LYP/6-31G (d, p) and B3LYP/DEF2SVP level.

Excite state electronic transition	**ΔE_{ST} (eV)**	**SOC (cm^{-1})**
$S_1 \leftrightarrow T_1$	1.015	1.920
$S_1 \leftrightarrow T_2$	0.003	0.57
$S_2 \leftrightarrow T_1$	1.238	0.87
$S_2 \leftrightarrow T_2$	0.226	2.36
$S_3 \leftrightarrow T_2$	0.551	2.18
$S_3 \leftrightarrow T_3$	0.141	0.69
$S_3 \leftrightarrow T_4$	0.116	0.223
$S_3 \leftrightarrow T_5$	0.096	0.47
$S_4 \leftrightarrow T_3$	0.234	2.04
$S_4 \leftrightarrow T_4$	0.209	1.87
$S_4 \leftrightarrow T_5$	0.189	2.43

$S_4 \leftrightarrow T_6$	0.087	3.13
$S_4 \leftrightarrow T_7$	0.041	2.97
$S_5 \leftrightarrow T_4$	0.571	1.95
$S_5 \leftrightarrow T_5$	0.551	0.28
$S_5 \leftrightarrow T_6$	0.449	0.48
$S_5 \leftrightarrow T_7$	0.403	0.77
$S_5 \leftrightarrow T_8$	0.265	0.39
$S_5 \leftrightarrow T_9$	0.167	0.96
$S_5 \leftrightarrow T_{10}$	0.122	1.43
$S_6 \leftrightarrow T_5$	0.571	2.87
$S_6 \leftrightarrow T_6$	0.469	1.84
$S_6 \leftrightarrow T_7$	0.423	1.76
$S_6 \leftrightarrow T_8$	0.285	1.67
$S_6 \leftrightarrow T_9$	0.187	0.97
$S_6 \leftrightarrow T_{10}$	0.142	2.23
$S_7 \leftrightarrow T_5$	0.694	2.93
$S_7 \leftrightarrow T_6$	0.592	1.42
$S_7 \leftrightarrow T_7$	0.546	1.61
$S_7 \leftrightarrow T_8$	0.408	1.89
$S_7 \leftrightarrow T_9$	0.31	1.23
$S_7 \leftrightarrow T_{10}$	0.265	0.74
$S_8 \leftrightarrow T_6$	0.619	0.93

$S_8 \leftrightarrow T_7$	0.573	0.85
$S_8 \leftrightarrow T_8$	0.435	1.22
$S_8 \leftrightarrow T_9$	0.337	0.84
$S_8 \leftrightarrow T_{10}$	0.292	0.81
$S_9 \leftrightarrow T_6$	0.692	0.56
$S_9 \leftrightarrow T_7$	0.646	0.75
$S_9 \leftrightarrow T_8$	0.508	1.36
$S_9 \leftrightarrow T_9$	0.41	1.47
$S_9 \leftrightarrow T_{10}$	0.365	1.72
$S_{10} \leftrightarrow T_6$	0.735	0.49
$S_{10} \leftrightarrow T_7$	0.689	0.56
$S_{10} \leftrightarrow T_8$	0.551	1.09
$S_{10} \leftrightarrow T_9$	0.453	1.13
$S_{10} \leftrightarrow T_{10}$	0.408	1.45

Table S14a Comparision of the SOCMEs with the most probable lowest excited singlet and triplet state transitions is conducted using the optimized isolated structures of previously reported PSs and conventional organic materials.

References		Materials	SOC (cm^{-1})
Present Work		**PPIS**	**10.88**
		THPIS	9.20
		APIS	5.73
a	*Adv. Mater.* **2022**, *34*, 2108146.	PTTe	0.28
9	*Angew. Chem. Int. Ed.* **2018**, *57*, 7997-8001.	o-MCBA	0.624

10	*ACS Nano* **2019**, *13*, 11283-11293.	TPAPyPF6	0.648015
b	*ACS Nano* **2020**, *14*, 16840-16853.	TPE-PTB	4.53
11	*ACS Nano* **2021**, *15*, 7328-7339.	MeTIN	1.242
12	*Chem. Sci.* **2020**, *11*, 10921-10927.	PTP	0.04
c	*J. Mater. Chem. B.* **2022**, *10*, 6228-6236.	gem-OMe-TPE-1CUM	0.340
d	*Nanoscale* **2016**, *8*, 17422-17426	$(OB4)_1$	0.42
13	*Phys. Chem. Chem. Phys.* **2023**, *25*, 24386-24394.	BODIPY heterodimers	0.74
14	*J. Phys. Chem. A 2007, 111, 10490-10499.*	monoaza[5]helicenes	0.1-3.0
15	*J. Phys. Chem. C.* **2023**, *127*, 2694-2704.	BT2O3Cz	0.462
e	*Biomaterials* **2021**, *275*, 120934.	TPAIN	0.7250

a, b, c, d, and e correspond to references 41, 40, 50, 29, and 49, respectively, present in the main manuscript.

Table S14b Calculated different excite state singlet (S) and triplet (T) state energy of the **RPNI-O** and **RPNI-S** derivatives via ORCA 5.0 at the B3LYP/6-31G (d, p) and B3LYP/DEF2SVP level.

Materials	**S (eV)**										**T (eV)**									
	S_1	**S_2**	**S_3**	**S_4**	**S_5**	**S_6**	**S_7**	**S_8**	**S_9**	**S_{10}**	**T_1**	**T_2**	**T_3**	**T_4**	**T_5**	**T_6**	**T_7**	**T_8**	**T_9**	**T_{10}**
PPIS	1.61	2.004	2.390	2.811	3.147	3.186	3.220	3.330	3.371	3.447	1.210	1.407	1.753	1.908	2.466	2.787	2.987	3.055	3.101	3.127
THPIS	1.595	1.987	2.191	2.597	2.785	3.095	3.154	3.203	3.278	3.380	1.177	1.393	1.740	1.893	2.174	2.554	2.731	2.868	3.020	3.049
APIS	1.613	2.005	2.313	2.434	2.823	2.865	3.210	3.224	3.269	3.365	1.227	1.406	1.752	1.907	2.313	2.512	2.789	2.885	3.049	3.082
PPI	2.677	3.152	3.456	3.521	3.556	3.634	3.689	3.768	3.860	3.888	1.474	2.847	2.945	2.962	3.104	3.246	3.347	3.378	3.438	3.497
THPI	2.403	2.864	3.128	3.425	3.493	3.512	3.635	3.662	3.703	3.758	1.422	2.367	2.871	2.925	2.952	2.975	3.088	3.241	3.334	3.375
API	2.513	2.736	3.061	3.154	3.516	3.536	3.659	3.686	3.759	3.802	1.498	2.510	2.920	2.945	2.965	3.067	3.113	3.251	3.349	3.394

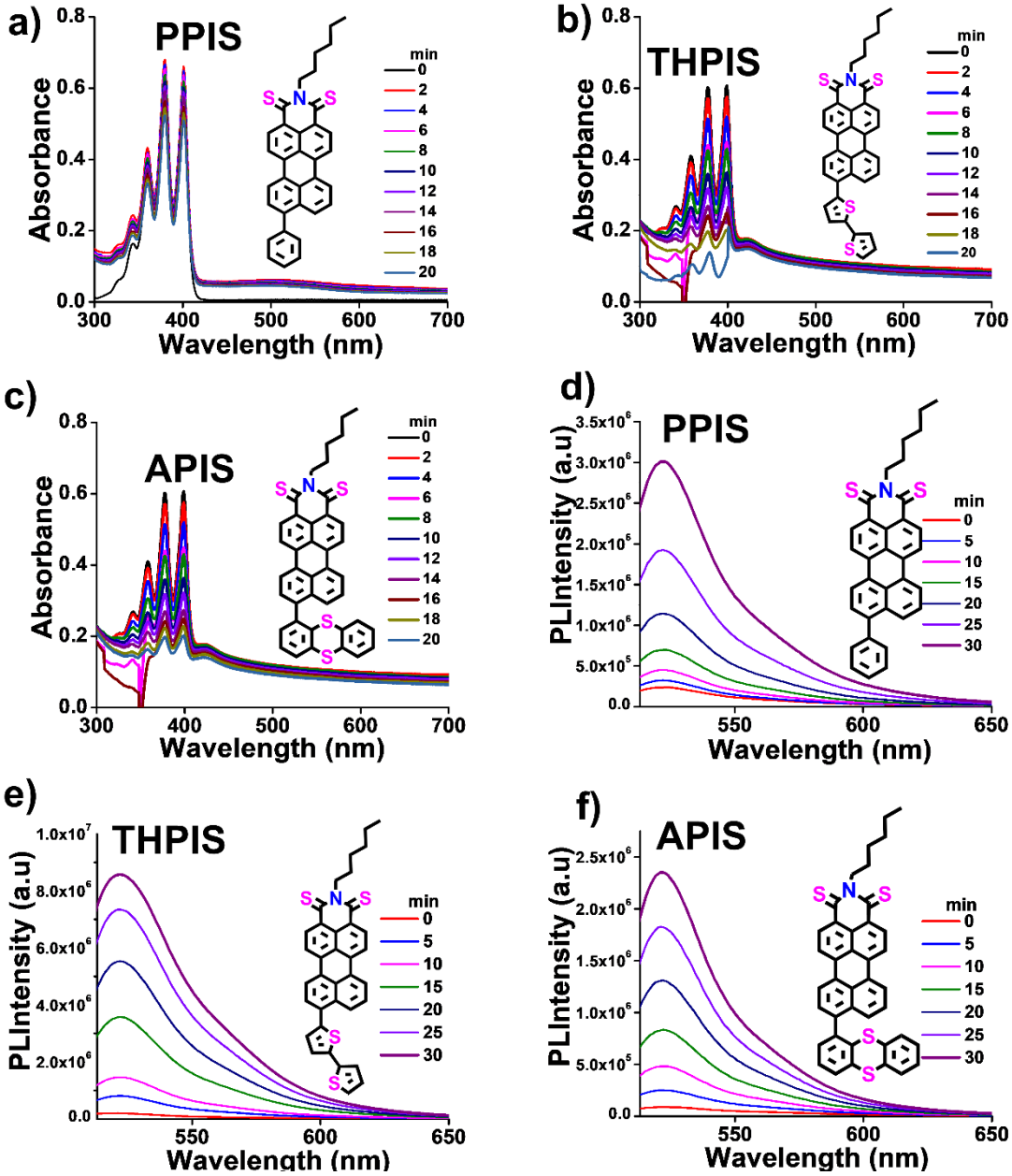

Fig. S12 ROS generation by the **RPNI-S** derivatives. (a-c) Plots of ABDA (100 μM) degradation rates at $\lambda_{abs.max}$ of 378 nm by the various PSs (100 μM) (a) **PPIS**, (b) **THPIS,** and (c) **APIS**, respectively and (d-f) Evaluation of the general ROS generation using DCFDA (10 μM) indicator by PSs (100 µM) (d) **PPIS**, (e) **THPIS** and (f) **APIS**, respectively upon white light excitation for different time periods at 99% PBS fraction in DMSO (λ_{ex}=500 nm). Inset: Chemical structure of the **RPNI-S** derivatives.

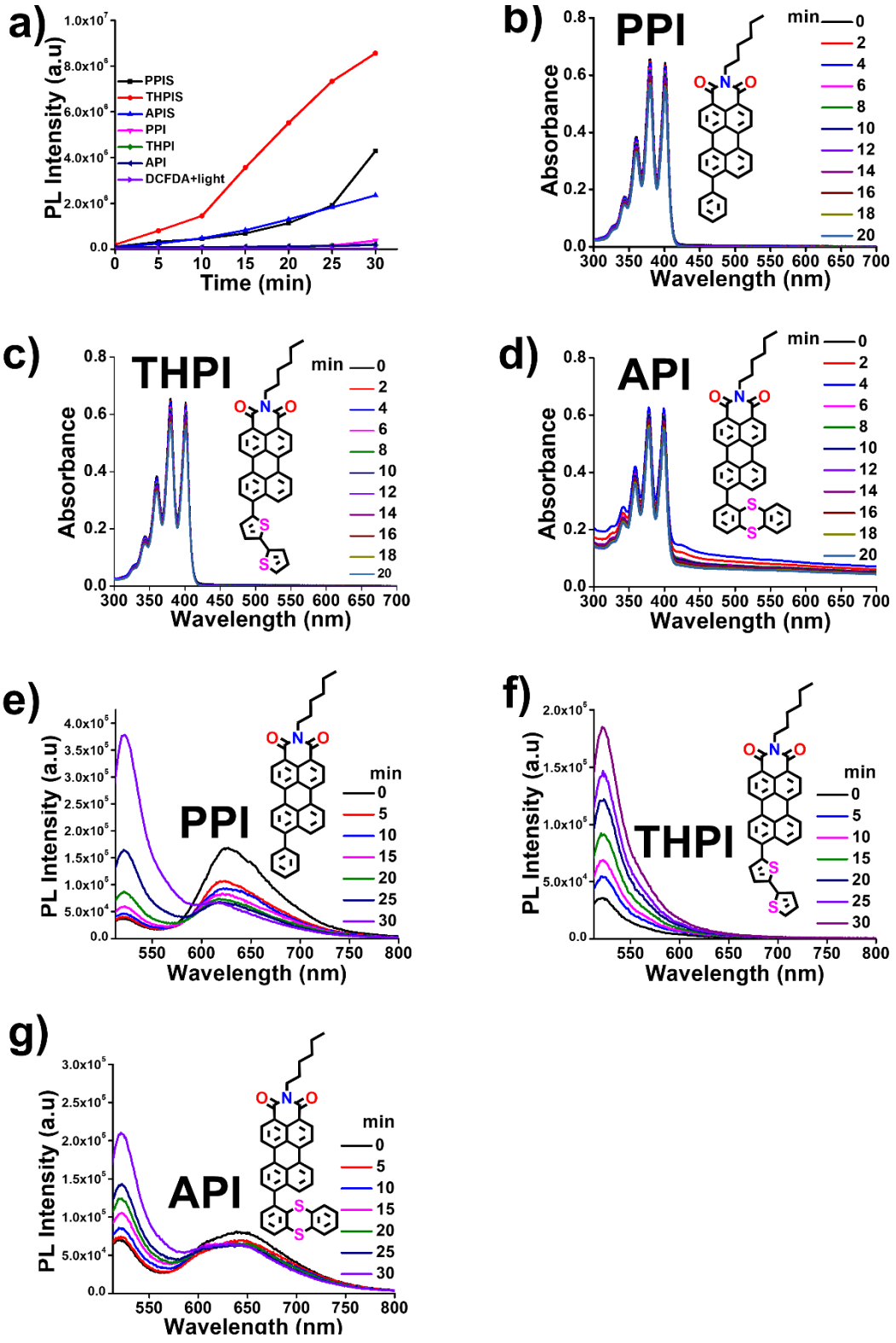

Fig. S13 (a) Plot of fluorescence intensities of DCFDA indicator in the presence of the **RPNI-O** and **RPNI-S** derivatives, respectively. ROS generation by the **RPNI-O** derivatives. (b-d) Plots of ABDA (100 μM) degradation rates at $\lambda_{abs.max}$ of 378 nm by the various PSs (100 μM) (b) **PPI**, (c) **THPI,** and (d) **API**, respectively and (e-g) Evaluation of the general ROS generation using DCFDA (10 μM) indicator by PSs (100 μM) (e) **PPI**, (f) **THPI**

and (g) **API**, respectively upon white light excitation for different time periods at 99% PBS fraction in DMSO (λ_{ex}=500 nm). Inset: Chemical structure of the **RPNI-O** derivatives.

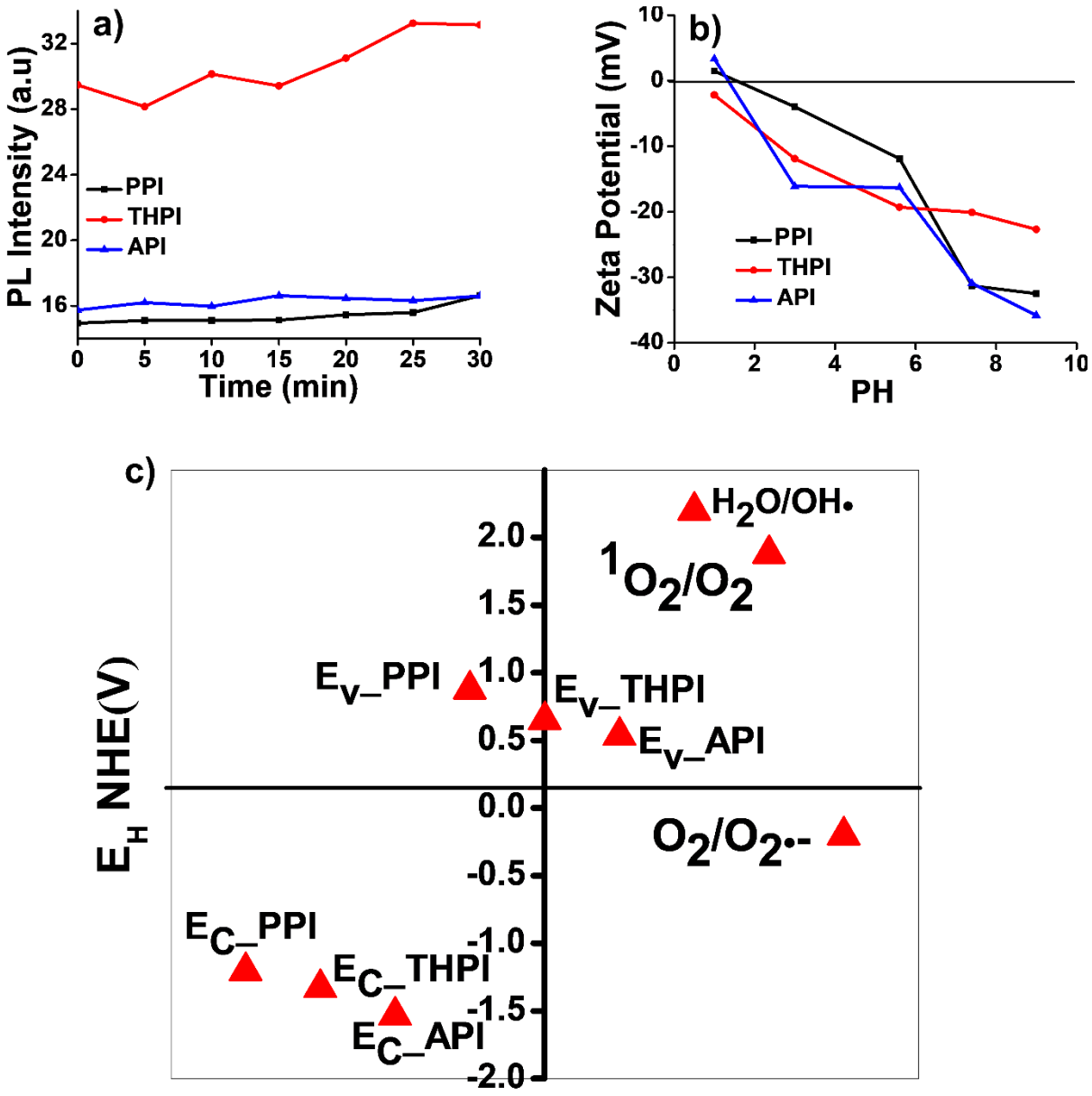

Fig. S14 (a) PL spectra of TA at 528 nm. (b) Zeta potential versus pH values of **RPNI-O** derivatives. (c) E_C and E_V of **RPNI-O** derivatives at pH 5.6. The energy scale is expressed in relation to NHE. E_H for $H_2O/HO^•$, $^1O_2/O_2$, and $O_2/O_2^{•-}$ are 2.2, 1.88, and −0.2 eV, respectively.

Table S15 Zeta potential data of **RPNI-O** and **RPNI-S** derivatives at different PH.

Materials	**PH**				
	1	**3**	**5.6**	**7.4**	**9**
PPIζ	1.49	-3.99	-11.90	-31.30	-32.50

THPIζ	-2.18	-11.90	-19.30	-20.10	-22.70
APIζ	3.35	-16.10	-16.30	-30.90	-35.80
PPISζ	2.68	-1.89	-10.79	-21.13	-22.45
THPISζ	2.18	-7.90	-18.20	-19.10	-20.70
APISζ	4.35	-13.4	-14.30	-31.90	-38.80

ζ is the zeta potential of the respective materials.

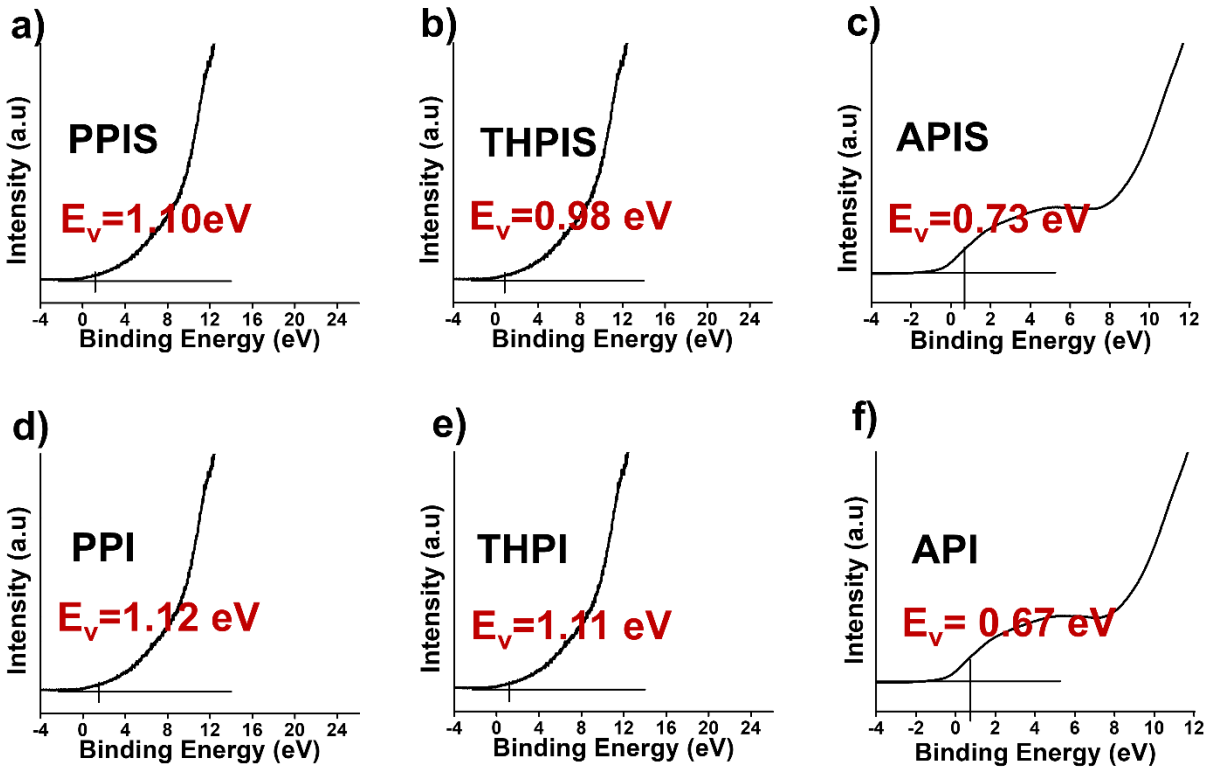

Fig. S15 XPS spectra displaying valence band energy **(E_v):** (a) **PPIS,** (b) **THPIS,** (c) **APIS,** (d) **PPI,** (e) **THPI,** and (f) **API,** respectively.

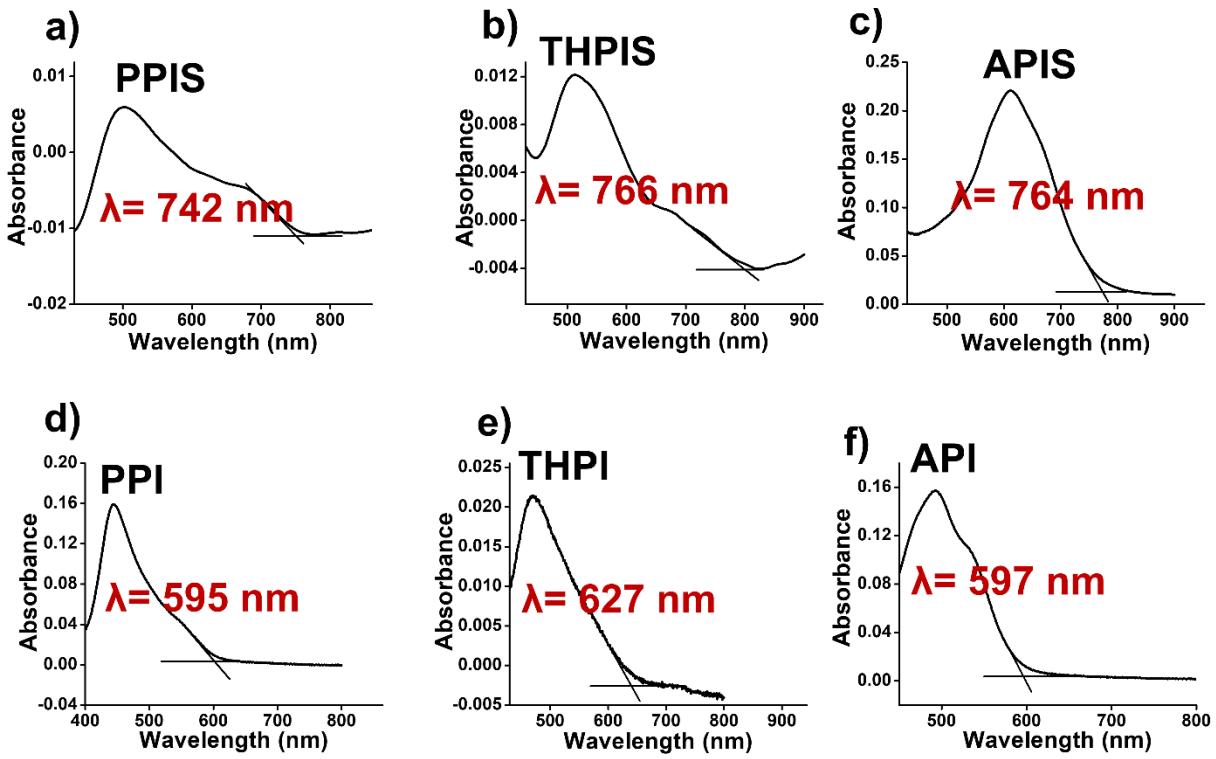

Fig. S16 UV-vis spectroscopy of exhibiting onset absorption (a) **PPIS,** (b) **THPIS,** (c) **APIS,** (d) **PPI,** (e) **THPI,** and (f) **API,** respectively.

Table S16 Optical band gap data of **RPNI-O** and **RPNI-S** derivatives calculated from the onset absorption of the UV-vis spectroscopy.

Materials	**λ_{onset}**	**E_g (eV)**
PPIS	742	1.67
THPIS	766	1.61
APIS	764	1.62
PPI	595	2.08
THPI	627	1.98
API	597	2.07

λ_{onset} onset UV-vis absorption

Table S17 E_C and E_V at a pH of 5.6 of **RPNI-O** and **RPNI-S** derivatives**.**

Materials	**Eg**	**E_{HOMO}**	**E_{LUMO}**	**E_v**	**E_c**	**PZZP**	**$E_{V,5.6}$**	**$E_{C,5.6}$**

PPIS	1.67	-5.60	-3.93	1.10	-0.57	2.68	0.92772	-0.74228
THPIS	1.61	-5.48	-3.87	0.98	-0.63	2.18	0.77822	-0.83178
APIS	1.62	-5.23	-3.61	0.73	-0.89	4.35	0.65625	-0.96375
PPI	2.08	-5.62	-3.54	1.12	-0.96	1.49	0.87751	-1.20249
THPI	1.98	-5.61	-3.63	1.11	-0.87	-2.18	0.65098	-1.32902
API	2.07	-5.17	-3.10	0.67	-1.40	3.35	0.53725	-1.53275

PZZP, the point of zero zeta potential

Table S18 Calculated Gibbs free energy of **O_2** using **ORCA 5.0** at the B3LYP/6-31G (d, p) and B3LYP/DEF2SVP level using quantum mechanism package.

Materials	**G (Eh)**		**ΔG (Kcal mol^{-1})**
PPIS	O_2	-150.09346315	-0.548
	PPIS+O_2	-2310.53867284	
	PPIS	-2160.44608328	
THPIS	O_2	-150.09346315	-40.83
	THPIS+O_2	-3182.63436769	
	THPIS	-3032.55916191	
APIS	O_2	-150.09346315	-10.26
	APIS+O_2	-3336.04242916	
	APIS	-3185.96532129	

Table S19 Calculated Gibbs free energy of **O_2** using ORCA 5.0 at the B3LYP/6-31G (d, p) and B3LYP/DEF2SVP level using a quantum mechanism package.

O_2

GIBBS FREE ENERGY

The Gibbs free energy is G = H - T*S

Total enthalpy ... -150.07131287 Eh

Total entropy correction ... -0.02215028 Eh -13.90 kcal/mol

Final Gibbs free energy ... -150.09346315 Eh

For completeness - the Gibbs free energy minus the electronic energy

G-E(el) ... -0.01441918 Eh -9.05 kcal/mol

Timings for individual modules:

Sum of individual times ... 12.524 sec (= 0.209 min)

GTO integral calculation ... 2.186 sec (= 0.036 min) 17.5 %

SCF iterations ... 4.342 sec (= 0.072 min) 34.7 %

Analytical frequency calculation... 5.995 sec (= 0.100 min) 47.9 %

Table S20 Calculated Gibbs free energy of **PPIS** using ORCA 5.0 at the B3LYP/6-31G (d, p) and B3LYP/DEF2SVP level using quantum mechanism package.

PPIS

GIBBS FREE ENERGY

The Gibbs free energy is G = H - T*S

Total enthalpy ... -2160.36500661 Eh

Total entropy correction ... -0.08107666 Eh -50.88 kcal/mol

Final Gibbs free energy ... -2160.44608328 Eh

For completeness - the Gibbs free energy minus the electronic energy

G-E(el) ... 0.46404158 Eh 291.19 kcal/mol

Timings for individual modules:

Sum of individual times ... 2449.244 sec (= 40.821 min)

GTO integral calculation ... 3.581 sec (= 0.060 min) 0.1 %

SCF iterations ... 217.116 sec (= 3.619 min) 8.9 %

Analytical frequency calculation... 2228.548 sec (= 37.142 min) 91.0 %

Table S21 Calculated Gibbs free energy of **PPIS** and **O_2** using ORCA 5.0 at the B3LYP/6-31G (d,p) and B3LYP/DEF2SVP level using a quantum mechanism package.

GIBBS FREE ENERGY **PPIS +O_2**

The Gibbs free energy is G = H - T*S
Total enthalpy ... -2310.44123598 Eh
Total entropy correction ... -0.09743686 Eh -61.14 kcal/mol

Final Gibbs free energy ... -2310.53867284 Eh
For completeness - the Gibbs free energy minus the electronic energy
G-E(el) ... 0.45873772 Eh 287.86 kcal/mol
Timings for individual modules:
Sum of individual times ... 19281.091 sec (= 321.352 min)
GTO integral calculation ... 103.385 sec (= 1.723 min) 0.5 %
SCF iterations ... 12827.456 sec (= 213.791 min) 66.5 %
SCF Gradient evaluation ... 2722.936 sec (= 45.382 min) 14.1 %
Geometry relaxation ... 24.973 sec (= 0.416 min) 0.1 %
Analytical frequency calculation... 3602.340 sec (= 60.039 min) 18.7 %

Table S22 Calculated Gibbs free energy of **THPIS** using ORCA 5.0 at the B3LYP/6-31G (d,p) and B3LYP/DEF2SVP level using quantum mechanism package.

THPIS

```
------------------
GIBBS FREE ENERGY
------------------
The Gibbs free energy is G = H - T*S
Total enthalpy ... -3032.47582297 Eh
Total entropy correction ... -0.08333893 Eh -52.30 kcal/mol
-----------------------------------------------------------------
Final Gibbs free energy ... -3032.55916191 Eh
For completeness - the Gibbs free energy minus the electronic
energy
G-E(el) ... 0.47671745 Eh 299.14 kcal/mol
Timings for individual modules:
Sum of individual times ... 3337.858 sec (= 55.631 min)
GTO integral calculation ... 4.858 sec (= 0.081 min) 0.1 %
SCF iterations ... 251.657 sec (= 4.194 min) 7.5 %
Analytical frequency calculation... 3081.344 sec (= 51.356
min) 92.3 %
```

Table S23 Calculated Gibbs free energy of **THPIS** and **O_2** using ORCA 5.0 at the B3LYP/6-31G (d, p) and B3LYP/DEF2SVP level using a quantum mechanism package.

THPIS+O_2

```
------------------
GIBBS FREE ENERGY
------------------
The Gibbs free energy is G = H - T*S
Total enthalpy ... -3182.55043554 Eh
Total entropy correction ... -0.08393215 Eh -52.67 kcal/mol
-----------------------------------------------------------------
Final Gibbs free energy ... -3182.63436769 Eh
For completeness - the Gibbs free energy minus the electronic
energy
G-E(el) ... 0.48055338 Eh 301.55 kcal/mol
Timings for individual modules:
Sum of individual times ... 5309.271 sec (= 88.488 min)
GTO integral calculation ... 3.579 sec (= 0.060 min) 0.1 %
SCF iterations ... 2394.155 sec (= 39.903 min) 45.1 %
Analytical frequency calculation... 2911.537 sec (= 48.526
min) 54.8 %
```

Table S24 Calculated Gibbs free energy of **APIS** using ORCA 5.0 at the B3LYP/6-31G (d,p) and B3LYP/DEF2SVP level using quantum mechanism package.

APIS

GIBBS FREE ENERGY

The Gibbs free energy is G = H - T*S

Total enthalpy ... -3185.87795057 Eh

Total entropy correction ... -0.08737072 Eh -54.83 kcal/mol

Final Gibbs free energy ... -3185.96532129 Eh

For completeness - the Gibbs free energy minus the electronic energy

G-E(el) ... 0.52321755 Eh 328.32 kcal/mol

Timings for individual modules:

Sum of individual times ... 4288.483 sec (= 71.475 min)

GTO integral calculation ... 2.835 sec (= 0.047 min) 0.1 %

SCF iterations ... 288.080 sec (= 4.801 min) 6.7 %

Analytical frequency calculation... 3997.568 sec (= 66.626 min) 93.2 %

Table S25 Calculated Gibbs free energy of **APIS** and **O_2** using ORCA 5.0 at the B3LYP/6-31G (d, p) and B3LYP/DEF2SVP level using a quantum mechanism package.

APIS+O_2

GIBBS FREE ENERGY

The Gibbs free energy is G = H - T*S

Total enthalpy ... -3335.95158265 Eh

Total entropy correction ... -0.09084651 Eh -57.01 kcal/mol

Final Gibbs free energy ... -3336.04242916 Eh

For completeness - the Gibbs free energy minus the electronic energy

G-E(el) ... 0.52511206 Eh 329.51 kcal/mol

Timings for individual modules:

Sum of individual times ... 7444.600 sec (= 124.077 min)

GTO integral calculation ... 73.874 sec (= 1.231 min) 1.0 %

SCF iterations ... 2387.693 sec (= 39.795 min) 32.1 %

Analytical frequency calculation... 4983.033 sec (= 83.051 min) 66.9 %

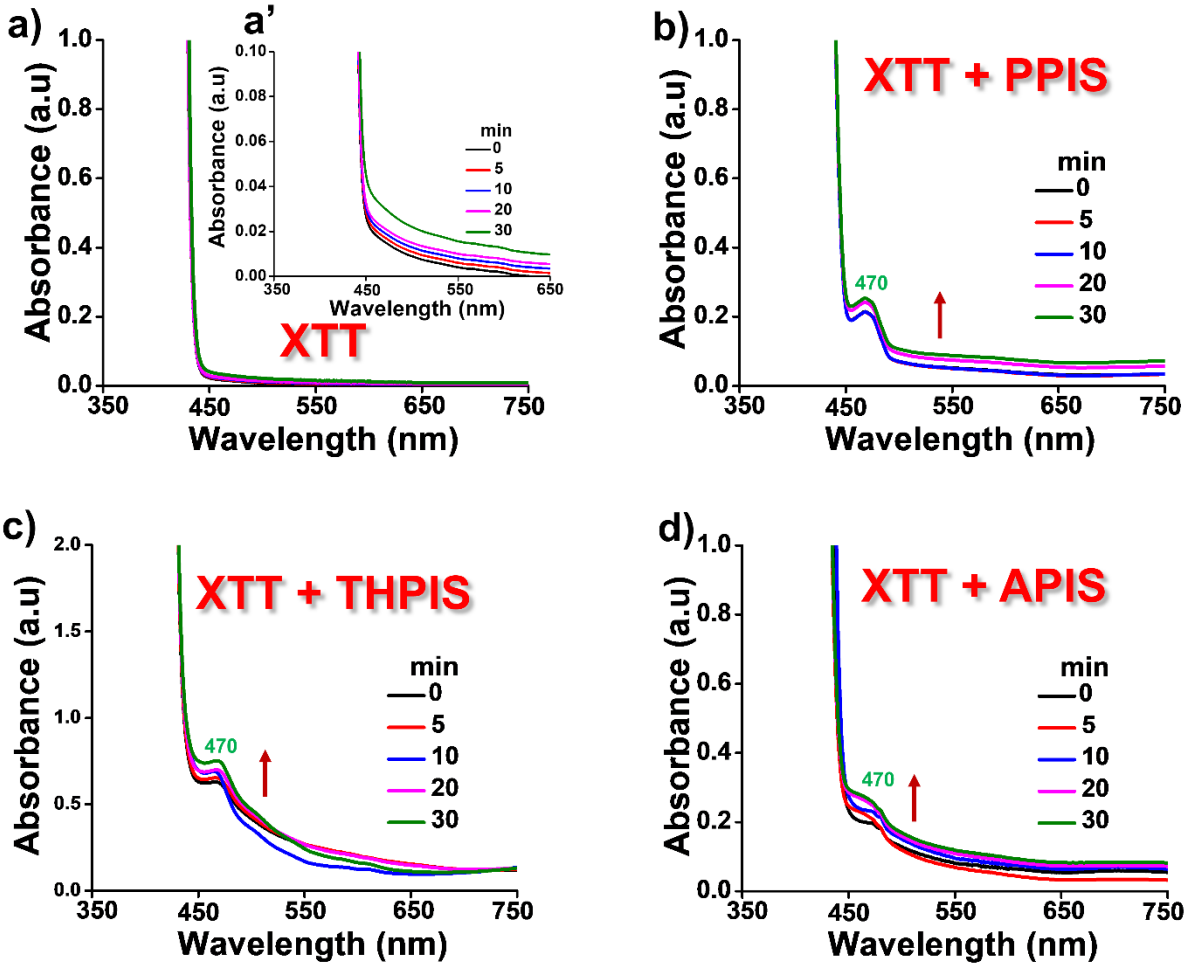

Fig. S17 $O_2^{\bullet-}$ production of three **RPNI-S** using the reduction product of XTT as the indicator. (a) UV-vis spectra changes of XTT alone, and (b-d) UV-vis spectra changes of XTT in the presence of (b) **PPIS**, (c) **THPIS**, and (d) **APIS** PSs, respectively, under the white light irradiation with different time. [Inset: (a') represents the partial magnified parts of Fig. a].

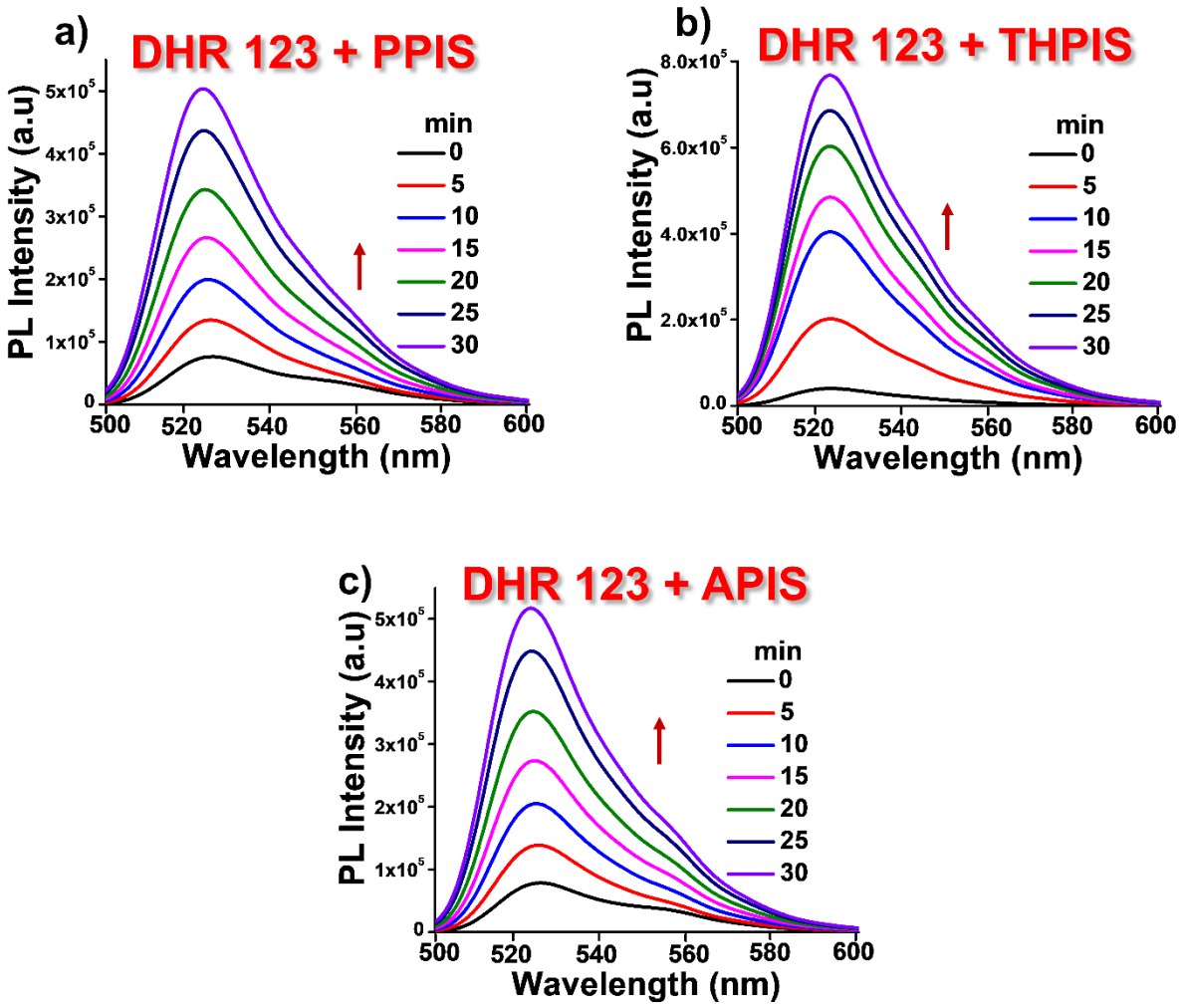

Fig. S18 $O_2^{\bullet-}$ generation of three **RPNI-S** PSs using the DHR 123 indicator. PL spectra of DHR 123 in 99% PBS in DMSO, f_{PBS} in the presence of (a) **PPIS**, (b) **THPIS**, and (c) **APIS**, respectively, after exposure to white light irradiation at different times. [**RPNI-S**] =100 μM, [DHR 123] = 10 μM].

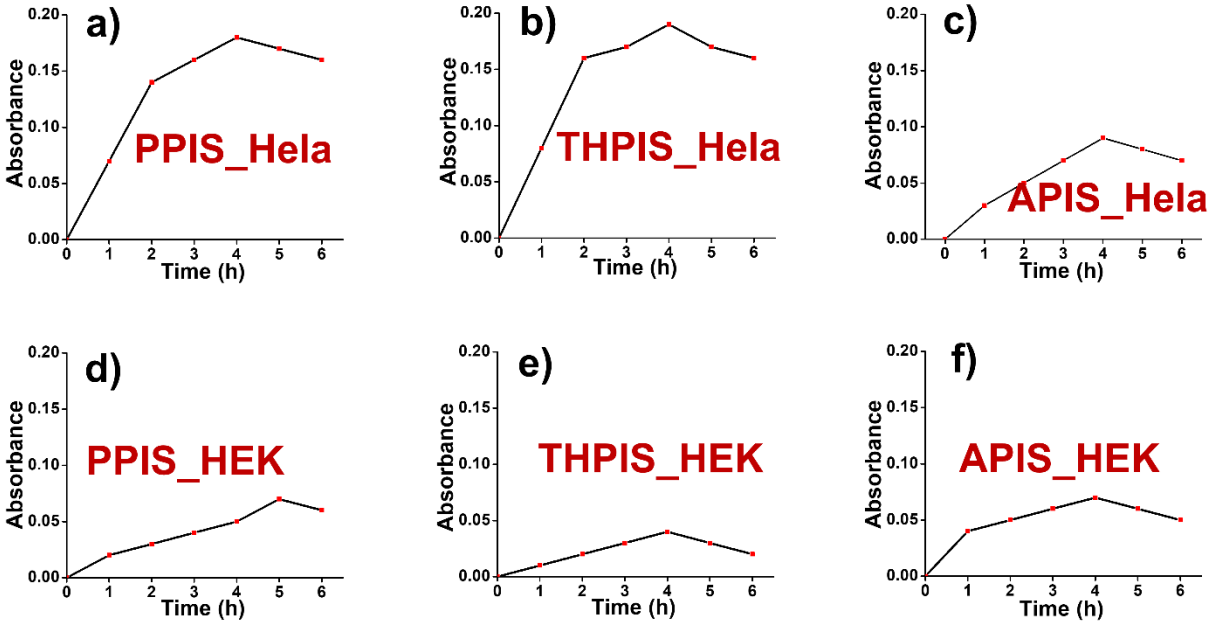

Fig. S19 (a-c) Cellular uptake data of the (a) **PPIS,** (b) **THPIS,** and (c) **APIS** in Hela cell. [concentration of **PPIS**, **THPIS,** and **APIS**: 20 μM]. (d-f) Cellular uptake data of the (d) **PPIS**, (e) T**HPIS,** and (f) **APIS** in HEK 293T. [concentration of **PPIS**, **THPIS,** and **APIS**: 100 μM].

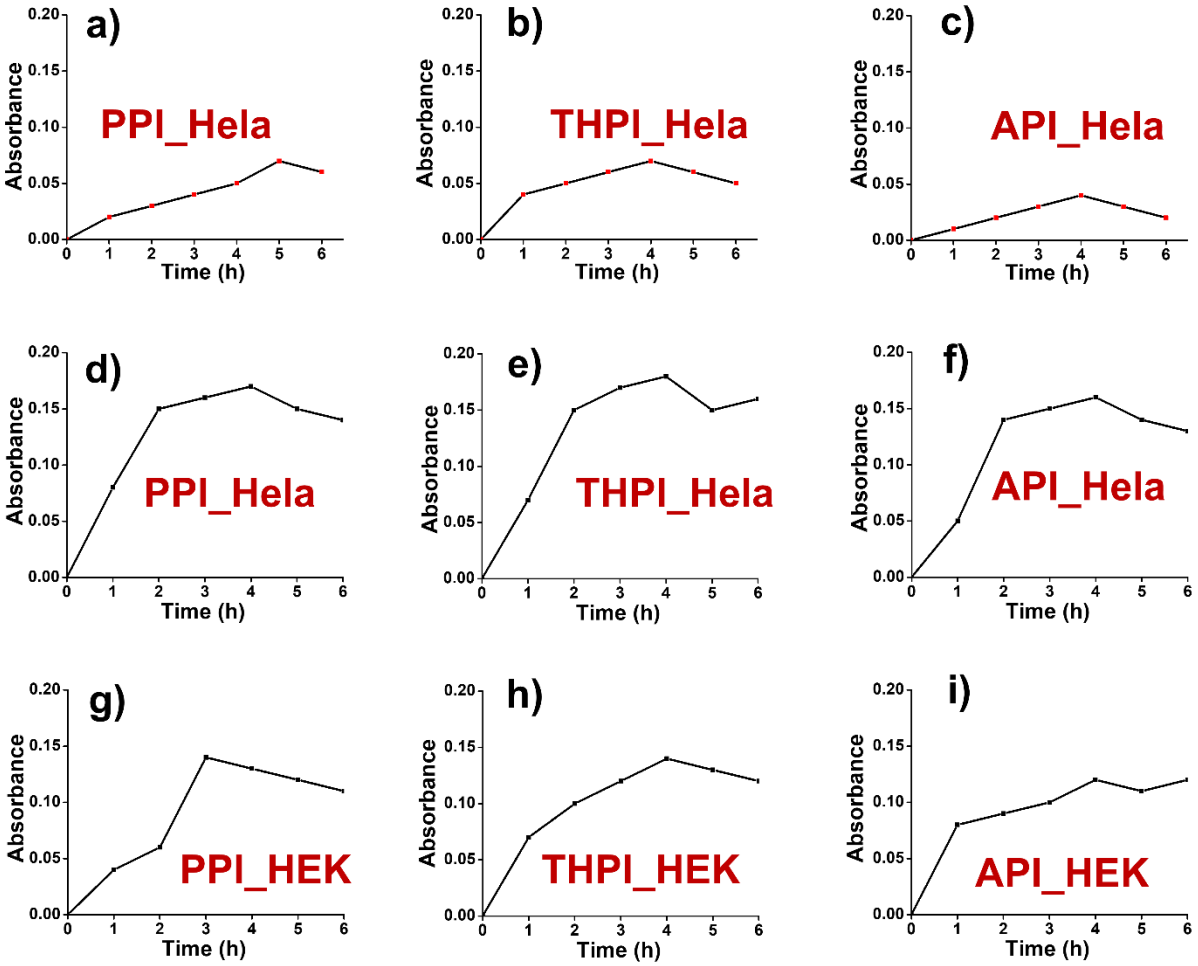

Fig. S20 (a-c) Cellular uptake data of the (a) **PPI**, (b) **THPI,** and (c) **API** in Hela cell. [concentration of **PPI**, **THPI,** and **API**: 20 μM]. (d-f) Cellular uptake data of the (d) **PPI**, (e) **THPI,** and (f) **API** in Hela cell. [concentration of **PPI**, **THPI,** and **API**: 100 μM]. (g-i) Cellular uptake data of the (g) **PPI**, (h) **THPI,** and (i) **API** in HEK293. [concentration of **PPI**, **THPI,** and **API**: 100 μM].

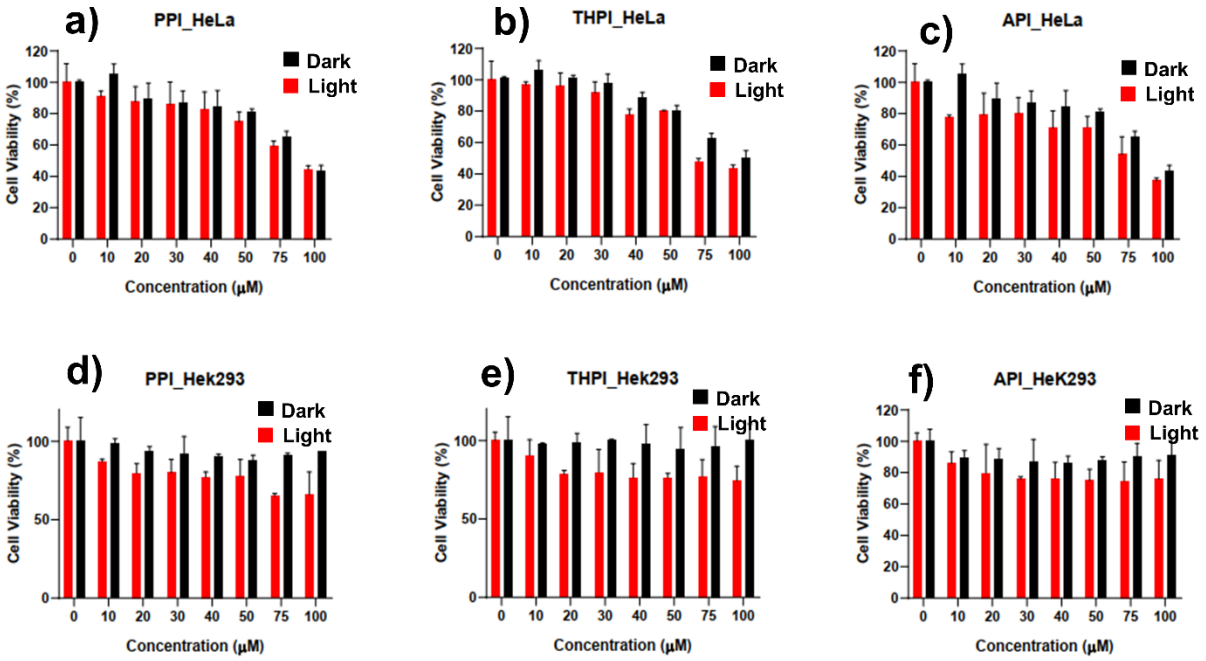

Fig. S21 (a-c) Cell viability of HeLa cells after treatment with different concentrations of (a) **PPI,** (b) **THPI,** and (c) **API**, respectively, along with white light irradiation. (d-f) Cell cytotoxicity of HEK293Tcells after treatment with different concentrations of (d) **PPI,** (e) **THPI,** and (f) **API**, respectively, along with white light irradiation.

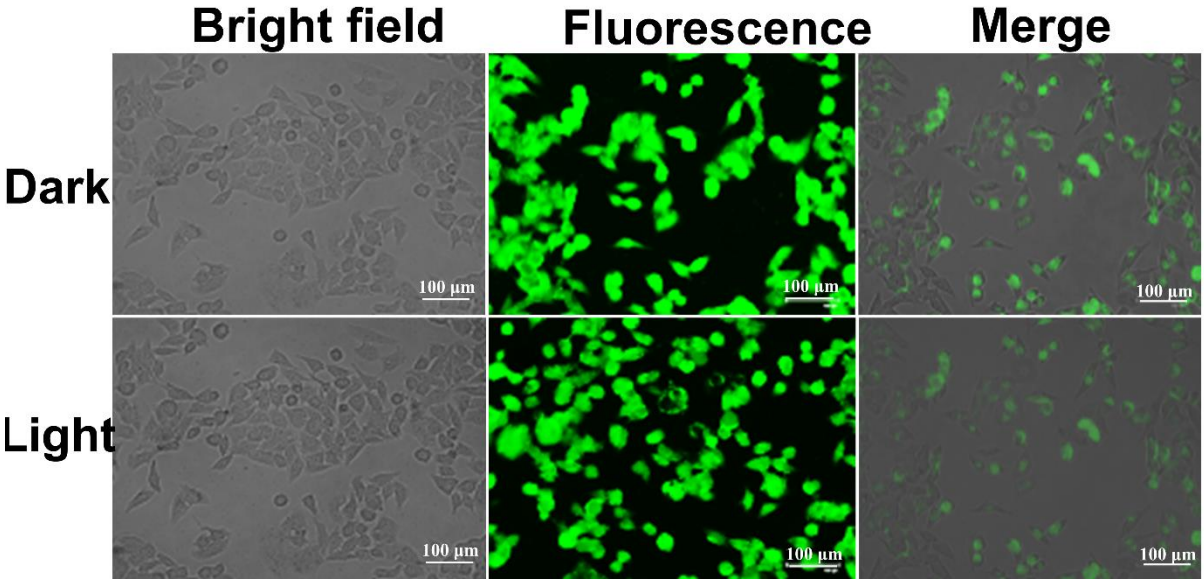

Fig. S22 Fluorescence microscope images of HeLa cells after treatment with **APIS** under normoxia and loaded with calcein-AM (2 μM, live cell marker). [Concentration of **APIS**: (50 μM, scale bar: 100 μm].

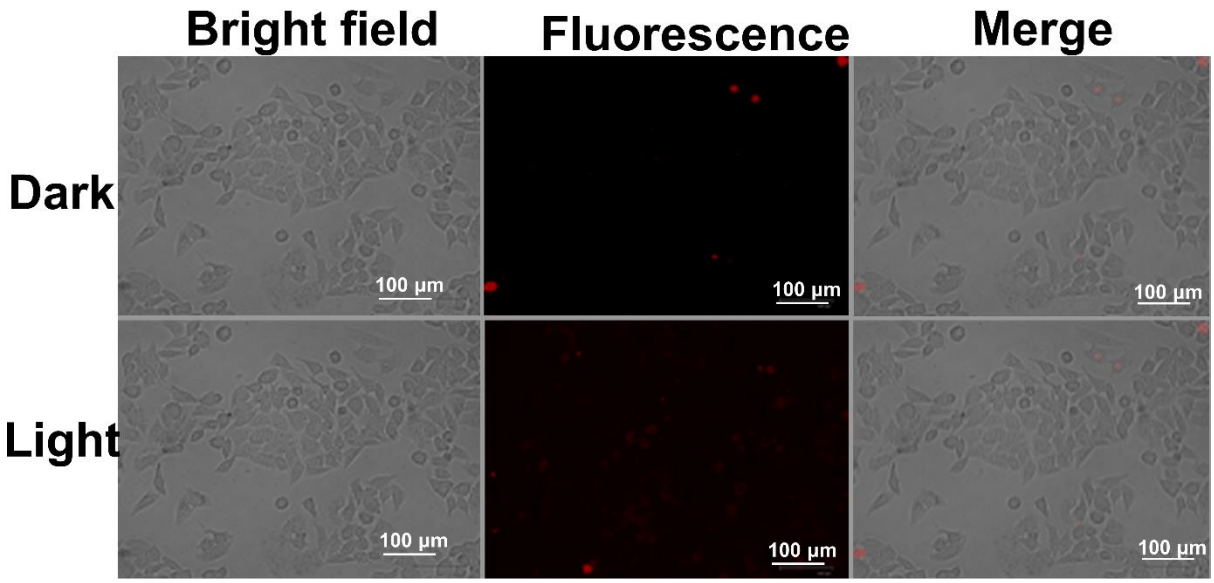

Fig. S23 Fluorescence microscope images of HeLa cells after treatment with **APIS** under normoxia and loaded with PI (4 μM, dead cell marker). [Concentration of **APIS**: (50 μM, scale bar: 100 μm].

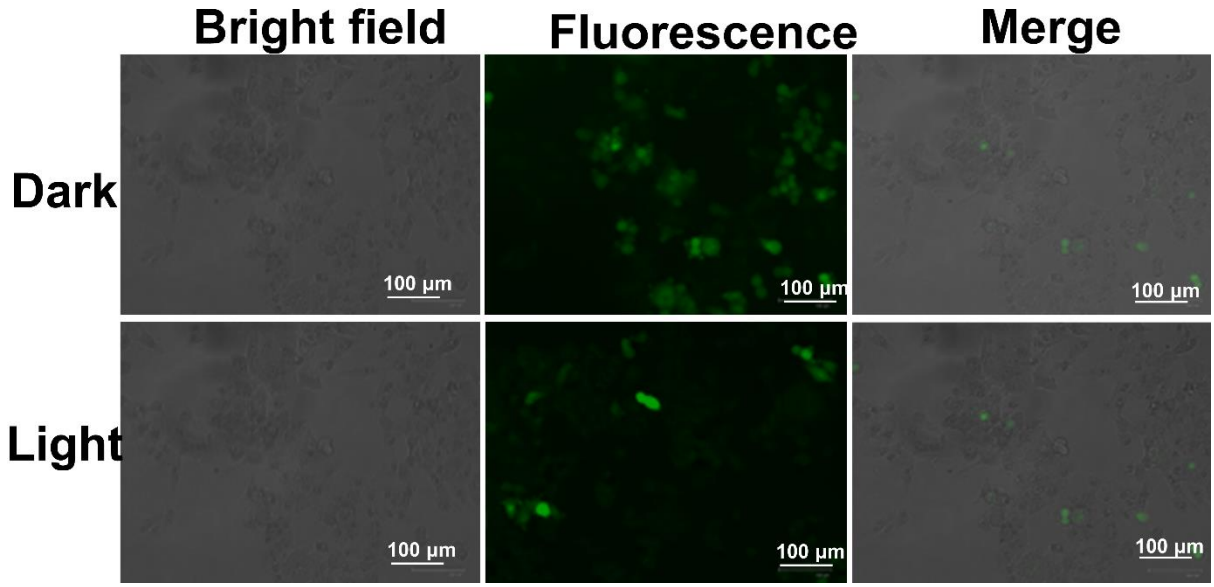

Fig. S24 Fluorescence microscope images of HeLa cells after treatment with **APIS** under normoxia and loaded with DCFDA (10 μM, ROS detection probe). [Concentration of **APIS**: (50 μM, scale bar: 100 μm].

2. Supporting figures

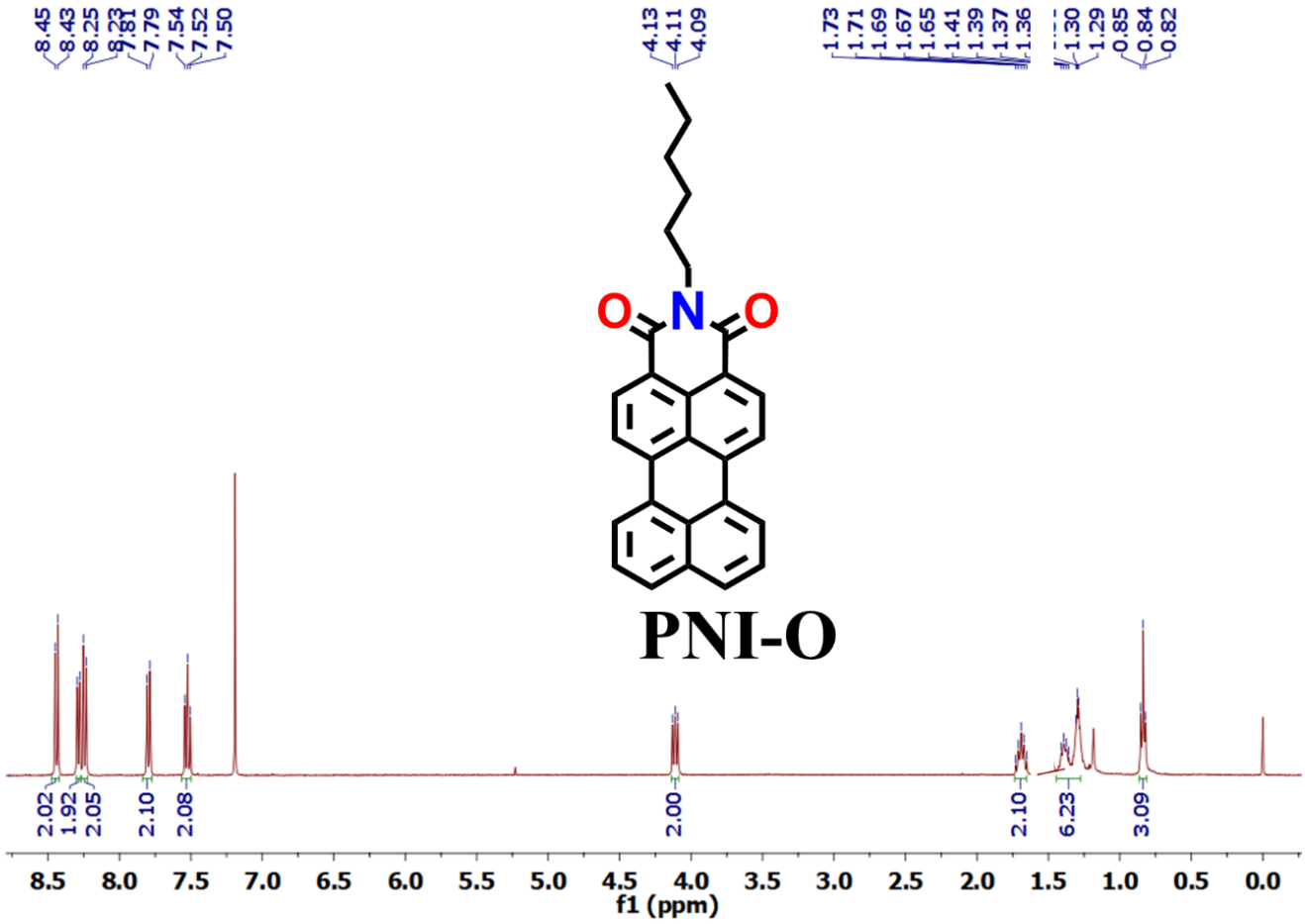

Fig. S25 ^{1}H NMR spectra of **PNI-O**.

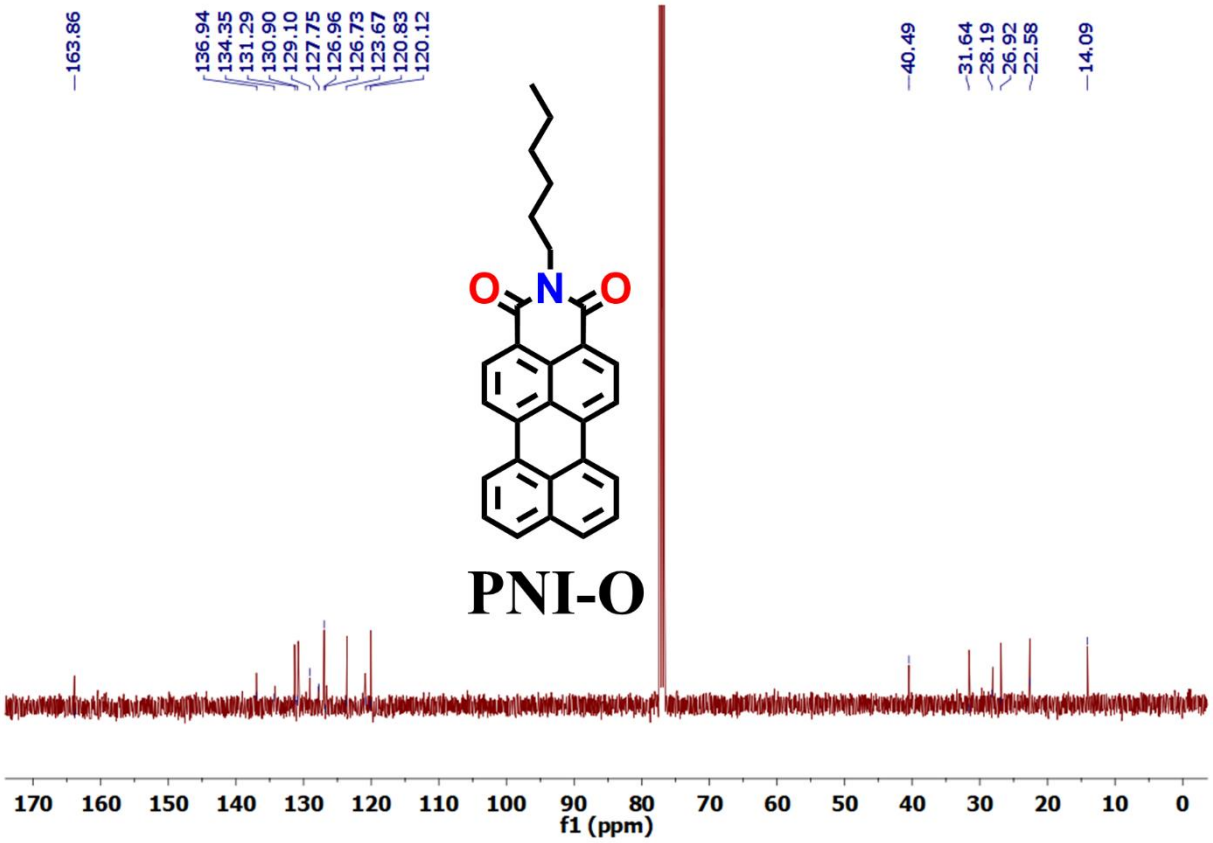

Fig. S26 ^{13}C NMR spectra of **PNI-O.**

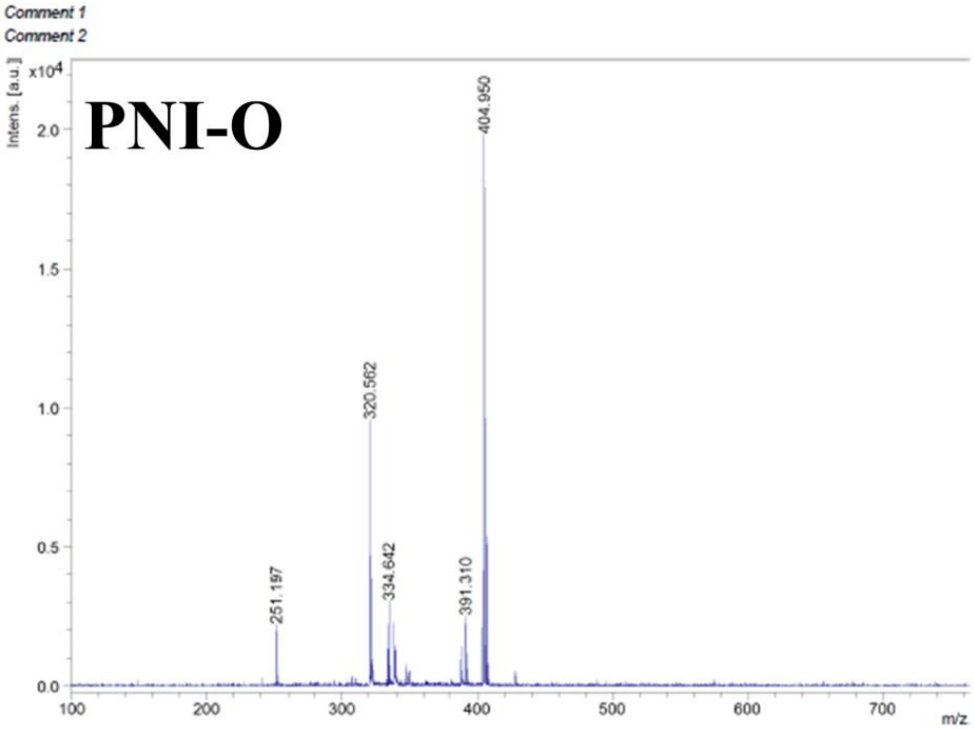

m/z	S/N	Quality Fac.	Res.	Intens.	Area
251.197	106		3340	2172	185
320.562	298		3062	9515	1277
334.642	92		3009	3013	408
387.886	44		3542	1422	227
391.310	77		2760	2486	391
404.950	629		3931	19790	2350

Fig. S27 Maldi-TOF spectra of **PNI-O**.

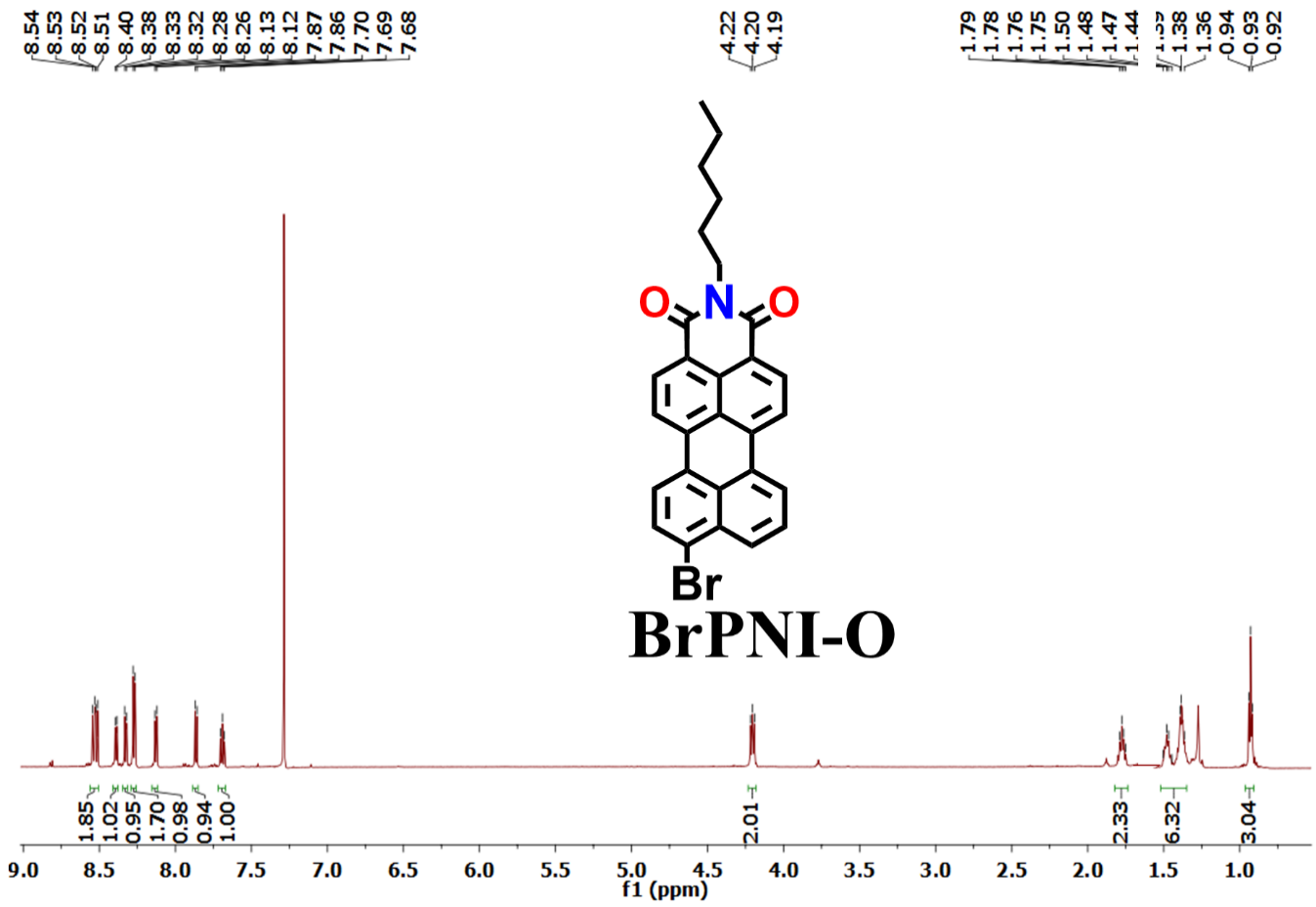

Fig. S28 ^{1}H NMR spectra of **BrPNI-O.**

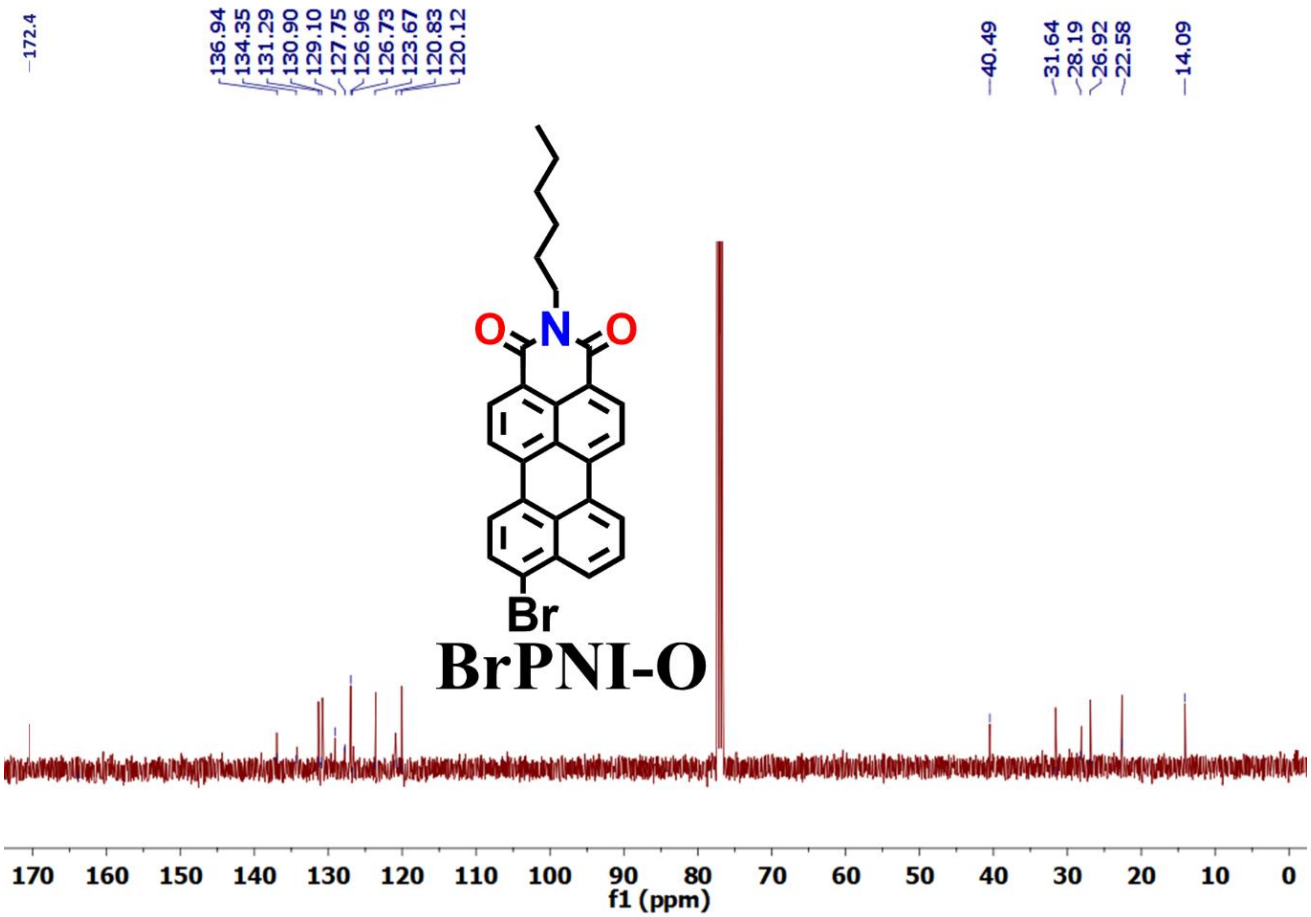

Fig. S29 ^{13}C NMR spectra of **BrPNI-O**.

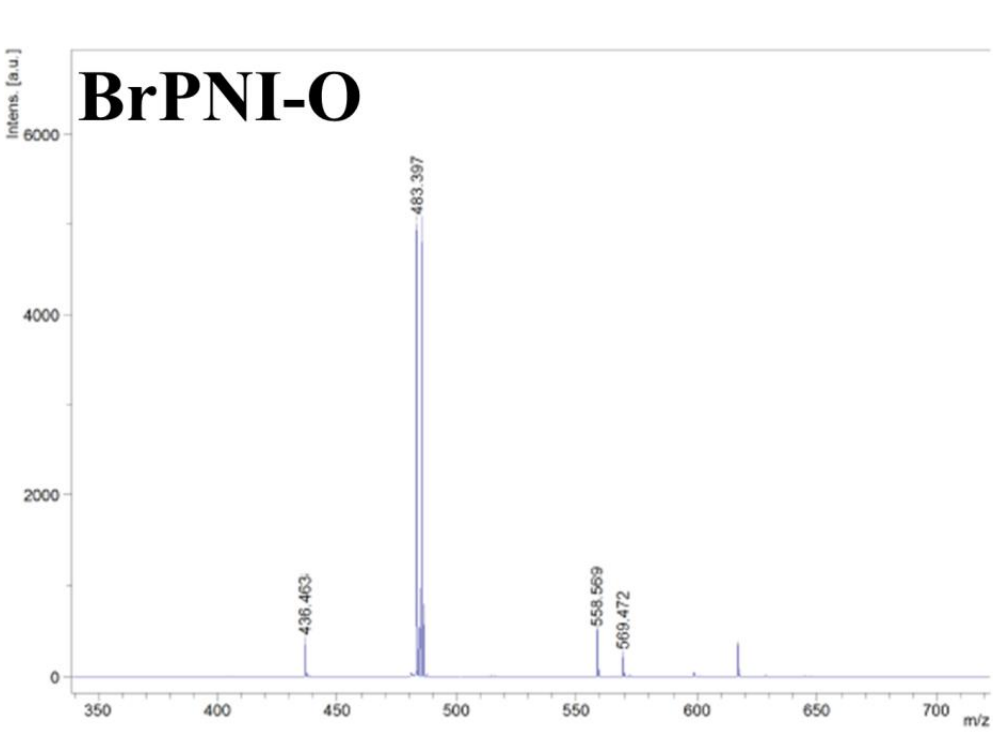

m/z	S/N	Quality Fac.	Res.	Intens.	Area
436.463	12		5242	440	80.6
483.397				4994	
484.408	30		225	984	2069
558.569	20		6983	528	94.5
569.472				276	

Fig. S30 Maldi-TOF spectra of **BrPNI-O.**

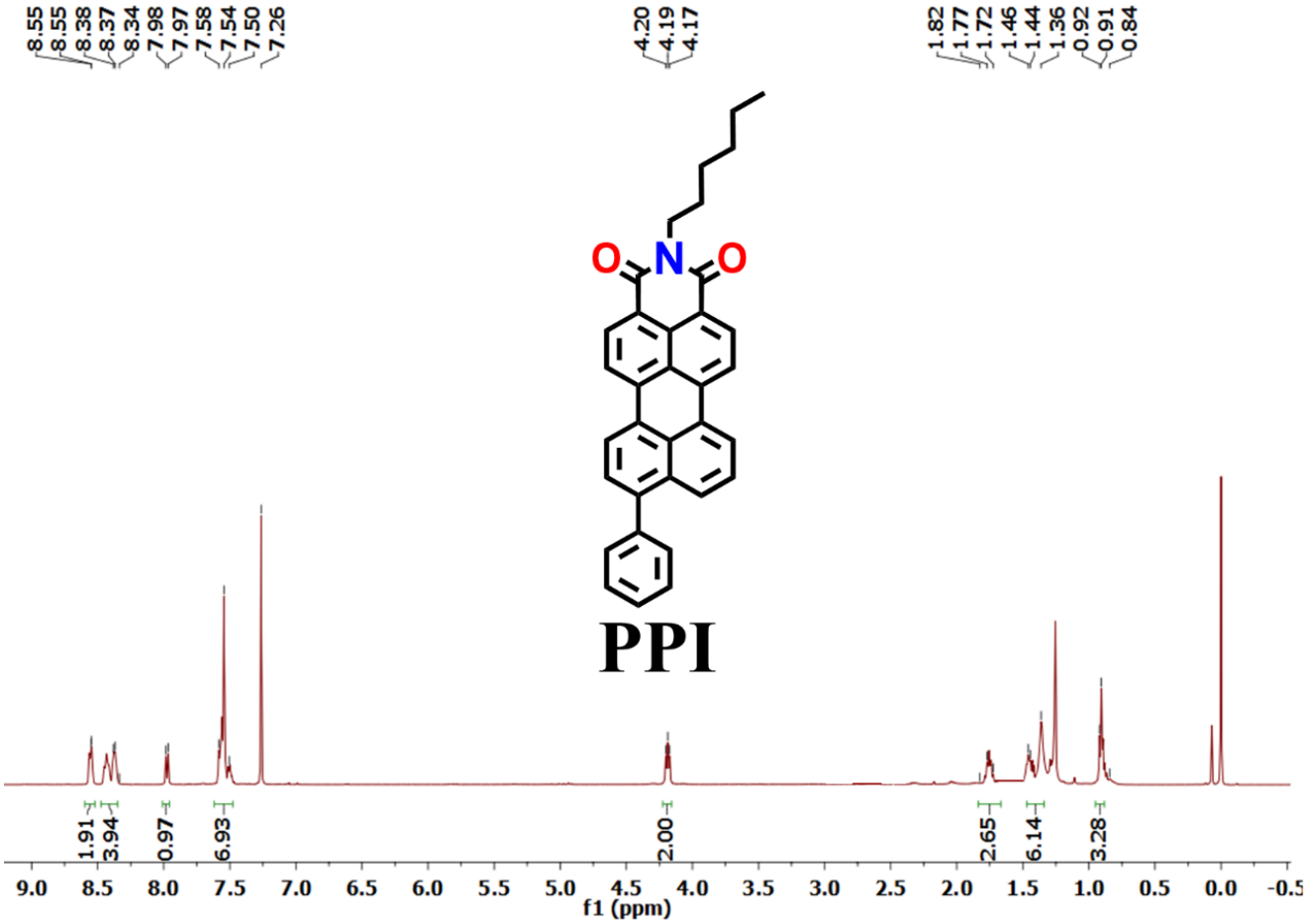

Fig. S31 ^{1}H NMR spectra of **PPI**.

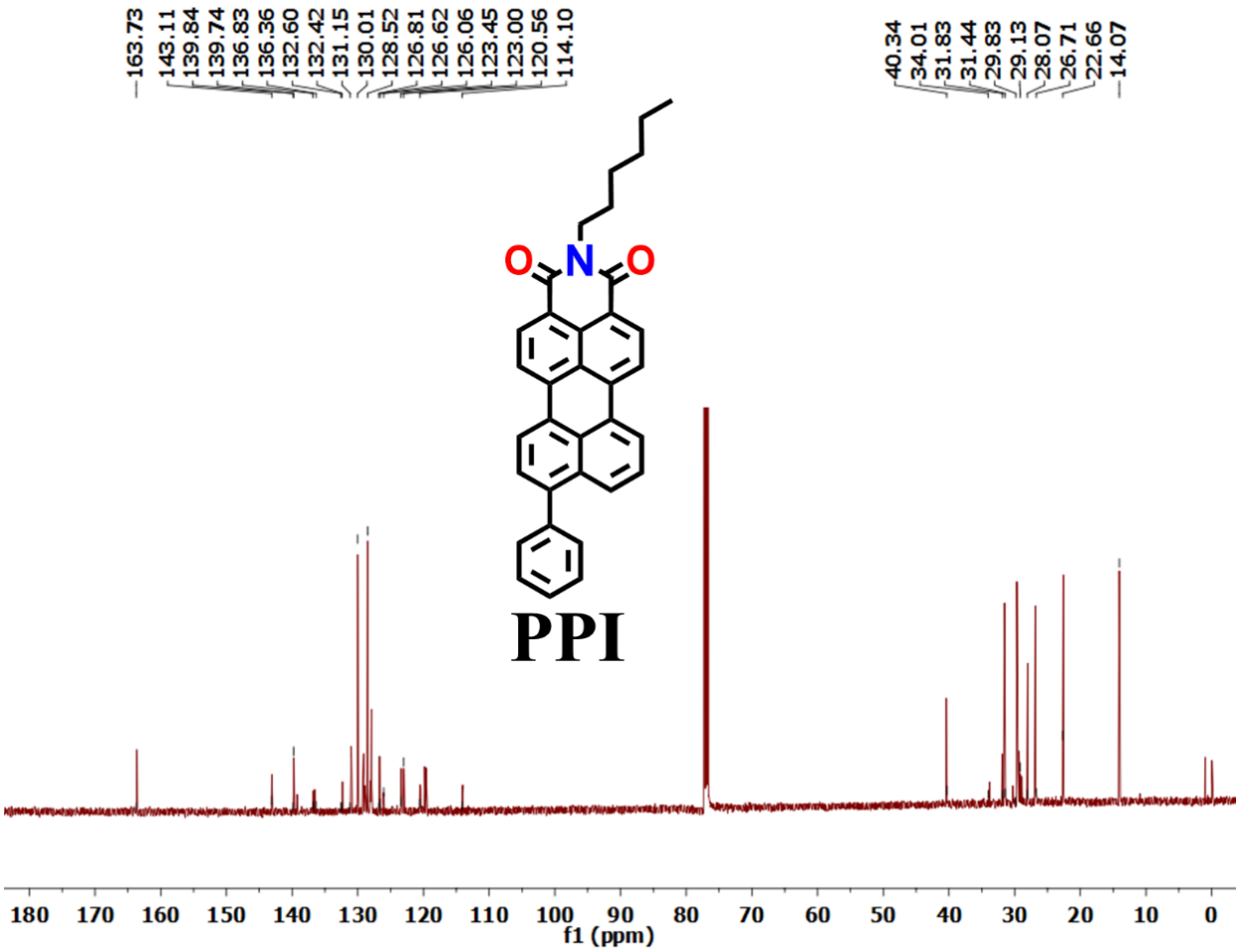

Fig. S32 ^{13}C NMR spectra of **PPI.**

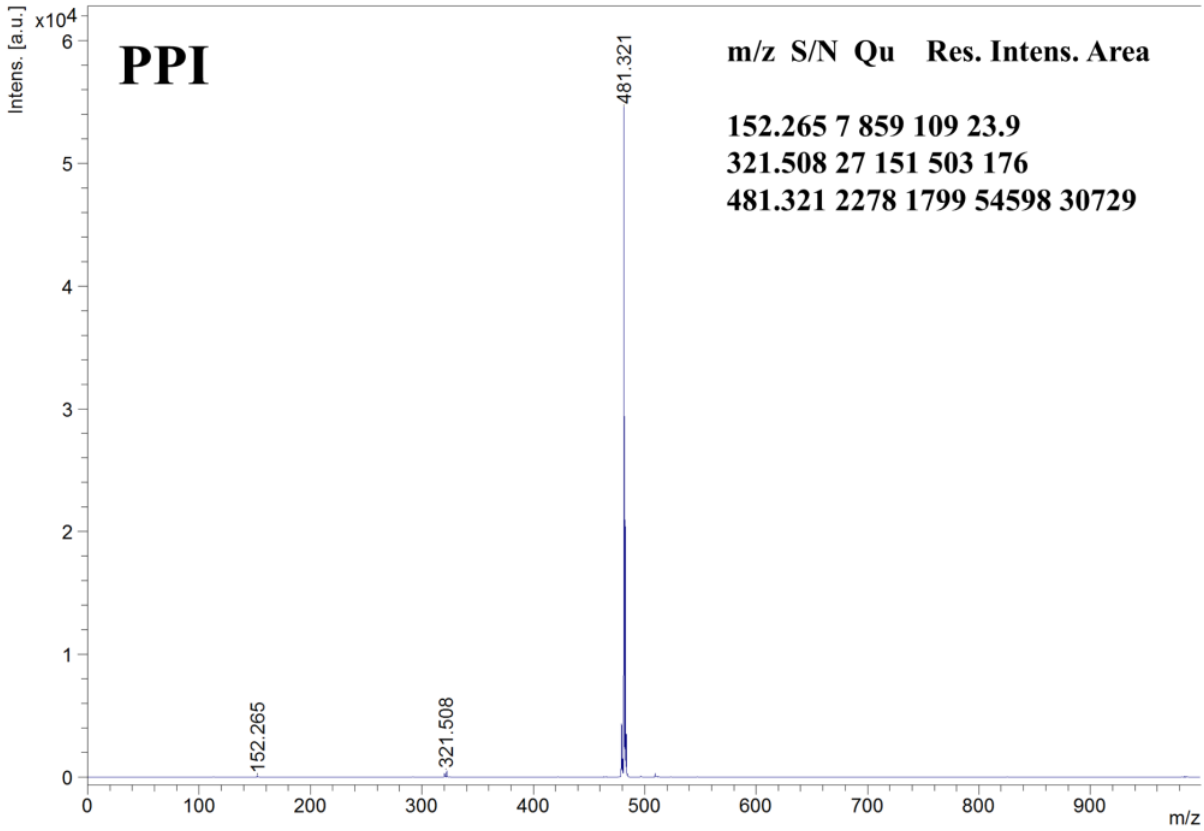

Fig. S33 Maldi-TOF spectra of **PPI**.

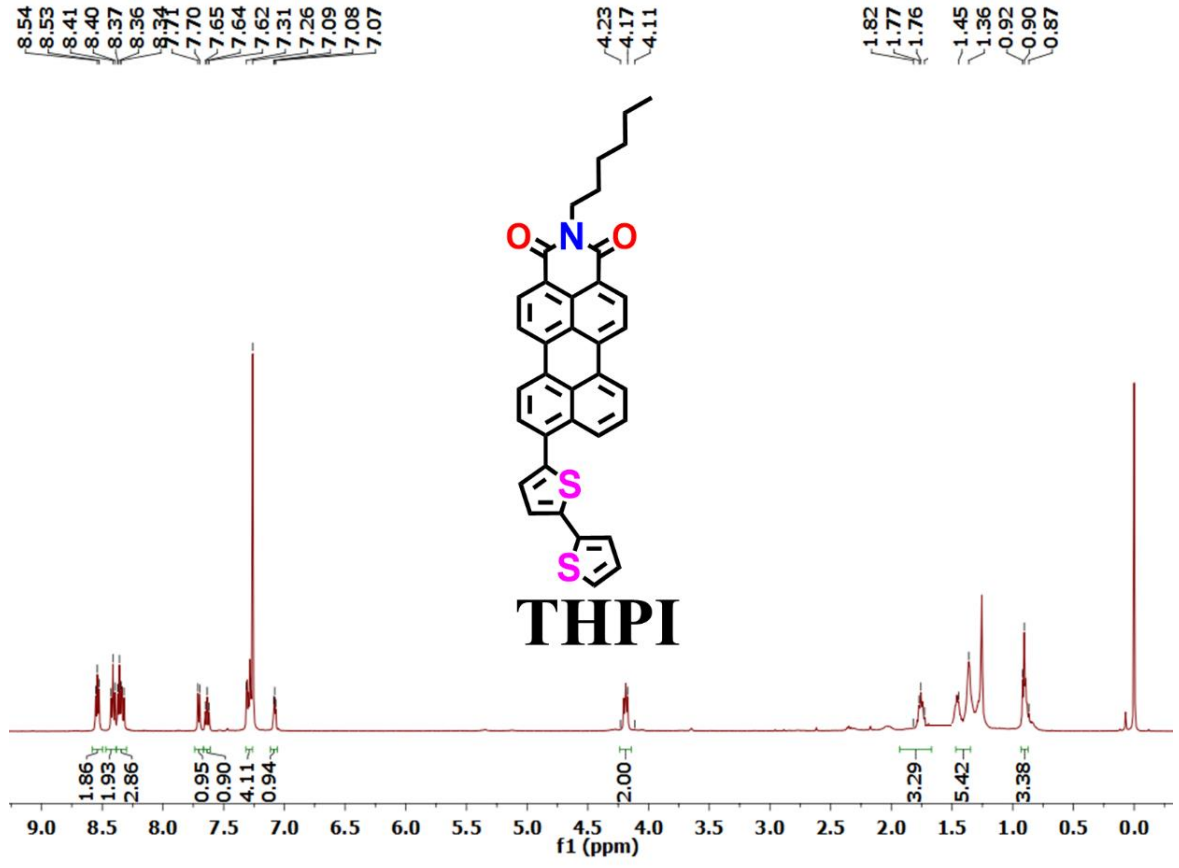

Fig. S34 ^{1}H NMR spectra of **THPI**.

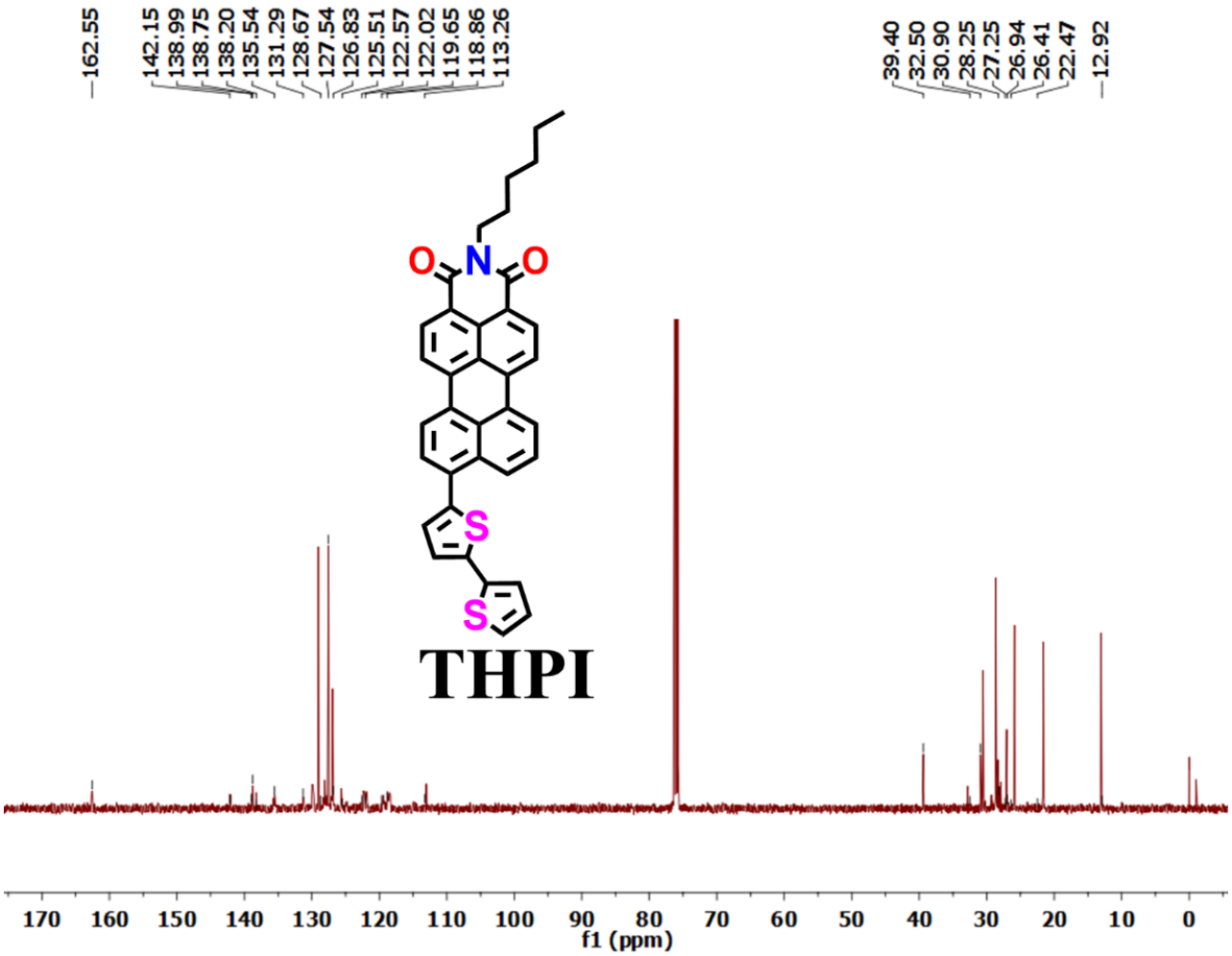

Fig. S35 ^{13}C NMR spectra of **THPI**.

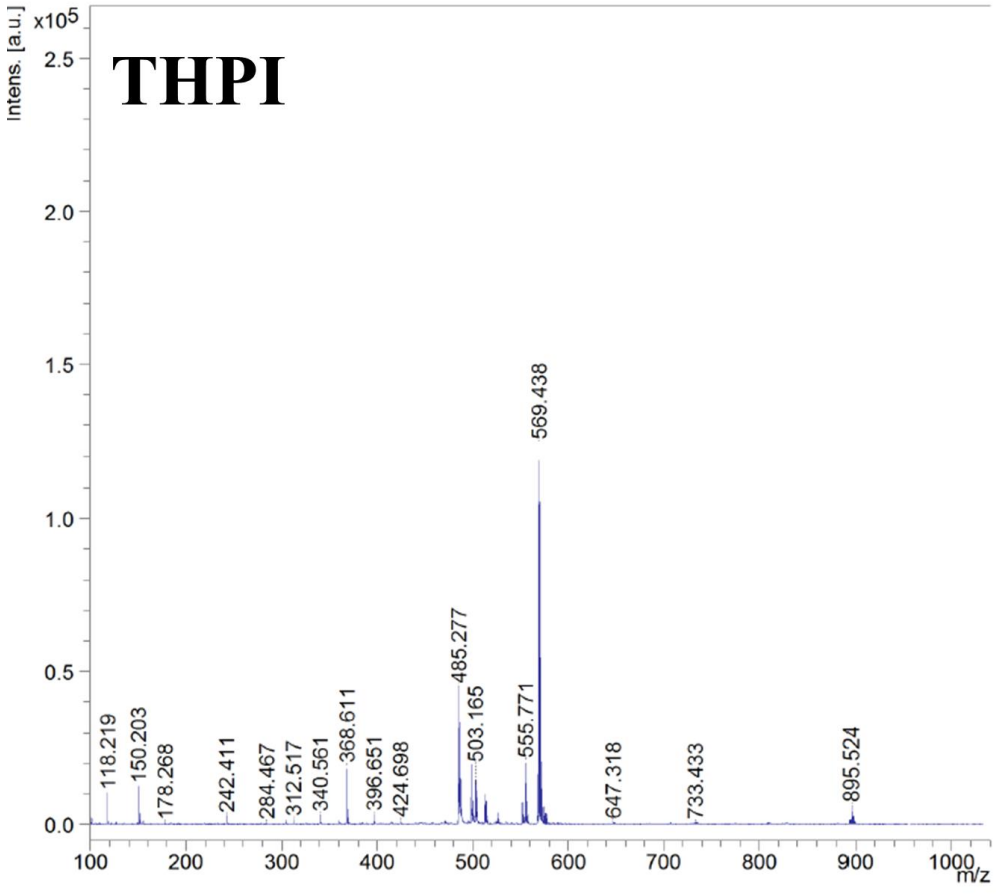

m/z	S/N	Quality Fac.	Res.	Intens.	Area
100.206	38	7546	1065	2442	256
102.222	32	3733	1078	2022	214
105.142	6	1466	794	407	60.4
109.162	11	4456	921	679	92.9
111.093	8	4332	685	539	113
118.219	175	5889	1182	11096	1249
121.195	10	409	1069	620	79.2
123.182	7	3721	895	474	80.4
127.049	15	3091	932	992	174
130.246	7	393	1139	469	60.7
135.183	6	4303	1066	394	58.1
147.193	6	6569	1067	405	66.7
150.203	199	8552	1309	13342	1751
151.168	8	264	1150	541	97.8
152.202	59	4648	1304	3958	529
155.246	20	612	1303	1363	186
178.268	8	1058	1556	581	78.5
224.188	8	2580	1485	600	111
233.140	9	5248	1345	649	150
242.411	43	3878	1704	3298	570

Fig. S36 Maldi-TOF spectra of **THPI**.

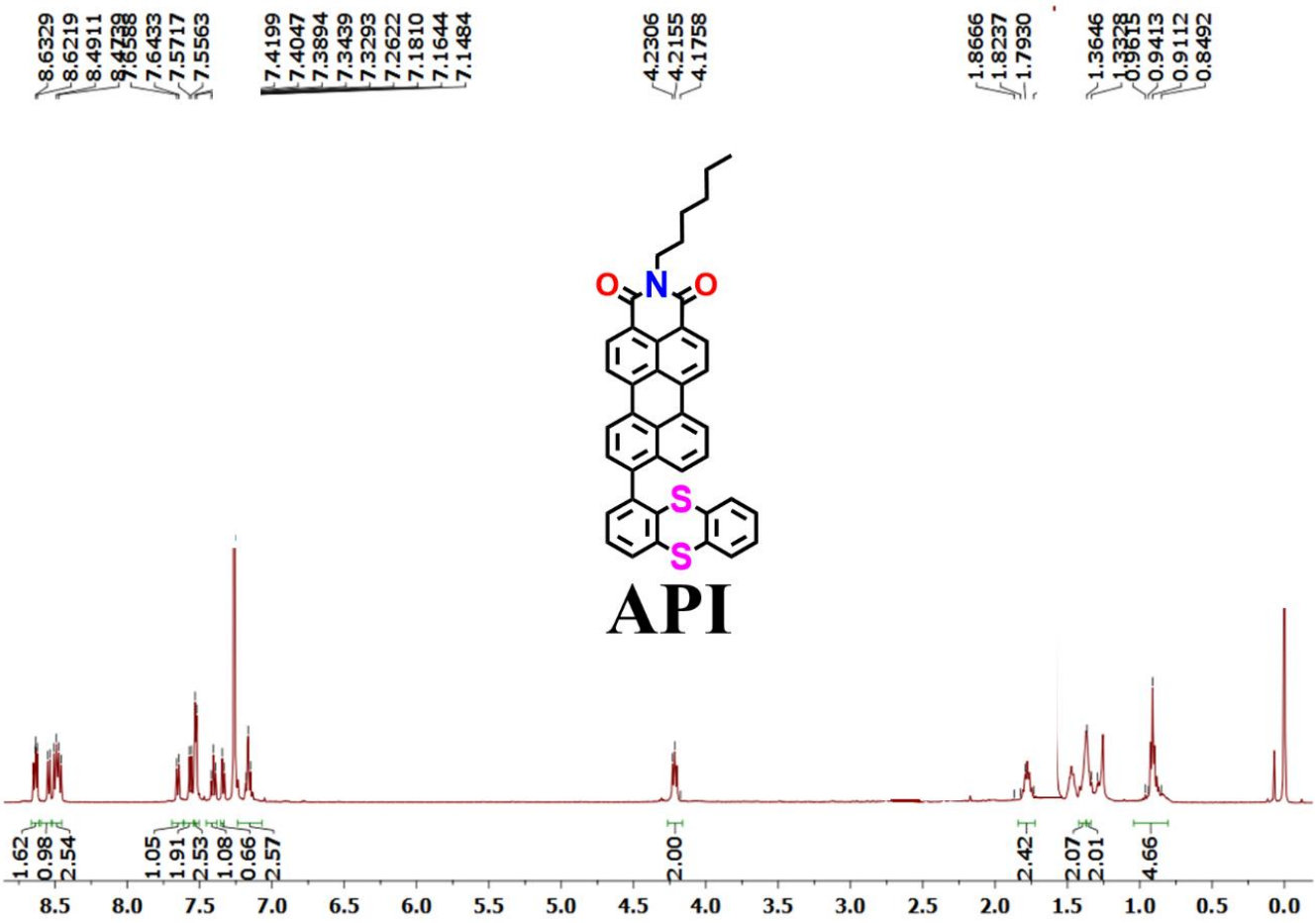

Fig. S37 ^{1}H NMR spectra of **API**.

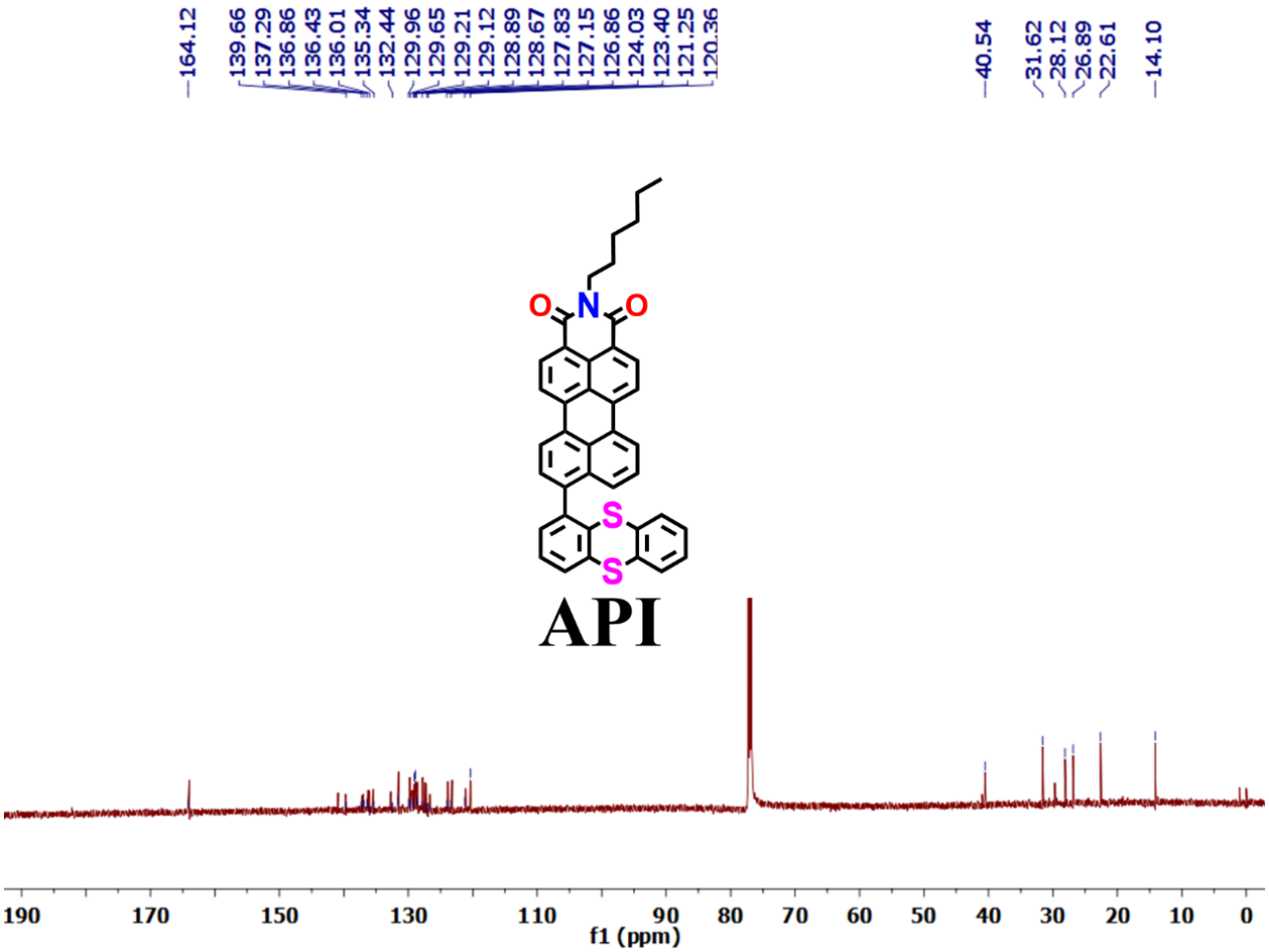

Fig. S38 ^{13}C NMR spectra of **API**.

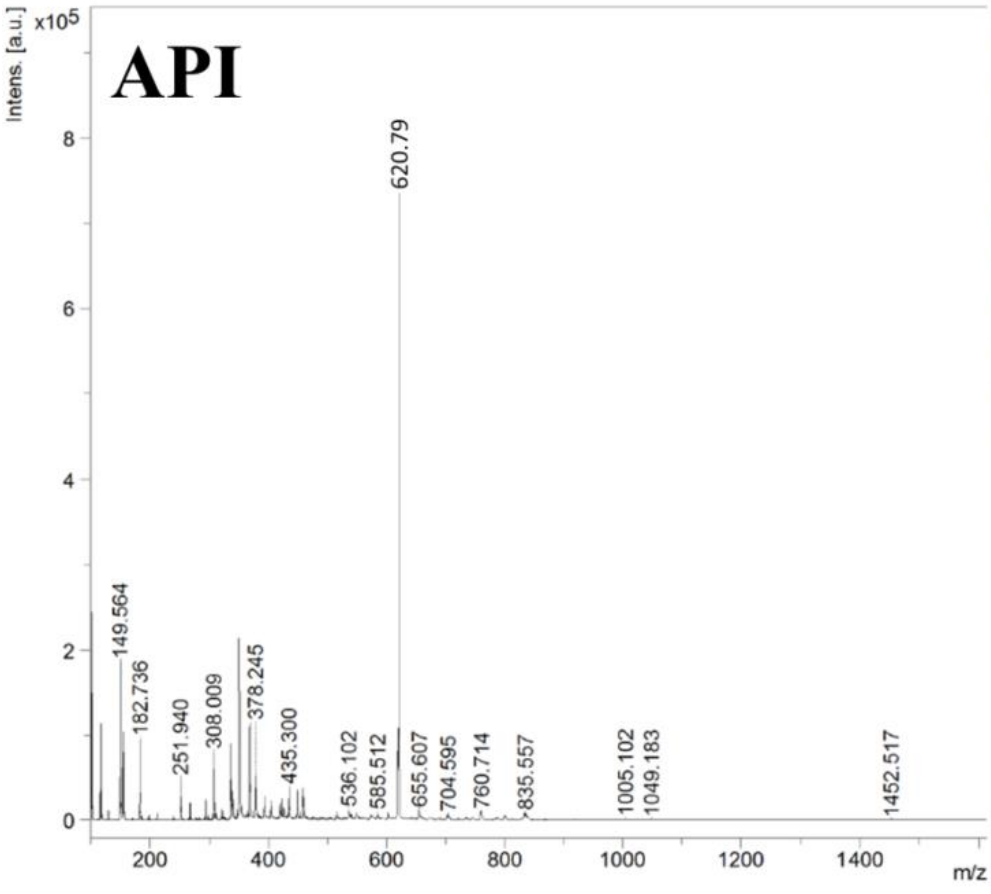

m/z	S/N	Quality Fac.	Res.	Intens.	Area
101.448	1065		395	2445 87	8379 2
112.188	7		557	1472	334
117.492	538		454	1137 93	3867 1
129.568	56		600	1153 2	2989
142.565	5		652	1052	359
149.564	844		514	1868 84	9695 4
154.632	439		511	1040 91	4663 0
169.708	9		656	2205	1674
182.736	337		603	9548 4	4361 4
197.778	14		87.7	4248	5078
211.734	22		733	7508	3962
251.940	68		3816	4980 2	2978 7
267.850	26		995	2065 7	9913
278.388	3		231	2975	2224
294.025	25		1206	2494 2	1635 4
299.009	5		924	5561	3119
308.009	73		961	8043 5	6157 3
322.021	10		847	1288 7	1129 5
337.080	22		257	2902 2	1013 84
350.057	335		890	4605 12	4729 18

Fig. S39 Maldi-TOF spectra of **API**.

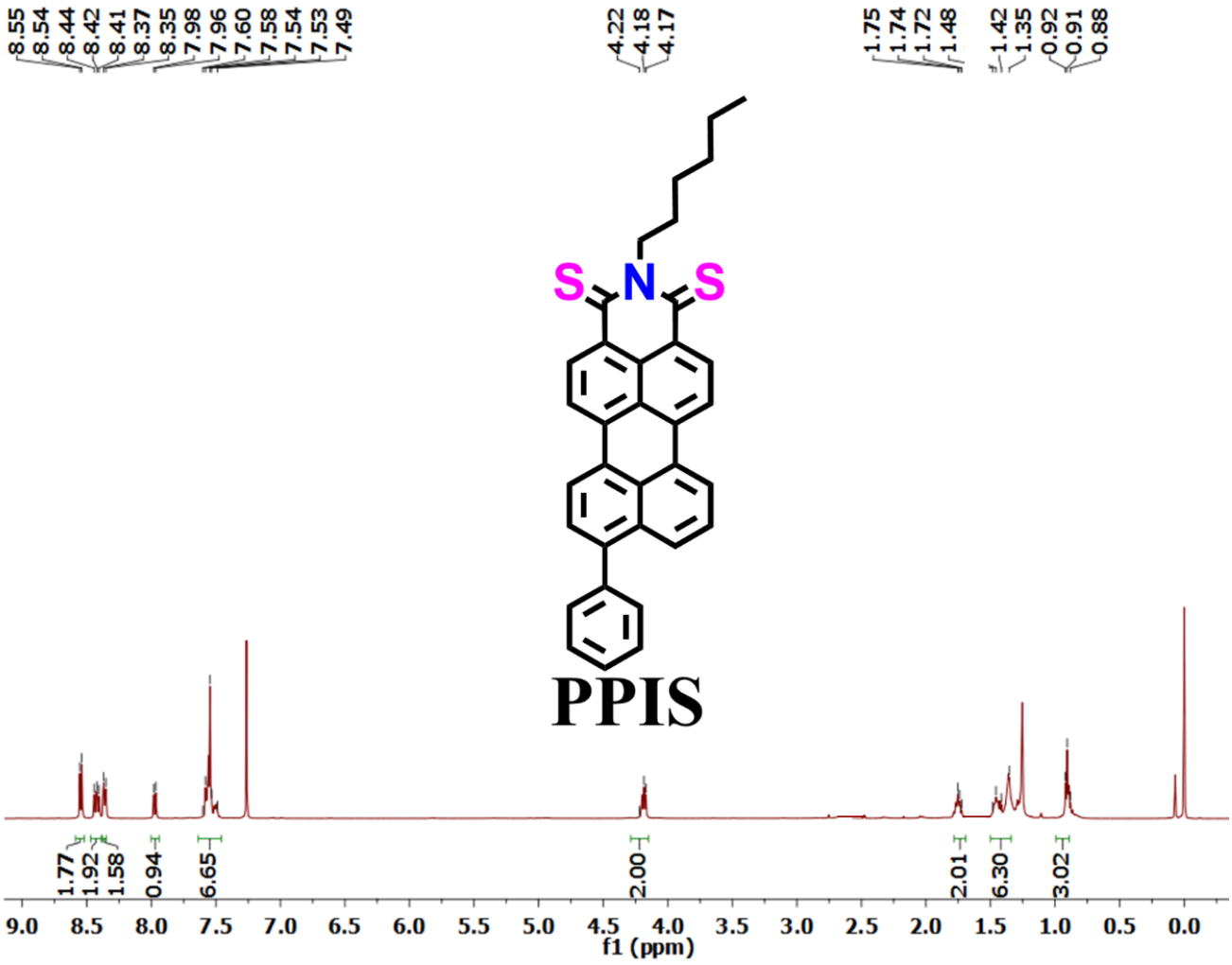

Fig. S40 ^{1}H NMR spectra of **PPIS**.

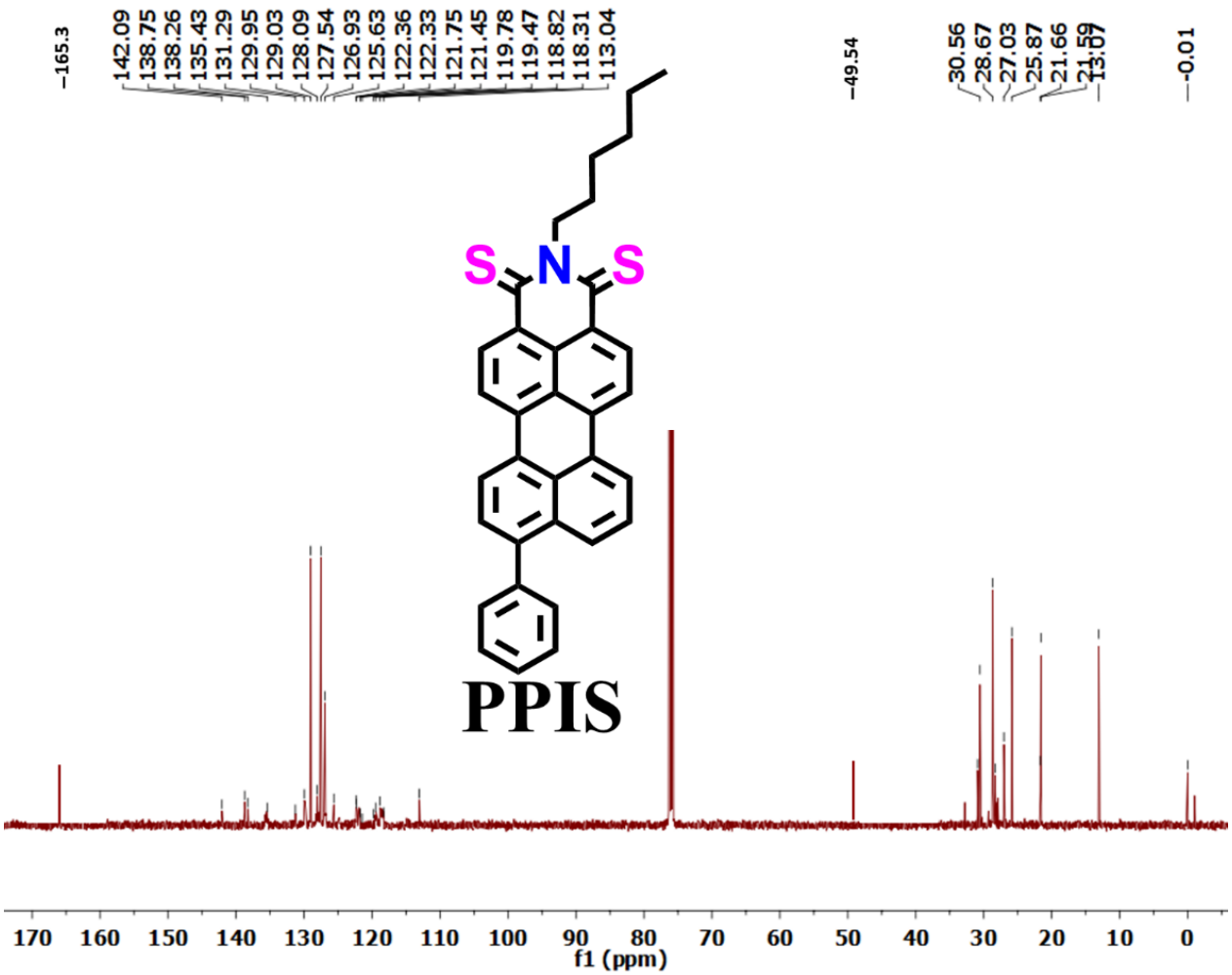

Fig. S41 ^{13}C NMR spectra of **PPIS**.

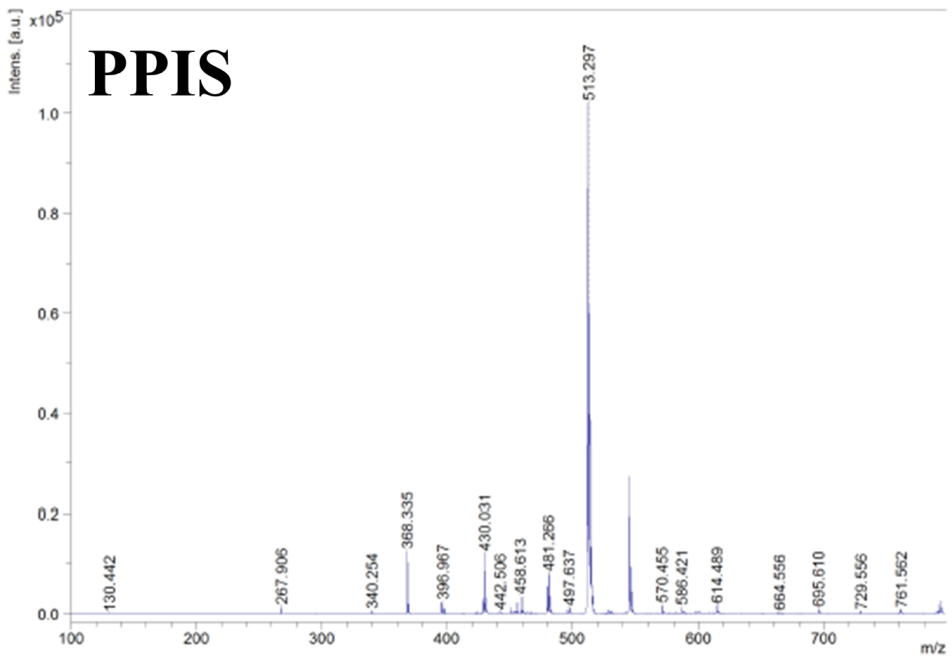

m/z	S/N	Quality Fac.	Res.	Intens.	Area
130.442	7		968	56.0	12.8
267.906	106		1636	1530	279
340.254	18		1756	573	142
368.335	323		1549	12588	4499
396.967	27		366	1166	1540
430.031	223		1255	12220	8161
442.506	8		344	447	518
458.613	62		109	3558	3687
481.266	142		364	8183	7400
497.637	22		217	1291	1156
513.297	1093		385	62030	114126
570.455	39		5299	1831	971
586.421	30		1747	1343	1526
599.454	10		166	444	990
614.489	45		1714	1775	1630
664.556	7		155	224	498
695.610	40		551	1010	999
729.556	14		555	313	368
761.562	24		615	498	790
792.547	133		2607	2655	3042

Fig. S42 Maldi-TOF spectra of **PPIS**.

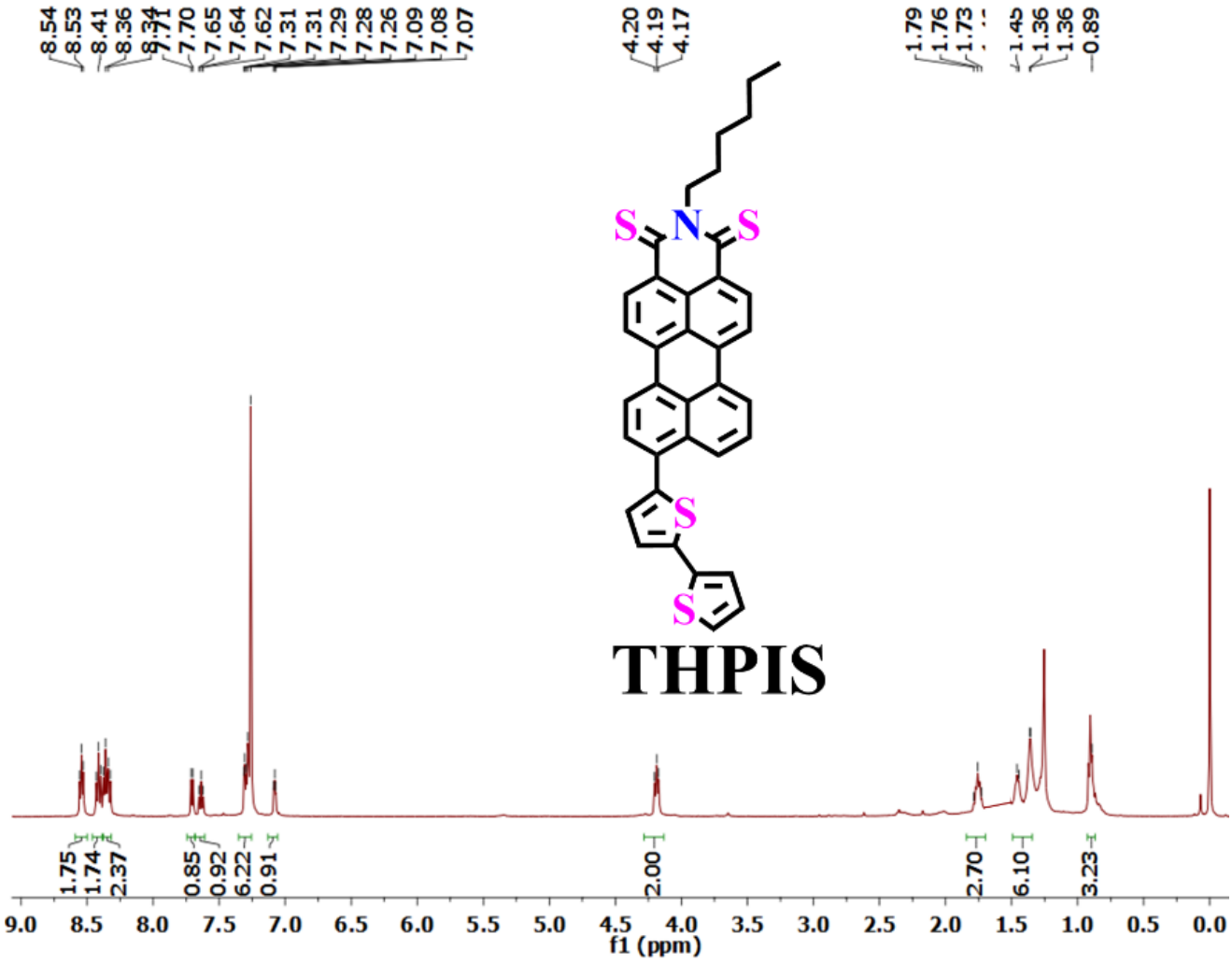

Fig. S43 ^{1}H NMR spectra of **THPIS**.

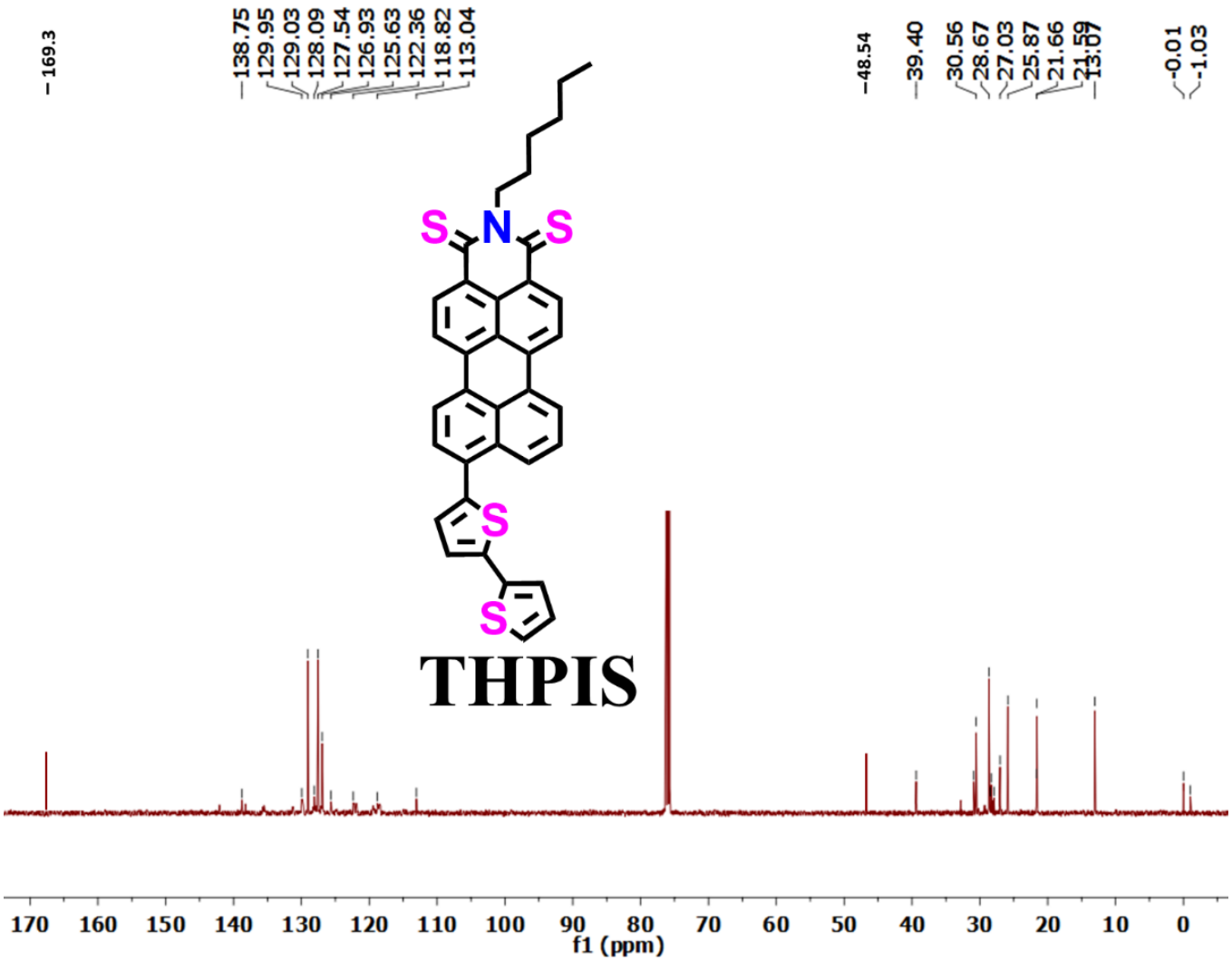

Fig. S44 ^{13}C NMR spectra of **THPIS**.

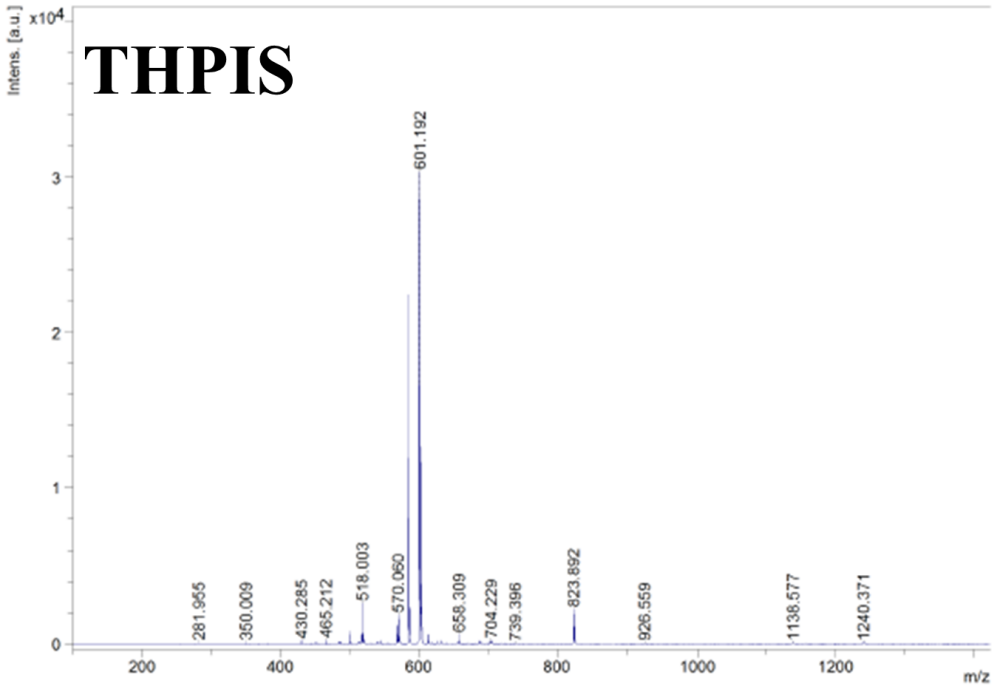

m/z	S/N	Quality Fac.	Res.	Intens.	Area
281.955	5		1705	80.0	14.8
350.009	5		2132	83.0	16.2
430.285	11		1941	203	64.1
444.288	4		1872	66.0	27.1
465.212	14		1307	245	76.1
485.389	8		216	149	150
500.375	46		2024	835	301
518.003	147		1625	2622	1613
570.060	111		361	1879	1980
586.531				2387	
601.192	1005		481	16598	29350
641.531	4		617	65.0	50.1
658.309	41		4029	627	410
704.229	4		271	58.0	290
711.757	4		345	54.0	53.2
739.396	3		328	46.0	88.8
823.892	182		710	2224	1641
926.559	5		770	55.0	86.5
1138.577	4		470	49.0	144
1155.625	3		264	36.0	127
1240.371	6		239	64.0	229

Fig. S45 Maldi-TOF spectra of **THPIS**.

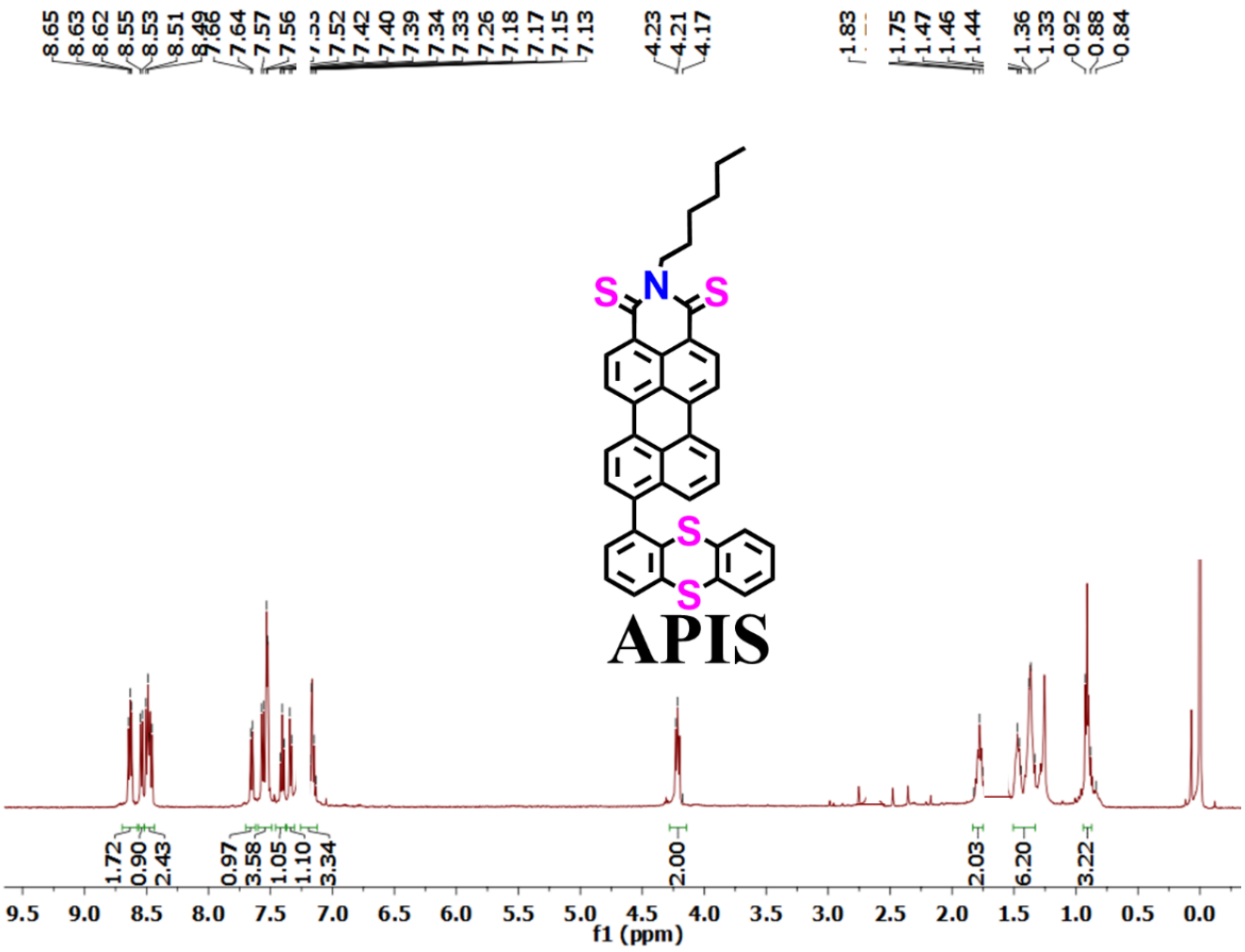

Fig. S46 ^{1}H NMR spectra of **APIS**.

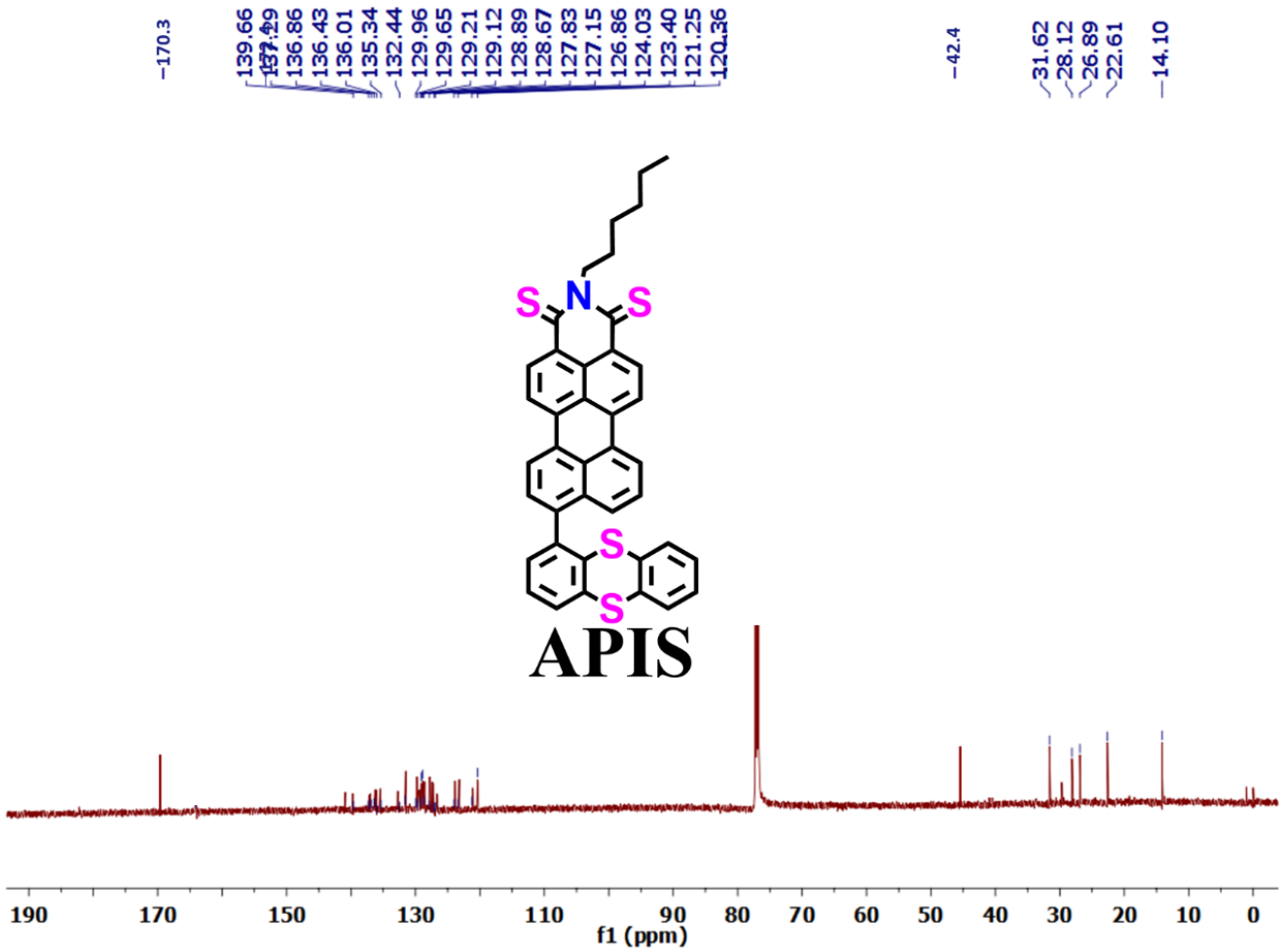

Fig. S47 ^{13}C NMR spectra of **APIS**.

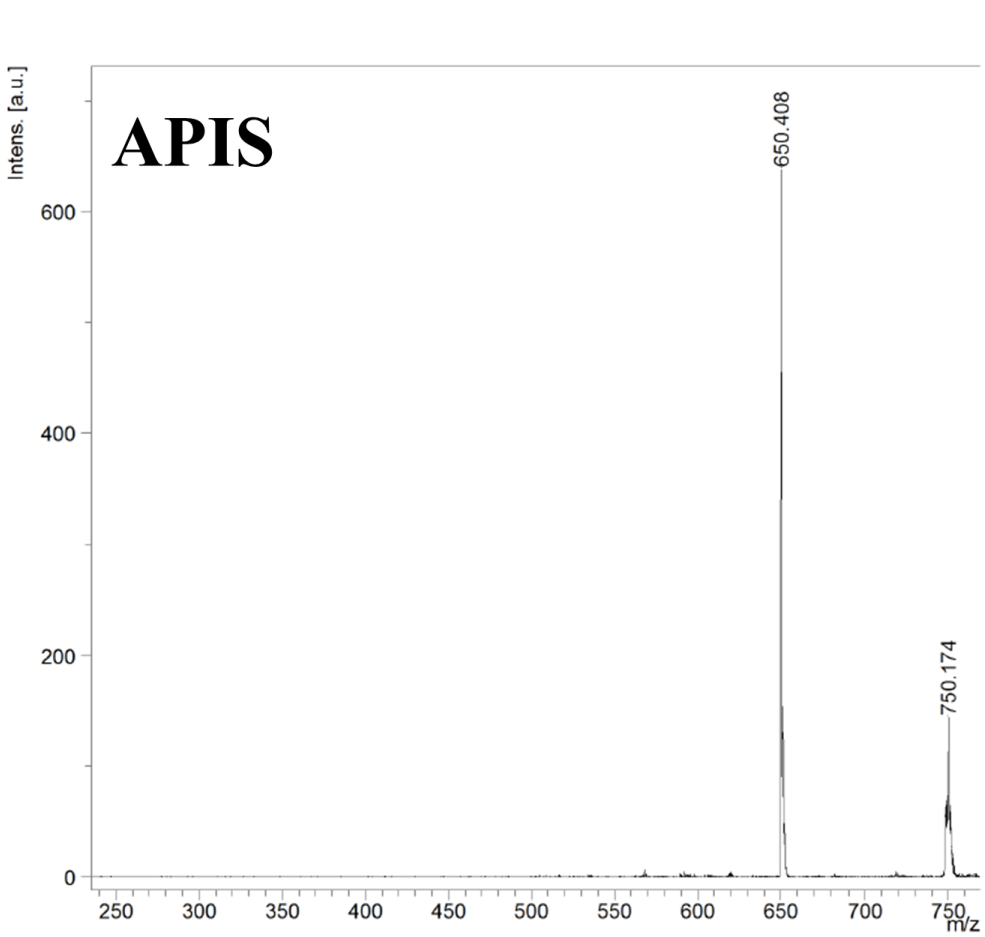

m/z	S/N	Quality Fac.	Res.	Intens.	Area
650.408	15		1815	638	427
750.174	4		505	144	248
782.755	11		568	419	824
807.910	3		322	108	355
834.419	12		531	378	762
865.638	374		483	11282	24753

Fig. S48 Maldi-TOF spectra of **APIS**.

3. References

1 A. D. Becke, *J. Chem. Phys.* 1993, **98**, 5648-5652.

2 M. J. Frisch, G. W. Trucks, H. B. Schlegel, G. E. Scuseria, M. A. Robb, J. R. Cheeseman, G. Scalmani, V. Barone, G. A. Petersson, H. Nakatsuji, X. Li, M. Caricato, A. Marenich, J. Bloino, B. G. Janesko, R. Gomperts, B. Mennucci, H. P. Hratchian, J. V. Ortiz, A. F. Izmaylov, J. L. Sonnenberg, D. Williams-Young, F. Ding, F. Lipparini, F. Egidi, J. Goings, B. Peng, A. Petrone, T. Henderson, D. Ranasinghe, V. G. Zakrzewski, J. Gao, N. Rega, G. Zheng, W. Liang, M. Hada, M. Ehara, K. Toyota, R. Fukuda, J. Hasegawa, M. Ishida, T. Nakajima, Y. Honda, O. Kitao, H. Nakai, T. Vreven, K. Throssell, J. A. Montgomery, Jr., J. E. Peralta, F. Ogliaro, M. Bearpark, J. J. Heyd, E. Brothers, K. N. Kudin, V. N. Staroverov, T. Keith, R. Kobayashi, J. Normand, K. Raghavachari, A. Rendell, J. C. Burant, S. S. Iyengar, J. Tomasi, M. Cossi, J. M. Millam, M. Klene, C. Adamo, R. Cammi, J. W. Ochterski, R. L. Martin, K. Morokuma, O. Farkas, J. B. Foresman, and D. J. Fox, Gaussian, Inc., Wallingford CT, 2016.

3 F. Neese, *WIREs Comp. Mol. Sci.*, 2018, **8**, 1327.

4 F. Neese, *WIREs Comp. Mol. Sci.*, 2022, **12**, 1606.

5 D. Wang, M. M. S. Lee, G. Shan, R. T. K. Kwok, J. W. Y. Lam, H. Su, Y. Cai and B. Z. Tang, *Adv. Mater.*, 2018, **30**, 1802105.

6 W. Wu, D. Mao, S. Xu, M. Panahandeh-Fard, Y. Duan, F. Hu, D. Kong and B. Liu, *Adv. Funct. Mater.*, 2019, **29**, 1901791.

7 X. Shi, S. H. P. Sung, J. H. C. Chau, Y. Li, Z. Liu, R. T. K. Kwok, J. Liu, P. Xiao, J. Zhang, B. Liu, J. W. Y. Lam and B. Z. Tang, *Small Methods*, 2020, **4**, 2000046.

8 Y. Li, W. Zhang, J. Niu and Y. Chen, *ACS Nano*, 2012, **6**, 5164-5173.

9 Y. Xiong, Z. Zhao, W. Zhao, H. Ma, Q. Peng, Z. He, X. Zhang, Y. Chen, X. He, J. W. Y. Lam and B. Z. Tang, *Angew. Chem., Int. Ed.*, 2018, **57**, 7997-8001.

10 Z. Liu, H. Zou, Z. Zhao, P. Zhang, G.-G. Shan, R. T. K. Kwok, J. W. Y. Lam, L. Zheng and B. Z. Tang, *ACS Nano*, 2019, **13**, 11283-11293.

11 Z. Yang, Z. Zhang, Z. Lei, D. Wang, H. Ma and B. Z. Tang, *ACS Nano*, 2021, **15**, 7328-7339.

12 X. Wang, Y. Song, G. Pan, W. Han, B. Wang, L. Cui, H. Ma, Z. An, Z. Xie, B. Xu and W. Tian, *Chem. Sci.*, 2020, **11**, 10921-10927.

13 Z. Wang, L. Ma, H. Zhao, Y. Wan, X.-F. Zhang, Y. Li, Z. Kuang and A. Xia, *Phys. Chem. Chem. Phys.*, 2023, **25**, 24386-24394.

14 K. Schmidt, S. Brovelli, V. Coropceanu, D. Beljonne, J. Cornil, C. Bazzini, T. Caronna, R. Tubino, F. Meinardi, Z. Shuai and J.-L. Brédas, *J. Phys. Chem. A*, 2007, **111**, 10490-10499.

15 D. Barman and P. K. Iyer, *J. Phys. Chem. C*, 2023, **127**, 2694-2704.